Elsevier Editorial System(tm) for Geomorphology

Manuscript Draft

Manuscript Number: GEOMOR-6067R2

Title: The role of topography in the scaling distribution of landslide areas: A cellular automata modeling approach

Article Type: Research Paper

Keywords: Landslide area; Topography; Cellular automata; Scaling

Corresponding Author: Ms. Luisa Liucci,

Corresponding Author's Institution: University of Perugia

First Author: Luisa Liucci

Order of Authors: Luisa Liucci; Laura Melelli; Cristian Suteanu; Francesco Ponziani

Abstract: Power law scaling has been widely observed in the frequency distribution of landslide sizes. The exponent of the power-law characterizes the probability of landslide magnitudes and it thus represents an important parameter for hazard assessment. The reason for the universal scaling behavior of landslides is still debated and the role of topography has been explored in terms of possible explanation for this type of behavior. We built a simple cellular automata model to investigate this issue, as well as the relationships between the scaling properties of landslide areas and the changes suffered by the topographic surface affected by landslides. The dynamics of the model is controlled by a temporal rate of weakening, which drives the system to instability, and by topography, which defines both the quantity of the displaced mass and the direction of the movement. Results show that the model is capable of reproducing the scaling behavior of real landslide areas and suggest that topography is a good candidate to explain their scale-invariance. In the model, the values of the scaling exponents depend on how fast the system is driven to instability; they are less sensitive to the duration of the driving rate, thus suggesting that the probability of landslide areas could depend on the intensity of the triggering mechanism rather than on its duration, and on the topographic setting of the area. Topography preserves the information concerning the statistical distribution of areas of landslides caused by a driving mechanism of given intensity and duration.

GREEN: Reviewer
RED: Authors

The authors would like to thank the Reviewer for the positive opinion expressed on the paper, and once again for helping us to catch the mistake that we made with the data analysis in the first version of the paper. Below we address all the points raised by the Reviewer in his second revision. To summarize, we implemented in the paper all of his suggestions at points 2 and 3, and in part, those at point 1. Please see below for more details.

The authors performed a thorough revision of their manuscript. In my first review I mainly criticized a mistake in the data analysis with the consequence that fixing it will bring the main result (D) far away form landslides in nature. As I hoped and already mentioned, changing the parameter values has brought the D value closer to nature again. After doing so, the D values obtained in this study are still somewhat at the edge of the D values obtained in nature. In this sense it is somewhat difficult to believe that the model really captures the statistical properties of landslides well, but on the other hand the approach is indeed promising, and the discussion given in the revised version is appropriate. I would therefore recommend publication of the manuscript, but would suggest to address the following points before publication:

(1) Several diagrams contain results leading to D values which are far off from the ``realistic'' range. I would suggest to remove those simulations where the D value is really too large in order to reduce the number of (sub)figures a bit.

We see that this request is quite justified and because of this – when we started working on the revision of the paper – we changed both Fig. 4 and Fig. 7 by removing all the subfigures which show values of *D* outside of the range observed for real landslides. However, when we went through the text to change it accordingly, we realized that the removal of those subfigures in Fig. 4 would result in either a loss of clarity for the reader (if describing results without any reference to the figure) or a loss of information (if removing the text which can no longer find any correspondence with the figure). In order to better explain this issue, we show below how the portion of text related to Fig. 4 (extracted from Section 3) would look like by reducing the number of subfigures in Fig. 4. The potential changes are marked, and in the appended comments we explain the reasons for our concern, which finally drove us to the choice of leaving all the subfigures in Fig. 4.

*From Section 3:*

"For each $w$ and $t_w$ tested t~~T~~he complementary of the cumulative frequency distribution of landslide areas obtained from the model~~ for each $w$ and $t_w$ tested, along with~~ and their scaling properties were investigated.~~, are shown in Fig. 4~~.
Overall, landslide areas increase with increasing $w$ and vary from $2\times10^3$ to $2\times10^7$ $m^2$, which are values comparable with the range observed for real landslide areas (Pelletier et al., 1997; Guthrie and Evans, 2004; Malamud et al., 2004), although the highest order of magnitude represented in most real datasets is of $10^6$ $m^2$, while landslides obtained from the model reach $10^7$ $m^2$. Such large landslides are not often present in landslide inventories, since they require particular conditions in order to occur, that is, very high slope gradients like those observed in deeply incised river valley, and high-intensity rainfall events (Korup et al., 2007). Moreover, particular structural settings may favor the instability of large slope portions. In terms of slope gradients and rainfall intensity, these conditions match those of the system modeled. Indeed, the river valleys are up to 70° steep, and landslide areas with a magnitude of $10^7$ $m^2$ are obtained when the highest values for the rate of weakening are applied (w=2.5 and w=2.75), which according to the interpretation given in Section 2.2, correspond to the highest intensities of the triggering event. Moreover, as explained above, coalescent landslides are identified in the model as a single landslide, thus leading to larger areas.
The ~~graphs in Fig. 4 show that the~~ right tails of the frequency distributions of landslide areas obtained from the model always follow a power law trend (R > 0.99) (Eq.3).

$$N \propto A^{-(D-1)} \qquad (3)$$

In Eq. 3, $N$ is the number of landslides with area greater than or equal to $A$, and $D$ is the scaling exponent. The scaling exponents $D$ range from 2.67 to 5.75, with uncertainty intervals at the 95% confidence level between 0.07 and 0.19. Overall, scaling behavior is observed in ranges of landslide areas from 0.6 orders of magnitude ~~(Figs.4d and 4f: series obtained at 1,000 model steps)~~ to 2 orders of magnitude ~~(Figs.4b and 4c: series obtained at 2,000 and 1,000 model steps, respectively)~~.

The graphs in Fig. 4 show the results obtained for $w$ between 2 and 2.75, which, as it will be shown later in this section, are the $w$-values that lead to realistic $D$-exponents.

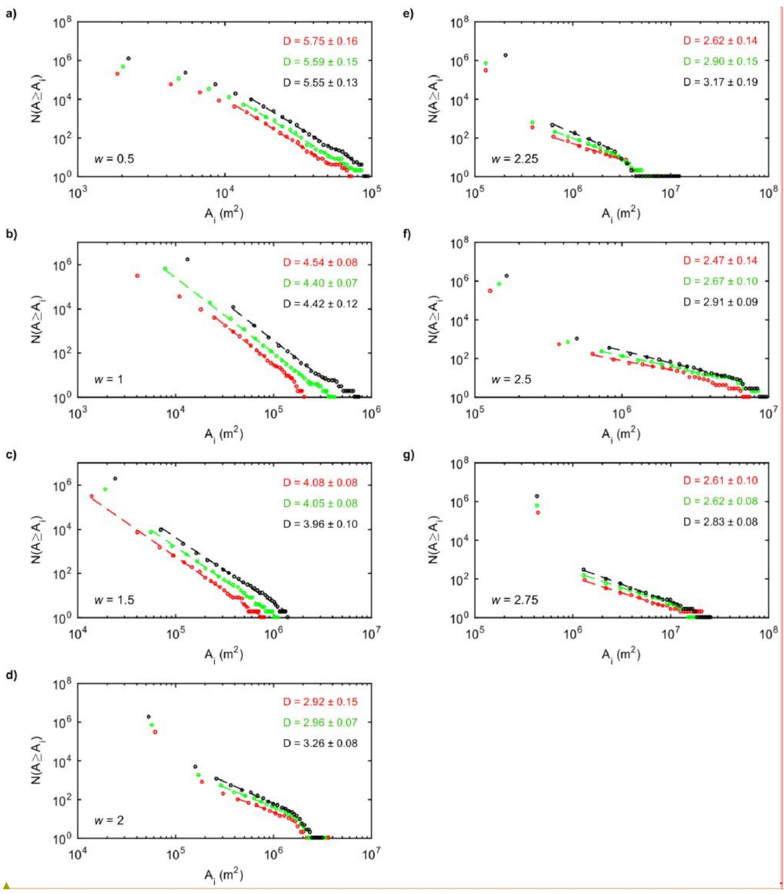


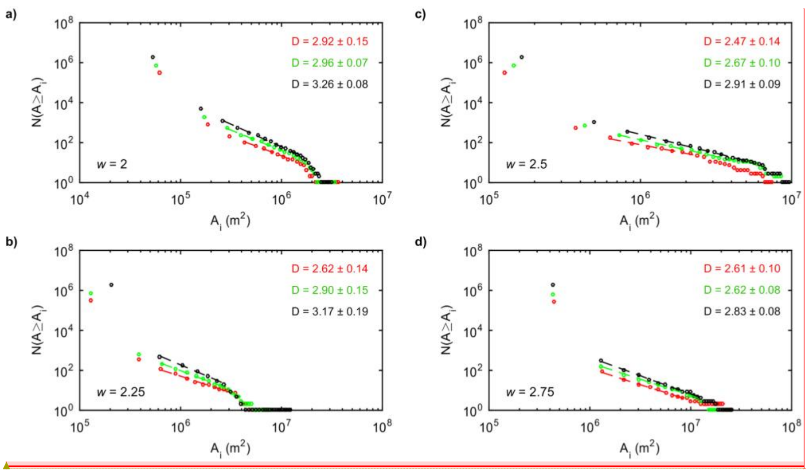


**Comment [Authors1]:** Related to the text above, we thought that we could restructure the manuscript as shown, without making major changes. As the Reviewer can see, here we would still provide information about the landslide areas and the scaling exponents obtained with all the $w$-values tested. We think that this information must be provided, since – because of the reasons explained in the previous response to Reviewers and in Section 3 - in the subsequent elaborations we use the $D$-values obtained with all the rates of weakening and not just those obtained with the $w$-values that lead to realistic $D$-exponents.
Since the figure would change as shown below, some of the values of landslide areas and $D$-exponents mentioned in the text could no longer be observed in the diagrams. Of course, this could also be done, since not necessarily all the information provided in the text must be illustrated. However, in our opinion, the situation would be more complex in the next part of the paper. Please, see comment 4 for details.

**Comment [Authors2]:** Original figure.

**Formatted:** Font: (Default) Times New Roman

**Comment [Authors3]:** New figure after removing the graphs leading to unrealistic $D$-values.

**Formatted:** Font: (Default) Times New Roman

**Fig. 4** Complementary of the cumulative frequency distributions (*CFDs*) of landslide areas ($A_i$ in m$^2$) obtained with a) *w* = ~~0.5~~2, b) *w* = ~~1~~2.25, c) *w* =~~1~~2.5, d) *w* = 2.75~~, e) *w* = 2.25, f) *w* = 2.5, g) *w* = 2.75~~, for different time spans (1,000 model steps in red, 2,000 in green, and 5,000 in black). The dotted lines indicate the portions of the *CFD*s taken in consideration for the identification of the power law (dotted lines). For each power law the respective scaling exponent *D* is shown.

~~A flattening of the frequency distributions is observed when landslide areas are lower than 10$^4$ m$^2$ (Fig.4a and 4b), thus indicating that small landslides are less frequent than predicted by the power law. A deviation from the power law at the smallest landslide sizes is also recognized in the *CFDs* obtained from real datasets. However, in the real world small landslides show a specific statistical behavior that is not observed in our *CFDs*: when non-cumulative frequency distributions are used, the interval corresponding to the smallest landslide areas is characterized by an opposite trend, with positive slope, followed by a rollover above which landslide areas start following the power law (Guzzetti et al., 2002; Guthrie and Evans, 2004; Malamud et al., 2004). Such a rollover is not present in the outcomes of this model: non-cumulative frequency distributions calculated for the same landslide data series for which the cumulative distributions are shown in Fig. 4a and 4b, exhibit a flattening rather than a rollover for the smallest sizes of landslide areas. As explained in Section 1, the rollover in real landslide inventories may be associated with a range of explanations, such as an underestimation of small landslides (Stark and Hovious, 2001; Brardinoni and Church, 2004), and the physics of processes controlling the occurrence of small landslides (Stark and Guzzetti, 2009, Milledge et al., 2014). In this regard, our model does not consider the physical parameters and processes invoked to explain the frequency distribution of small landslides, and it cannot be affected by the resolution of the data sources of the landslide inventory either. This could explain why the *CFDs* obtained do not exhibit a rollover. In our model, the only variable affecting landslide areas is the topography. Thus, the flattening that we observe for these series at the smallest landslide areas is expected to be related to the constraints represented by the topographic surface.~~
The first part of the frequency distributions obtained with *w* from 2 to 2.75 (Figs. from 4d to 4g) exhibits a behavior that it is not the same with the one from real landslide inventories. In particular, although the smallest sizes of these series are in a range at which scaling behavior is observed in nature, in this part of the *CFD* the number of the modeled landslides is higher than that predicted by the power law. The difference can ~~again~~ be related to the fact that the only constraint to model dynamics is represented by topography: as we deduced from Fig. 3, topographic adjustments occur in response to the large landslides caused by high rates of weakening, thus leading to a high number of slope failures with smaller area.
While model choices affect the first part of the area-frequency distributions, results indicate that the model is capable of reproducing the scaling properties of real landslides. The values of *D* were compared to those observed for real landslide inventories by taking as a reference the work by Van Den Eeckhaut et al. (2007)…"

**Comment [Authors4]:**
The flattening that we are referring to, can be observed in subfigures 4a and 4b, which have been removed in the updated figure. The parts of this paragraph highlighted in yellow are those where we explicitly refer to those graphs, and that allow us to compare the behavior of small landslides in real inventories and in our model.
In the attempt of adapting this paragraph to the new figure, we would thus have two options:
- 1) leave it as it is, only removing the references to Figs. 4a and 4b, that is, to provide the information highlighted in yellow and the related discussion without the possibility for the reader to find any correspondence in the figure,
- 2) to remove this whole paragraph from the text (as shown) and no longer address the issue related to the frequency distribution of small landslides.
We think that none of them would be a good choice.
- If we apply option 1, we are concerned that the reader would get lost in the text and not understand what we are speaking about.
- If we apply option 2, the removal of the paragraph would imply that we would no longer make any consideration about the behavior of small landslide sizes, while we think that a paper that deals with landslide area frequency statistic should mention this aspect of the distribution, which has been widely depicted and debated in literature. Also, one of the main clarifications asked by the other Reviewer in the first review was about the reasons why our model does not reproduce well this part of the distribution, and if we remove this part we will no longer provide any explanation regarding that.

*Last rows of Section 4:*

"These outcomes also suggest that the fact that the model does not accurately represent the first part of the frequency distribution of real landslides (Section 3) is not due to the scale of analysis but rather, as hypothesized in the previous section, due to the choice of topography as the main way of describing the spatial variability of the system."

**Comment [Authors5]:**
The considerations above also apply to the last rows of Section 4, which should be either left as they are without having shown – in Section 3 – any graphical information, or removed from the text, although they proved to the other Reviewer (and more in general, they prove to the reader) that the resolution does not affect the statistical behavior of small landslides in the model.

Because of the reasons explained above, we finally decided to leave Fig. 4 and the text in Section 3 as they were in the first review. However, in order to better point out that some *w*-values lead to unrealistic *D*-exponents, we reiterated this concept through the paper, where appropriate. In the file 'Liucci et al._changes marked', the Reviewer can see – highlighted in yellow – the parts of text where this concept was already present, and – highlighted in green – the parts where it has been repeated.
As for Fig. 7, we followed Reviewer's suggestion and removed the two subfigures where the *D*-values where too high. The text still explains that we compared results for two rates of weakening, since we think that this makes the results of the comparison stronger. We hope that the Reviewer agrees with the decisions made.

(2) The second part of the paper (from Fig. 8 on) discusses results of the model in great detail. Taking into account that we cannot be completely sure about the relationship of the model for real landslides, the authors might think about tightening this part a bit and reducing the overall length of the paper.

We followed the Reviewer's suggestion and removed some sentences from the manuscript (from Section 5 to Section 7), which either provided too detailed information about marginal aspects of results or stressed the possibility of a link between the model and reality.

(3) The log scales in the diagrams are not consistent. Some diagrams use axes with 10^... (what I would prefer for clarity), while others use labels such as log(A) and number like 5, 6, ... Maybe the authors could use a uniform style for this.

Thank you for helping us notice this. We uniformed the log scales of the diagrams by converting the axes in Fig. 7 in the format of 10^…

I think the authors can establish at least some of these suggestions, and I will be happy to recommend publication of this interesting and in general well written paper then.

# Highlights

- A Cellular Automata model for the study of landslide scaling behavior is proposed.
- The rate of weakening of the system affects landslide area frequency distribution.
- Topography is a good candidate to explain the scaling behavior of landslide areas.
- Topography conserves information about the probability of landslide magnitudes.

# The role of topography in the scaling distribution of landslide areas: A cellular automata modeling approach

AUTHORS:

**1**. Luisa Liucci (Corresponding Author)

**2.** Laura Melelli

**3.** Cristian Suteanu

**4.** Francesco Ponziani

AFFILIATIONS

**1; 2**: Department of Physics and Geology, University of Perugia, Via Alessandro Pascoli snc, 06123 Perugia, Italy

**3**: Department of Geography & Environmental Studies and Department of Environmental Science, Saint Mary's University, 923 Robie St., Halifax, Nova Scotia, B3H 3C3 Canada

**4**: Umbria Region Civil Protection Department, Via Romana Vecchia, 06034 Foligno, Perugia, Italy

CORRESPONDING AUTHOR

email Luisa.Liucci.LL@gmail.com

Tel +393405816613

Fax +390755840302

**Abstract**

Power law scaling has been widely observed in the frequency distribution of landslide sizes. The exponent of the power-law characterizes the probability of landslide magnitudes and it thus represents an important parameter for hazard assessment. The reason for the universal scaling behavior of landslides is still debated and the role of topography has been explored in terms of possible explanation for this type of behavior. We built a simple cellular automata model to investigate this issue, as well as the relationships between the scaling properties of landslide areas and the changes suffered by the topographic surface affected by landslides. The dynamics of the model is controlled by a temporal rate of weakening, which drives the system to instability, and by topography, which defines both the quantity of the displaced mass and the direction of the movement. Results show that the model is capable of reproducing the scaling behavior of real landslide areas and suggest that topography is a good candidate to explain their scale-invariance. In the model, the values of the scaling exponents depend on how fast the system is driven to instability; they are less sensitive to the duration of the driving rate, thus suggesting that the probability of landslide areas could depend on the intensity of the triggering mechanism rather than on its duration, and on the topographic setting of the area. Topography preserves the information concerning the statistical distribution of areas of landslides caused by a driving mechanism of given intensity and duration.

Keywords: Landslide area; Topography; Cellular automata; Scaling

## 1. Introduction

Landslide occurrence is controlled by the interaction of many factors, such as geology, topography, hydrology, land use and climate. These factors affect both the proneness to slope failures and the type and magnitude of landslides. However, regardless of the local characteristics, it has been widely shown that landslide patterns (Goltz, 1996; Liucci et al., 2015) and the frequency distribution of landslide areas and volumes exhibit scaling properties (Malamud and Turcotte, 1999; Stark and Hovius, 2001; Guzzetti et al., 2002, Martin et al. 2002; Brardinoni and Church, 2004; Guzzetti et al., 2005; Korup, 2005; Brunetti et al., 2009). In particular, landslide sizes follow a power law with negative scaling exponent, which can also be similar for landslides triggered by different mechanisms (Pelletier et al., 1997; Malamud et al., 2004; Hergarten, 2013). This trend is found from medium to large landslide sizes, while an opposite trend is identified at smaller sizes. Several models have been built to investigate this behavior and hypotheses have been discussed that the scaling properties of landslides could arise in Self-Organized Critical dynamics (Malamud and Turcotte, 1999; Hergarten, 2003, 2013).

According to the work by Van Den Eeckhaut et al. (2007), who reviewed the values of the scaling exponent observed for about thirty landslide datasets around the world, the exponent of the non-cumulative frequency distribution of landslide areas ranges between 1.42 and 3.36.

Compared to regolith landslides, rockfalls exhibit, on average, smaller scaling exponents (Malamud et al. 2004, Brunetti et al., 2009), and this could depend on the physics of processes leading to rockfalls, which are different from those responsible for regolith landslides (Malamud et al., 2004). The comparison between the scaling behavior of these two types of mass movement commonly takes into account the mobilized volumes.

The understanding of the factors controlling this power law decay and the value of the scaling exponent is of much interest, since it would provide valuable information concerning the probability of occurrence of landslides of different magnitudes. Several studies suggested possible explanations for the characteristic shape of the landslide frequency distribution and for the factors responsible for landslide sizes. Katz and Aharonov (2006) induced landslides in a vibrating box of cohesive sands through the application of both horizontal and vertical acceleration. The analysis of the frequency-size distribution of the generated landslides showed that the power law behavior observed for medium to large sizes is due to the strength heterogeneity of the material caused by the fracture systems that form in response to the acceleration applied. Lehmann and Or (2012) used a hydromechanical physically based hillslope model inspired by concepts of Self-Organized Criticality (SOC) (Bak et al., 1988), to study the frequency distribution of rainfall-induced shallow landslide volumes. They observed that root reinforced soils and high slope angles lead to smaller values of the scaling exponent of landslide volumes, while soil textural class and rain intensity have less of an impact on its value. Conversely, the work by Alvioli et al. (2014) showed that the shape of the frequency distribution for medium to large landslides changes with rainfall intensity and rainfall duration, for given geotechnical parameters. Frattini and Crosta (2013) observed that topography exhibits power law scaling with a rollover at smaller scales, similarly to what was observed for landslide size-frequency distributions, and that the scaling exponent of the frequency distribution of areas of patches (triangular units used to tile the topographic surface) increases with the slope gradient of relief. This indicates that topography is characterized by a low number of large areas with high slopes. They conclude that the low number of large patches with a slope gradient high enough to have slope failure causes an increase of the scaling exponent of the frequency distribution of landslides compared to the case of unlimited availability of high-slope patches. However, the investigation of synthetic landslide inventories showed that the main factor controlling the scaling exponent of landslide sizes is the variation of the geotechnical properties with depth. Katz et al. (2014) investigated the possible factors controlling the size and geometry of an individual landslide through the use of a numerical model. They hypothesized that the size of small landslides is controlled by the amount of material disintegrated by pre-sliding rupture processes, which in turn is controlled by the peak strength of the material and by the slope angle, while the size of medium to large landslides is not necessarily related to material disintegration and is mainly affected by the preexisting discontinuity setting. Milledge et al. (2014) proposed a slope stability model to predict the size of shallow landslides. They suggested that the low number of small landslides observed in real inventories and their size depend on the so called ‘critical area’, defined as the minimum area necessary to overcome resistive forces like friction and (when present) cohesion and thus to become prone to failure. The critical area is controlled by the critical failure depth, which is the depth at which the critical area is minimized, and in both cohesion and cohesionless soils it is affected by the position of the water table, which thus indirectly controls landslide sizes. They also found that the critical area closely corresponds to the peak of the frequency distribution of landslide areas on the reference site. This peak delimitates the rollover that marks the transition from the part of the frequency distribution corresponding to small landslide areas and characterized by positive slope, to the part corresponding to the medium to large landslide areas, which follows a power law with negative exponent (Guzzetti et al., 2002; Guthrie and Evans, 2004; Malamud et al., 2004). There is a wide debate about the reasons for the rollover. A possible explanation is an underestimation of small landslides because of the resolution of the original data sources used to build the dataset (Stark and Hovious, 2001; Brardinoni and Church, 2004). For example, raster data with a certain spatial resolution do not allow us to identify landslides with areas lower than the resolution of cells. Moreover, erosional processes quickly remove the fingerprint of small landslides (Guzzetti et al., 2002) - the level of conservativeness of landforms increases with their size.

Another possible explanation for the low number of small landslides concerns the geomechanical properties of soil and their relative importance in the rupture mechanism, which depends on the scale at with the process occurs (Stark and Guzzetti, 2009). Another category of models widely applied to the study of the dynamics of such natural phenomena is that of cellular automata (CA) models. A cellular automaton is a discrete numerical model, in which the studied system is discretized in cells. Each cell is characterized by a state representing one or more physical properties. The states of cells are evaluated and updated at discrete time steps according to rules that concern the states of the neighboring cells. One can then study the overall behavior of the system in space and time as an effect of local interactions. One of the strengths of these models stems from their capability of reproducing the complexity of real world patterns by using a small number of input parameters and by reducing processes to simple rules, capable of fruitfully describing their dynamics. Although in reality the dynamics are quite more complex and the factors involved are many, in CA models complex patterns emerge from simple rules (Wolfram, 2002); that is, they manifest emergent behavior (Bonabeau et al., 1995) just like complex natural systems do.

Two pivotal CA models are the Bak-Tang-Wiesenfeld model (Bak et al., 1988) and the Olami-Feder-Christensen model (Olami et al., 1992). The former, known as 'sandpile model', describes the behavior of a system subject to constant input that drives the system to instability: the equivalent of adding grains to a sand pile causes local instabilities that may propagate throughout the system, in a chain reaction, as a function of local states, producing scale invariant features both in space and in time. Constant input is thus leading to outputs in a wide range of sizes, corresponding to a distribution governed by a power law. The second one belongs to the group of CA spring-block models and it was built to study earthquake dynamics. In this model, cells represent blocks connected with each other through springs. In its theoretical formulation, blocks are also connected to a rigid driver plate, slowly moving, thus increasing the forces acting on the blocks until one (or some of them) exceeds the static friction and becomes unstable. When the block becomes unstable it is displaced, possibly initiating a chain-reaction involving neighboring cells. The OFC model is considered as a paradigm for non-conservative SOC because it involves dissipation: the potential energy gradually accumulated in the springs is partially transferred to the driver plate, while a part of it is lost from the system.

Like other phenomena, landslides seem suitable to be treated as avalanche processes. For slides occurring on slopes of overconsolidated clay and clay shales, the development of a sliding surface follows a mechanism of progressive slope failures (Bjerrum, 1967): the instability starts in a small region and destabilizes the neighborhood, thus allowing the instability to propagate. Moreover, the behavior of CA models can be thought of as a self-similar inverse cascade (Turcotte et al., 2002), and this idea can be fruitfully applied to landslides by considering the cascade as a coalescence of metastable regions: small failures coalesce to form a large failure plane.

Attempts have been made to apply the sandpile model (Bak et al., 1988) and the OFC model (Olami et al., 1992) to landslides, but results showed that none of them works on a quantitative level if the surface gradient is the only parameter used to describe the state of cells in the model (Hergarten, 2003). Hergarten and Neugebauer (2000) presented a new type of model, which introduces a second variable to the one describing the state of cells. The second variable represents a time-dependent weakening, and when the model is applied to landslides it consists of a temporal decrease of the stability slope threshold of each site. The rate of weakening can be introduced in different ways in the stability criterion, for example as a sum approach or as a product approach. When the product approach is used, the model shows SOC behavior and the scaling exponent observed is in agreement with values observed for real landslides. Thus, when a second variable is introduced to describe slope stability, results improve.

The idea of a two-variable model was also applied by Piegari et al. (2006, 2009). Their model uses the inverse of a factor of safety as a dynamic variable describing the state of cells, while a second parameter drives the system to instability, which in practice is equivalent to the time-dependent weakening of Hergarten and Neugebauer (2000). In their model, the instability of cells is partly lost from the system, which means that unlike previous landslide models the system is non-conservative, in analogy with the non-conservative case of the OFC model. A good correspondence with real frequency-size distributions is obtained when a specific level of conservation and driving rate are used, and after spatially scaling the model. They conclude that the frequency-size distribution of landslides is controlled by the rate of approaching instability more than by the triggering mechanism. Hergarten (2013) points out that the introduction of a degree of dissipation represents a tuning parameter for the model, whose value cannot be conceptually interpreted based on physical arguments.

Both the CA by Hergarten and Neugebauer (2000) and by Piegari et al. (2006, 2009) describe landslides on an individual slope. However, as shown by Frattini and Crosta (2013), topography is a key factor affecting landslide sizes. The important role of topography in slope failure occurrence is also highlighted by landslide susceptibility analyses, which find the slope gradient to be a predominant factor in causing the instability of an area (Lee and Min, 2001; Ayalew and Yamagishy, 2005). More generally, the setting of the topographic surface plays a major role in all the geomorphological processes acting on the landscape. Topography is not a static property of an area. A topographic surface changes as a consequence of the processes acting on it and in turn it affects the dynamics of most of these processes. A large number of landscape evolution models aim to describe these mutual interactions (a recent review of these models is given by Chen et al., 2014), and the factors mainly considered are the tectonic uplift, the fluvial erosion, and the gravitational processes. Topography also implicitly contains information concerning the lithology and the structural aspects of the area, since the geological properties constrain the resulting landforms (Taramelli and Melelli, 2009; Melelli et al., 2014). Consequently, the variability of the topographic surface also reflects the variability of many other parameters and it can thus be considered representative of the specificities of an area.

The changes that the topographic surface incurs over time could play a key role in the explanation for the statistics of landslide sizes (Hergarten, 2013). This paper focuses on this specific aspect of landslide dynamics, in order to contribute to the understanding of the scaling properties observed for medium to large landslides. In particular, we explore the possible relationships between landslide scaling properties and the changes in topography, which to the authors' knowledge, represents a new contribution to the existing literature on this topic.

To this purpose, we use a cellular automata (CA) model. In the model, we consider the gravitational process as the only mechanism shaping the landscape, and the topographic surface as the only parameter defining the variability in the initial conditions. Given that the model does not take into account the subsoil and structural geology, it refers to shallow landslides involving the regolith layer of the slope, and triggered by moisture increase. Its basic structure is similar to the one proposed by Hergarten and Neugebauer (2000), which is also used in the non-conservative CA model by Piegari et al. (2006, 2009). The model dynamics is driven by two variables: a temporal rate of weakening and a variable describing the state of cells. However, the fundamental difference between the model proposed here and those models consists of the predominant role of topography in the evolution of the system and in landslide dynamics, since topography is decisive for both the displaced mass and the instability direction. Moreover, conversely to the model by Piegari et al. (2006, 2009), this model is based on the transfer of mass and thus it is conservative.

The steps involved in this work consisted in: *i*) building the CA model (described in Section 2); *ii*) investigating the frequency distribution of landslide areas resulting from the implementation of the model starting from a topographic surface (Section 3 and 4); *iii*) qualitatively and quantitatively investigating the changes undergone by the topographic surface (Sections 5); *iv*) exploring the possible relationships between the scaling behavior of landslide areas and the changes in topography (Section 6). Section 7 discusses the results and their implications in terms of landslide dynamics, the limitations of this study, and possible future developments.

## 2. A cellular automata model for landslides

### 2.1. Structure of the model

The cellular automata model presented in this study was designed and written by the authors using the Matlab® software. It consists of a square lattice of square cells. Each cell is characterized by an altitude value, which can change during the evolution of the model through local interactions between neighboring cells. The initial state of the system is represented by the altitude values acquired from the Digital Elevation Model (DEM) of a real area. The lattice has a size of 320×320 cells, while the original DEM corresponds to an area located in the Umbria region (central Italy) and has a cell size of 25x25m. The area represents a mountainous morphology characterized by steep river valleys with slopes up to about 68° and flat surfaces at the top of the slopes. Overall, the area exhibits low drainage density and wide interfluve areas. The maximum altitude is of 1,412 m a.s.l (Fig. 1). We would like to specify the fact that it is not our objective to study landslide phenomena in this specific area. Rather, we use a real DEM in order to represent the natural variability of topographic surfaces, which has been shown to possess self-affine statistics over a wide range of scales (Turcotte, 1997). The advantage of using a real topography instead of a synthetic self-affine surface is that the latter typically lacks some important features of the earth's surface, such as river valleys and morphological shapes resulting from a variety of processes, including tectonics (Hergarten, 2013). Moreover, real topographic surfaces exhibit deviations from scale invariance (Evans and McClean, 1995).

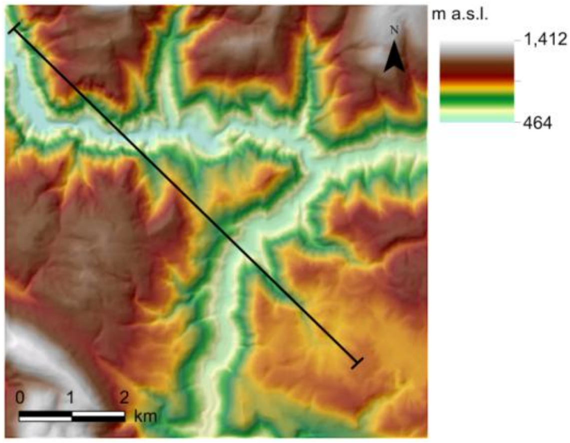


**Fig. 1** DEM of the area used as initial topographic surface in the CA model. The black line indicates the cross-section of profiles shown in Fig. 9.

The stability criterion for the cells is based on the local slope angle. The slope angle $\beta_c$ of each cell $c$ is defined as the maximum slope gradient between the cell and its eight Moore neighboring cells (Wolfram and Packard, 1985). The slope threshold is defined as the slope angle above which cells are unstable. The model starts from stable initial conditions; that is, the initial threshold $\alpha_0$ for all the cells is higher than the maximum $\beta_c$ of the area. Then, at each step the threshold decreases by a quantity $w$, driving the system towards instability. In analogy with the real world, the decrease of the stability threshold can be thought of as representative of the weakening of soil caused by triggering events such as rainfall and snowmelt, which produce a decrease of the resistive forces of soil until one or more slope failures occur. If the slope threshold of a cell at a given time $t$ has a value lower than or equal to $\alpha_{min}$, the decrease is no longer applied. The value used for $\alpha_{min}$ is 5°, which implies that a quasi-flat area is always stable. A cell $c$ is unstable when $\beta_c$ is higher than the slope threshold $\alpha_c$. When the cell $c$ is unstable, its altitude $e_c$ decreases by a quantity $\Delta e_c$. The value of $\Delta e_c$ is evaluated as the amount of altitude that $c$ must lose so that $\beta_c$ after perturbation becomes equal to $\alpha_c$, that is, the quantity necessary to bring cell $c$ back to a metastable state. The quantity $\Delta e_c$ is discharged to the $n_i$ neighboring cells identified as receiving cells ($n_i$, $i = 1\ldots, N$), thus resulting in an increase of their altitude $e_{n_i}$. Accordingly, in order to evaluate $\Delta e_c$ the model takes into account both the decrease of $e_c$ and the corresponding increase of $e_{n_i}$ of the receiving cells. There can be between one and three receiving cells ($1 \leq N \leq 3$) and they are evaluated based on the slope gradients between the eight Moore neighboring cells and the overcritical cell. The neighboring cell with the highest slope angle identifies the main landslide direction, which means that the avalanche follows the steepest descendent gradient. Then, if the two neighboring cells located at the two sides of the main landslide direction have an altitude that is lower than the altitude of $c$, they are also considered to be receiving cells. If $N > 1$, $\Delta e_c$ is anisotropically discharged among the $n_i$ cells. In particular, the fraction $f_{n_i}$ ($0 \leq f_{n_i} \leq 1$) of $\Delta e_c$ that each of the cells $n_i$ receives is proportional to the values of the slope angle between $c$ and the cells $n_i$. If $N = 1$, $\Delta e_c$ is shifted in its entirety to the receiving cell in the direction of the maximum slope gradient (i.e., $f_{n_i} = 1$). Thus, both the landslide direction and the transfer of mass are constrained by the local topographic features of the surface. After perturbation, the threshold $\alpha_c$ of cell $c$ is restored to its initial value $\alpha_0$. The instability of a cell may cause the instability of the neighboring cells, thus allowing the landslide to propagate within the system. At each model step $t$ and for each cell $c$, the rules governing the dynamics of the model are summarized in Eqs. 1 and 2, which represent the driving rule and the transition rule, respectively.

$$\alpha_c(t) = \alpha_c(t-1) - w \qquad (1)$$

$$\text{if} \quad \beta_c(t) > \alpha_c(t) \rightarrow \begin{cases} e_c(t+1) = e_c(t) - \Delta e_c \\ e_{n_i}(t+1) = e_{n_i}(t) + f_{n_i} \cdot \Delta e_c \\ \alpha_c(t+1) = \alpha_0 \end{cases} \qquad (2)$$

In the model, landslides are considered instantaneous compared to the time scale of the overall evolution of the system. Thus, when the condition described in the transition rule (Eq. 2) is verified for at least one cell of the lattice (i.e. when there is at least one landslide in progress) the driving rule (Eq. 1) is no longer applied until all the cells become stable again.

Moreover, our model does not take into account a regenerating process such as uplift, since it is based on the assumption that the time scale at which the modeled landslides occur is much shorter than that of tectonic processes: the effect of these processes on the evolution of the system is negligible at the temporal scale considered and it does not significantly affect landslide dynamics.

2.2. Implementation of the model

The model was applied to the investigation of the frequency distribution of landslide areas. We used a series of values for the rate of weakening $w$. For each of these values we measured the areas of landslides that occurred over time windows $t_w$ defined as a number of model steps. The area of a landslide is calculated as the number of adjacent cells affected by instability during a single event. For each landslide area series we investigated the scaling properties of the resulting cumulative frequency distribution.

The choice of the values to be used for $w$ was constrained by the model outputs. In the next section it will be shown that in the model, landslide areas increase with $w$. Thus, the value of $w$ affects the sizes of the resulting landslides as well as the shape of the size frequency distribution. Accordingly, the model outputs drove the selection of the values of $w$ capable of representing the range of landslide sizes and the values of scaling exponents observed in the real world. In particular, we first tested a low value for $w$ ($w$ = 0.5). Then, we repeatedly ran the model by progressively increasing the value of $w$ by 0.5, until values were reached for which the behavior of the system was similar to real world observations. In the range of $w$ for which such similarity was observed, we reduced the distance between subsequent $w$ values to 0.25, to investigate the behavior of the system in more detail. The values tested for $w$ are 0.5, 1, 1.5, 2, 2.25, 2.5, 2.75.

As explained in Section 2.1, the weakening $w$ applied in the model through a decrease in the slope angle stability threshold is meant to correspond to the effect of rainfall or snowmelt events, which weaken the soil thus causing the instability of some sites of the system. In the real world, the rate of soil weakening depends both on the intensity of the triggering event and on the physical response of the soil (Iverson, 2000), which in turn depends on its physical properties. In our model we apply a constant rate of weakening in space and in time, which means to assume that the factors that create unstable conditions are constant in time, and that the only variable affecting the response of the system is topography, while all the other physical properties are homogeneous in space. Thus, a higher $w$ can be associated with a higher rainfall intensity or snowmelt rate, or more generally with a higher rate of increase of the resulting pore pressure, under the assumption of homogeneous soil properties.

To summarize, the way we implement the model allows us to study how landslide dynamics evolves when the system is subjected to a constant driving mechanism over time, with different predefined intensities.

The time windows $t_w$ used for the model consist of 1,000; 2,000; and 5,000 model steps. Accordingly, $t_w$ represents the sum of the “landsliding steps”, that is, the steps at which the instability is communicated from the unstable cells to their neighbors, and the “weakening steps”, that is, the steps at which the decrease of the slope stability threshold is applied. This implies that for a given time window $t_w$, the larger the areas of landslides of the resulting landslide series, the higher the number of landslide steps in the $t_w$-window, since the avalanche process involves a larger number of cells.

Figure 2 shows an example of stability conditions (Fig. 2a) and of the pattern of the slope stability threshold (Fig. 2b) of the examined topography, after 1,000 steps and for $w$ = 2. In Fig. 2a, yellow denotes the unstable cells at the 1,000$^{th}$ step of the model. In Fig. 2b we observe that under the effect of the driving rule (Eq.1, taking $w$ = 2), the slope threshold $\alpha_c$, which at time $t$ = 0 is uniform for all cells of the matrix (Eq.1, with $\alpha_c$ =75°; that is, $\tan\alpha_c$=3.7), has become strongly variable after 1,000 steps: its values vary from cell to cell, depending on the stability history of the cells during this time span.

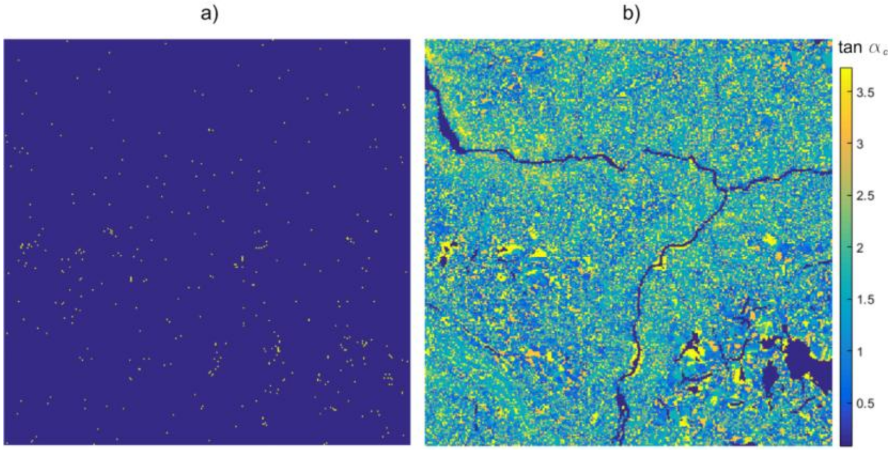


**Fig. 2** Stability conditions of the matrix, at the 1,000th step of the model. a) unstable cells (yellow) and stable cells (blue); b) Map of the tangent of the slope stability threshold $\alpha_c$.

## 3. Analysis of the probability of landslide areas obtained from the model

In this section, we first describe results obtained with all the rates of weakening ($w$) tested, and then compare these results with the real world observations in order to define the range of $w$-values capable of reproducing the behavior of real landslides.

For each number of iterations $t_w$ and for each $w$-value tested, the outputs from the model consist of a series of landslide areas $A_i$, expressed as a number of cells. These values were converted in in m$^2$ according to the resolution of the original DEM, in order to facilitate the comparison between the results obtained from the models and the behavior of real landslides.

Figure 3 shows how the mean area of landslides ($A_L$) of each landslide data series varies with the rate of weakening $w$ (Fig. 3a) and with the number of model steps $t_w$ (Fig. 3b). In both graphs we observe that the higher the value of $w$ the higher the mean area $A_L$. In particular, the two parameters are linked to each other by a linear equation (Fig. 3a). The increase of $A_L$ with $w$ is due to the spatial spread of instability, which increases with increasing rate of weakening. Indeed, according to the driving rule (Eq.1), a higher $w$ implies a faster decrease of the slope threshold $\alpha_c$ and thus a higher number of unstable cells with a higher probability to be in touch with each other. This results in larger landslide triggering areas, which consequently generate larger landslide bodies. Moreover, the wide spatial spread of instability can also cause the formation of coalescent landslides, which are identified in the model as a single landslide. Finally, a faster decrease of the slope threshold also implies that a larger mass must be lost from the unstable cell in order to restore equilibrium conditions. The increase of the landslide mass involved in the landslide process increases the probability for the neighboring cells that receive the mass to become in turn unstable and, as a result, landslide processes are more likely to generate large areas.

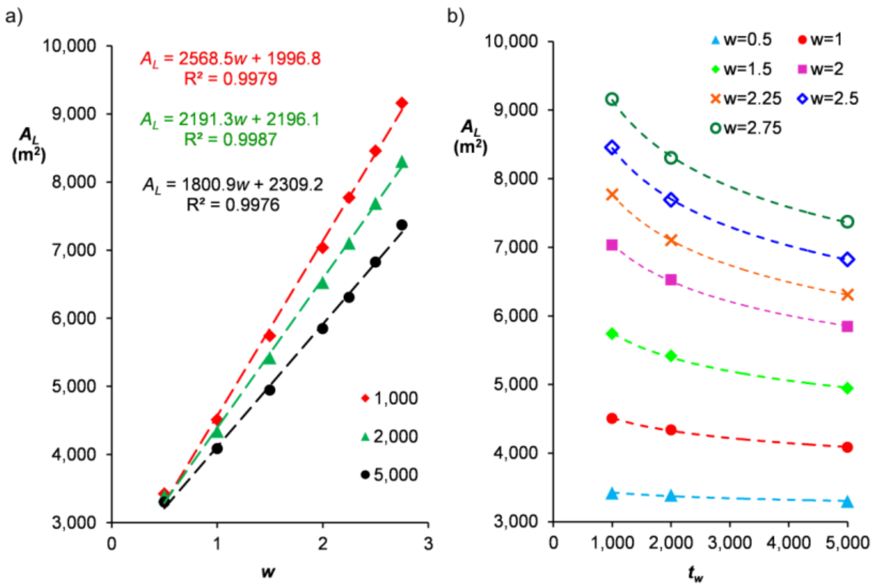


**Fig. 3** (a) For each number of model steps ($t_w$ = 1,000; 2,000; 5,000), mean area of landslides ($A_L$) of the respective landslide areas data series as a function of $w$, and the respective linear best fit. (b) For each $w$, $A_L$ as a function of $t_w$.

The slope of the linear best fit in Fig 3a decreases with increasing $t_w$, thus indicating that the largest landslides occur at the early stages of the evolution of the model, while the relative importance of smaller landslides in the data series increases with $t_w$, thus lowering the mean value of landslide areas $A_L$. This aspect of the behavior of the system is well depicted in Fig. 3b, where we observe that $A_L$ decreases with $t_w$, and that this decrease is higher for higher $w$. Since high values of $w$ lead to large landslide areas, we can hypothesize that like in real systems, relatively smaller topographic adjustments occur in response to large landslides, thus decreasing the value of $A_L$.

The complementary of the cumulative frequency distribution of landslide areas obtained from the model for each $w$ and $t_w$ tested, along with their scaling properties, are shown in Fig. 4.

Overall, landslide areas increase with increasing $w$ and vary from $2\times10^3$ to $2\times10^7$ $m^2$, which are values comparable with the range observed for real landslide areas (Pelletier et al., 1997; Guthrie and Evans, 2004; Malamud et al., 2004), although the highest order of magnitude represented in most real datasets is of $10^6$ $m^2$, while landslides obtained from the model reach $10^7$ $m^2$. Such large landslides are not often present in landslide inventories, since they require particular conditions in order to occur, that is, very high slope gradients like those observed in deeply incised river valley, and high-intensity rainfall events (Korup et al., 2007). Moreover, particular structural settings may favor the instability of large slope portions. In terms of slope gradients and rainfall intensity, these conditions match those of the system modeled. Indeed, the river valleys are up to 70° steep, and landslide areas with a magnitude of $10^7$ $m^2$ are obtained when the highest values for the rate of weakening are applied (w=2.5 and w=2.75), which according to the interpretation given in Section 2.2, correspond to the highest intensities of the triggering event. Moreover, as explained above, coalescent landslides are identified in the model as a single landslide, thus leading to larger areas.

The graphs in Fig. 4 show that the right tails of the frequency distributions of landslide areas always follow a power law trend (R > 0.99) (Eq.3).

$$N \propto A^{-(D-1)} \quad (3)$$

In Eq. 3, $N$ is the number of landslides with area greater than or equal to $A$, and $D$ is the scaling exponent.

The scaling exponents $D$ range from 2.67 to 5.75, with uncertainty intervals at the 95% confidence level between 0.07 and 0.19. Overall, scaling behavior is observed in ranges of landslide areas from 0.6 orders of magnitude (Figs.4d and 4f: series obtained at 1,000 model steps) to 2 orders of magnitude (Figs.4b and 4c: series obtained at 2,000 and 1,000 model steps, respectively). Later in this section we will show that only some of the *D*-values obtained are in the range detected for real landslides.

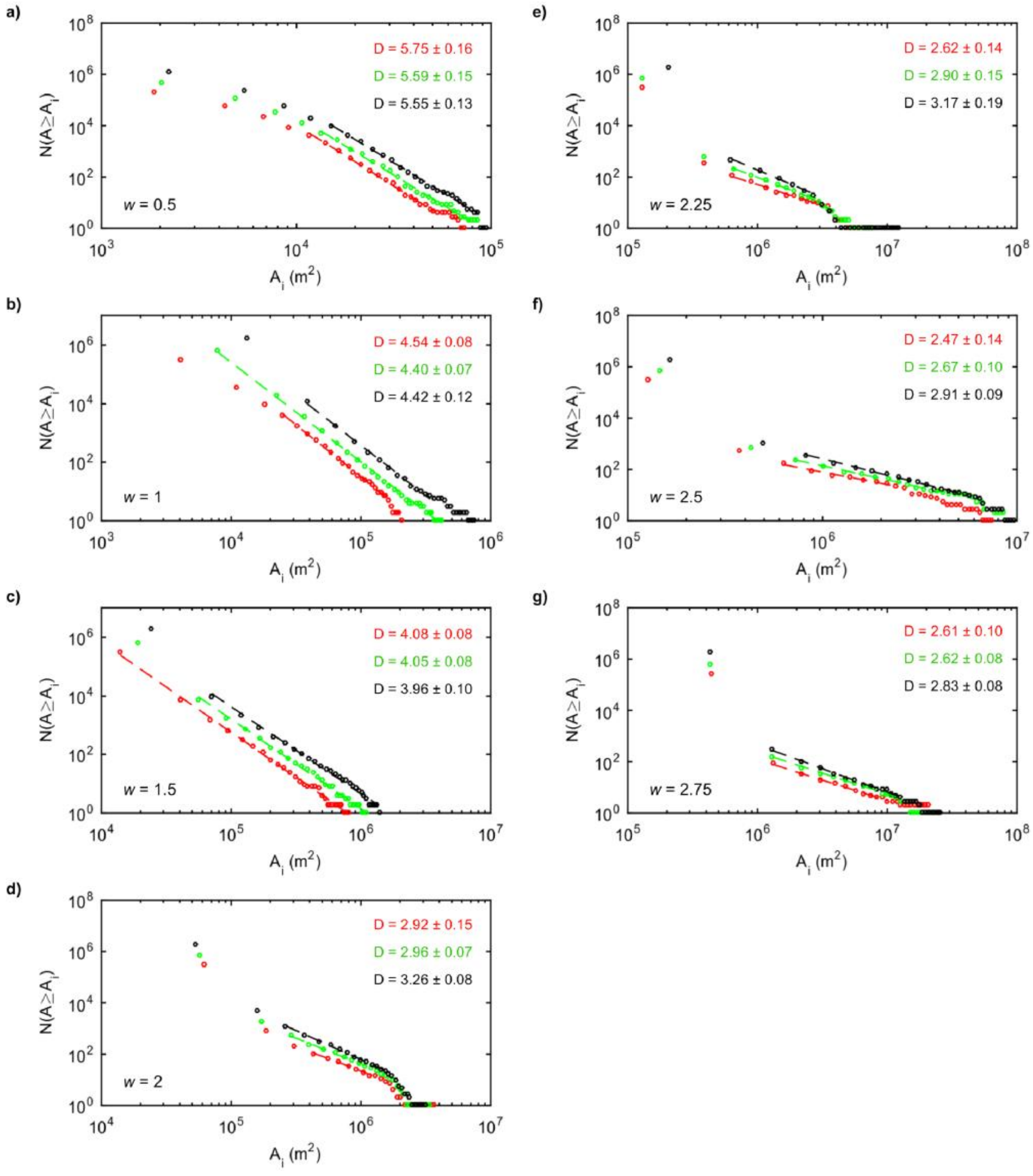


**Fig. 4** Complementary of the cumulative frequency distributions (*CFDs*) of landslide areas ($A_i$ in m$^2$) obtained with a) $w$ = 0.5, b) $w$ = 1, c) $w$ =1.5, d) $w$ = 2, e) $w$ = 2.25, f) $w$ = 2.5, g) $w$ = 2.75, for different time spans (1,000 model steps in red, 2,000 in green, and 5,000 in black). The dotted lines indicate the portions of the *CFD*s taken in consideration for the identification of the power law (dotted lines). For each power law the respective scaling exponent $D$ is shown.

A flattening of the frequency distributions is observed when landslide areas are lower than $10^4$ $m^2$ (Figs.4a and 4b), thus indicating that small landslides are less frequent than predicted by the power law. A deviation from the power law at the smallest landslide sizes is also recognized in the *CFD*s obtained from real datasets. However, in the real world small landslides show a specific statistical behavior that is not observed in our *CFD*s: when non-cumulative frequency distributions are used, the interval corresponding to the smallest landslide areas is characterized by an opposite trend, with positive slope, followed by a rollover above which landslide areas start following the power law (Guzzetti et al., 2002; Guthrie and Evans, 2004; Malamud et al., 2004). Such a rollover is not present in the outcomes of this model: non-cumulative frequency distributions calculated for the same landslide data series for which the cumulative distributions are shown in Fig. 4a and 4b, exhibit a flattening rather than a rollover for the smallest sizes of landslide areas. As explained in Section 1, the rollover in real landslide inventories may be associated with a range of explanations, such as an underestimation of small landslides (Stark and Hovious, 2001; Brardinoni and Church, 2004), and the physics of processes controlling the occurrence of small landslides (Stark and Guzzetti, 2009, Milledge et al., 2014). In this regard, our model does not consider the physical parameters and processes invoked to explain the frequency distribution of small landslides, and it cannot be affected by the resolution of the data sources of the landslide inventory either. This could explain why the *CFD*s obtained do not exhibit a rollover. In our model, the only variable affecting landslide areas is the topography. Thus, the flattening that we observe for these series at the smallest landslide areas is expected to be related to the constraints represented by the topographic surface.

The first part of the frequency distributions obtained with *w* from 2 to 2.75 (Figs. from 4d to 4g) exhibits a behavior that it is not the same with the one from real landslide inventories. In particular, although the smallest sizes of these series are in a range at which scaling behavior is observed in nature, in this part of the *CFD* the number of the modeled landslides is higher than that predicted by the power law. The difference can again be related to the fact that the only constraint to model dynamics is represented by topography: as we deduced from Fig. 3, topographic adjustments occur in response to the large landslides caused by high rates of weakening, thus leading to a high number of slope failures with smaller area.

While model choices affect the first part of the area-frequency distributions, results indicate that the model is capable of reproducing the scaling properties of real landslides, when specific values for the parameters of the model are used. The values of $D$ were compared to those observed for real landslide inventories by taking as a reference the work by Van Den Eeckhaut et al. (2007), which provides an overview of the values of $D$ observed for about thirty landslide inventories around the world, published in twenty-seven papers (please refer to Van Den Eeckhaut et al. (2007) for the related bibliography). According to this paper, for real landslide inventories the values of $D$ range between 1.42 and 3.36, with many of them around 2.5. The landslide inventories considered are both historical and post-event. Since like most CA models, the one presented in this paper does not have a timescale, for the comparison of the model outputs with reality we preferred not to refer to a specific type of inventory, but rather to include both post-event inventories and historical ones, also considering that the main difference between historical and post-event inventories is observed in the frequency distribution of small landslides, which is not the focus of this study, while in the portion of the frequency distribution that exhibits power law scaling, the scaling exponent does not show any specific behavior for the two types of datasets.

The comparison indicates that the power law decay of the modeled landslide areas is in accordance with that of real landslide inventories for rates of weakening between 2 and 2.75 (Figs. from 4d to 4g). Indeed, in this range of $w$ the exponents are comprised between 2.47 and 3.26, while for lower values of $w$ the exponent is too high compared to real values, thus indicating an underestimation of large landslides and suggesting that although power law behavior is observed for all the $w$ applied, only the highest rates of weakening among those tested are capable of reproducing the action exerted by real landslide triggering events. The histogram in Fig. 5 shows the values of the $D$-exponent in literature. The $D$ classes are 0.3 wide and the values in the x-axis represent the middle value of each class. Most of the real observations are in the $D$ class from 2.4 to 2.6. In Fig. 5, the arrow delimitates the range of $D$-exponents observed for the landslide series obtained from the model, with rates of weakening $w$ between 2 and 2.75. The comparison with literature shows that in this range of $w$-values, the scaling behavior of landslide areas is well reproduced by the model: the scaling exponents of the modeled landslide series range from 2.5 to 3.2.

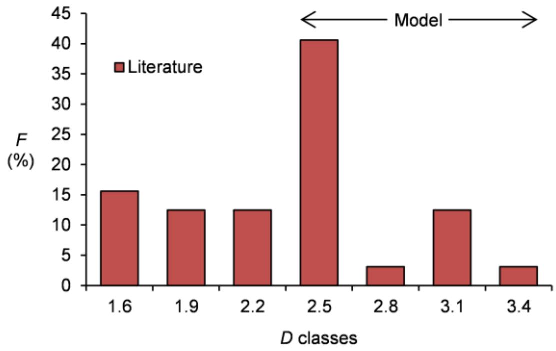


**Fig. 5** Comparison of the percentage frequency (*F*) of the values of *D* observed within each *D* class, in literature (Tab. 1 in Van Den Eeckhaut et al. (2007)) and for the landslide data series obtained with *w* from 2 to 2.75. The *D* classes are 0.3 wide.

In the next section we will show that the shape of the frequency distributions is not affected by the resolution of the DEM used, at least for the resolutions tested. This means that although the results presented in Fig. 4 correspond to landslide areas expressed in $m^2$ (based on the resolution of the original DEM of 25x25 m), the represented constraints exercised by topography on the landslide probability should correspond to a wider range of landslide areas than the one represented in the figure.

We studied the way the scaling exponents depend on (*i*) the rate of weakening *w* and (*ii*) time $t_w$. For this analysis, all the values of *w* were used, although only those higher than or equal to 2 lead to scaling exponents similar to the real ones (as shown above). This allows us to better explore the behavior of the system, which according to the results obtained and shown below and in the next sections, may be described by mathematical rules that can be fitted to the whole range of rates of weakening *w* tested. Graphs a, b, and c in Fig. 6 show that for each $t_w$, *D* linearly decreases with an increasing rate of weakening *w* ($R^2 > 0.98$), thus indicating that the faster the system is driven to instability the higher becomes the probability of large landslides. The decrease is described by:

$$D = -m_D \cdot w + c_D \qquad (4)$$

where $c_D$ is a constant.

This result indicates that a possible cause affecting the probability of occurrence of real landslide sizes is the rate at which the system is driven to instability, such as the rainfall intensity for rainfall triggered landslides. Fig. 6d indicates that when the rate of weakening *w* is lower than or equal to 1.5, *D* does not significantly change over time. Conversely, for higher $w$, $D$ slowly increases with $t_w$. However, the change of $D$ over time is much lower than that produced by the rate of weakening: for $t_w$ equal to 5,000 model steps, the maximum temporal change of $D$ is of 0.4 (Fig. 6d), while in the same time window, the change of $D$ with $w$ is of about 2.7. This result will be discussed in section 7.

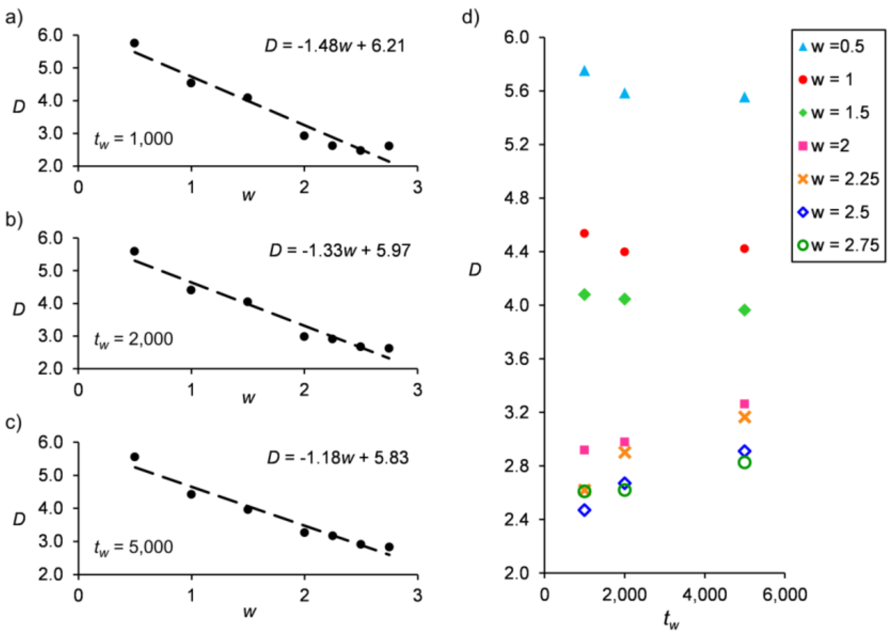


**Fig. 6** (a, b, c) For each $t_w$ (1,000; 2,000; 5,000 model steps), $D$ as a function of the rate of weakening $w$, and the respective linear best fit. (d) For each $w$, $D$ as a function of $t_w$.

## 4. Investigation of the effect of model choices and computational techniques

The model is based on a lattice of 320×320 cells, and the DEM used to define the altitude values of cells has a resolution of 25×25 meters, thus implying that the smallest possible landslide in the model is of 625 m$^2$ (i.e, when the instability involves only one cell). We investigated the ways in which these choices affect the landslide area distribution, by keeping the same area as the initial surface for the model, but changing the DEM resolution to 10×10 meters (the DEM was built by Tarquini et al., 2007, 2012). Accordingly, the resulting lattice has a size of 800×800 cells and the smallest possible landslide area is of 100 m$^2$. We used a low ($w$=1) and a high value ($w$=2.75) among the rates of weakening $w$ applied in the model~~: 1 and 2.75~~ (1,000 model steps were used for this comparison) and obtained similar results for both of them. ~~Results~~ The outcomes of the model for $w$=2.75 are shown in Fig. 7.

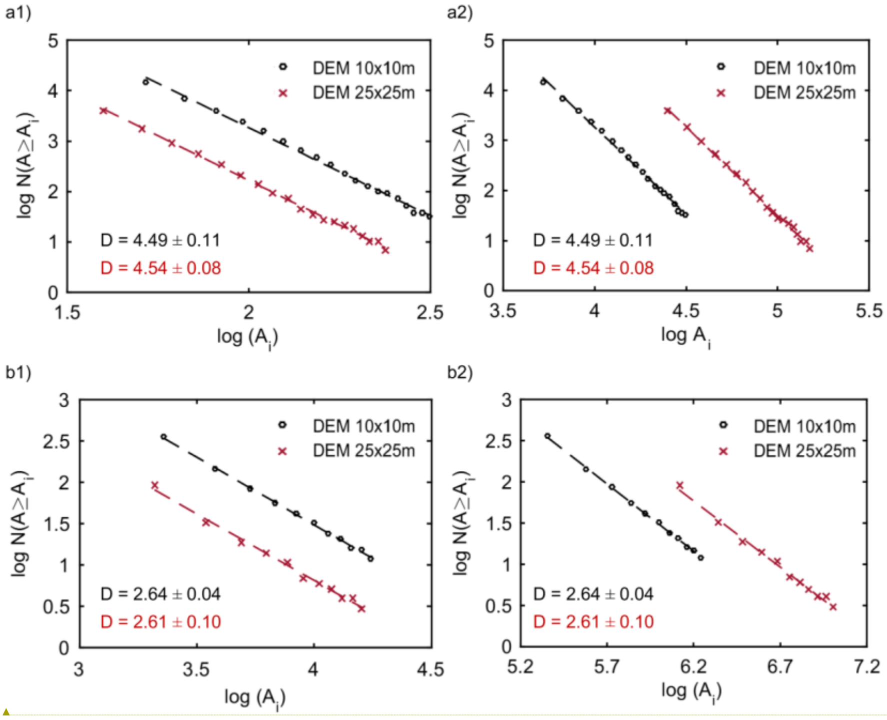


Formatted: Font: (Default) Times New Roman

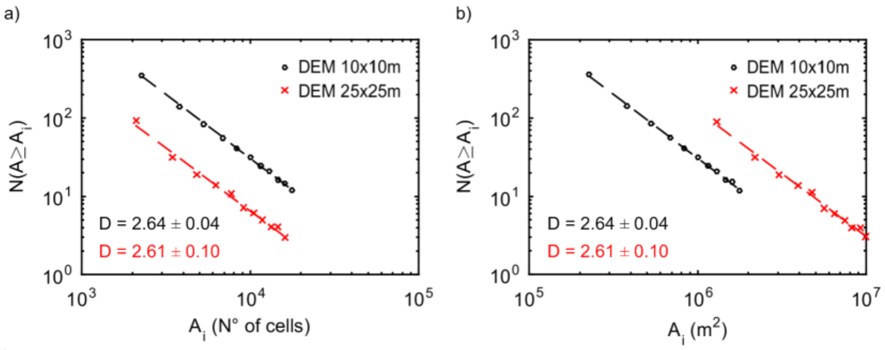


Formatted: Font: (Default) Times New Roman

**Fig. 7** Portions of the cumulative frequency distributions (*CFD*) of landslide areas ($A_i$) that can be described by power laws (dotted lines) and their respective scaling exponents (*D*), for the series of $A_i$ obtained with a DEM of 25×25 m (lattice size of 320×320 cells) and with a DEM of 10×10 m (lattice size of 800×800 cells) ($t_w$=1,000;), with a rate~~s~~ of weakening of ~~(a) *w* = 1 and (b)~~ *w* = 2.75: a~~1 and b1~~) $A_i$ values as number of cells; ~~a2 and~~ b~~2~~) $A_i$ values in m$^2$.

~~Graphs~~Figure 7a)~~1 and b1~~ shows the power law fit of the *CFD* of landslide areas, with the latter expressed as a number of cells, that is, without converting these values in m$^2$. ~~For both *w* = 1 (Fig. 7a1) and *w* = 2 (Fig. 7b1), t~~The range of landslide areas obtained from the model is about the same for the two DEMs used, while the number of landslides is higher for the DEM of 10×10m. The scaling exponents *D* of the power laws observed for the two DEMs are very similar, as well as their scaling ranges. This result shows that while the size of the lattice affects, as expected, the number of landslides (the higher the model size, the higher the number of cells available to become unstable, and the higher the number of landslides), it does not affect the shape of the distribution and the dynamics of the system. The same applies to the resolution of the original DEM, which according to the results obtained does not produce any significant effect on the value of the scaling exponent, for the two resolutions tested. This result suggests that the control of topography on the size frequency distribution of the modeled landslides is the same at the two scales of analyses used, and this may be explained by the scale-invariant character of topography (Frattini and Crosta, 2013). Accordingly, after converting landslide areas from number of cells to $m^2$ (Fig~~s~~. 7b~~1 and 7b2~~) the only effect is a shift of the power laws along the x-axis. As a result, while the range of the scaling regimes for the landslide series obtained from the two DEMs are different, the values of their exponents do not change. This also indicates that~~, for example (Fig. 7b2)~~ a *D*-value of about 2.6 characterizes the scaling behavior of landslide areas in a range from about $2{\times}10^5$ to $10^7$ (~~i.e, from 5.3 to 7 in terms of logarithms of landslide areas~~Fig. 7b), considering the scaling ranges observed for both the DEMs.

These outcomes also suggest that the fact that the model does not accurately represent the first part of the frequency distribution of real landslides (Section 3) is not due to the scale of analysis but rather, as hypothesized in the previous section, due to the choice of topography as the main way of describing the spatial variability of the system.

## 5. Changes of the topographic surface modeled

The initial topographic surface is subjected to changes caused by the mass distribution occurring during the time window $t_w$. In the present section we investigate these changes focusing on different morphometric and geomorphological features of the landscape. We must remember that according to the dynamics of the model, these changes represent the evolution of an area only subjected to the action of the gravitational process and whose variability is only represented by topography.

### 5.1 Topographic attributes

Fig. 8 shows the difference in altitude between the final surface obtained at $t_w$ = 5,000 steps, and the initial one, for $w$ equal to 1, 2 and 2.75, respectively. The difference is expressed in meters, according to the altitude values of the original DEM. Red zones indicate a decrease in altitude (areas affected by erosion), while blue zones indicate an increase in altitude (areas affected by deposition). When $w$ grows from 1 (Fig. 8a) to 2.75 (Fig. 8c), the difference in altitude increases. This is due to the observed property of the frequency distribution of landslides, which indicates that for the same $t_w$ the number of large landslides increases with increasing rate of weakening. Consequently, the higher $w$ the larger the change of the surface configuration.

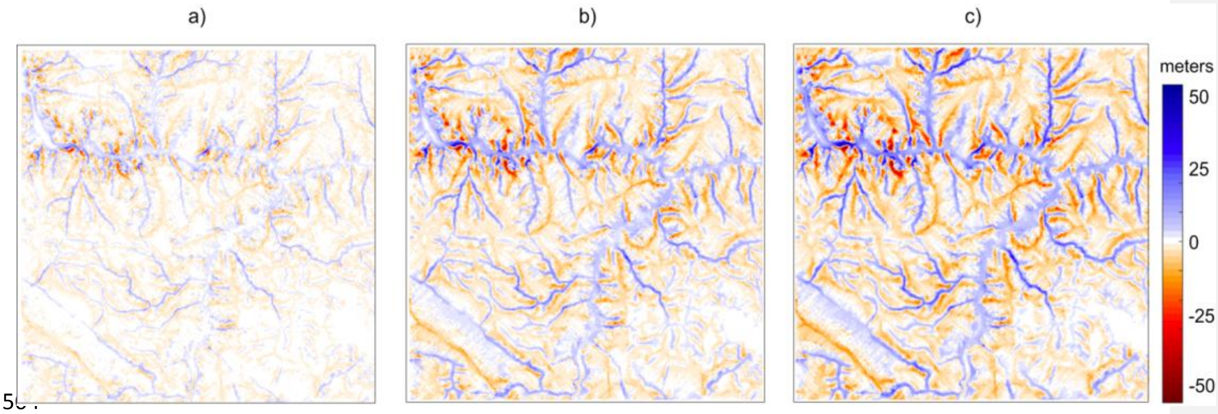


**Fig. 8** Difference in altitude between the final surface obtained at $t_w$ equal to 5,000, and the initial one. a) $w$=1; b) $w$=2; c) $w$=2.75.

In order to highlight the variation of specific topographic attributes a cross-section through the surface is made (Fig. 1). The section is traced so as to cross the main ridges and valleys to highlight the evolution of the slopes. Fig. 9 shows how specific topographic attributes change along the cross-section after an interval $t_w$ equal to 5,000 model steps and with $w$ = 2.75, i.e. the situation in which we observed the more pronounced topographic changes. Fig. 9a displays the initial and the final topographic profiles. The comparison of the two profiles indicates that landslides that occurred over the time interval $t_w$ cause a decrease of the altitude of mountain ridges and the filling of valleys, thus producing a smoothing of the relief. ~~The stronger smoothing occurs where the altitude difference between the top and the bottom of the slope is lower, thus suggesting that where the slope length is short, the material transfer due to landslides is more effective in changing the~~

~~topographic geometry.~~ Fig. 9b shows the initial and the final profile curvature ($P_c$) of the topographic surface (Moore et al., 1991), which describes the curvature of the surface along the direction of the steepest gradient. ~~We chose this secondary attribute among those that may describe a topographic surface (e.g., slope angle, planar curvature, aspect, roughness) because when a landslide occurs the geomorphic evidence consists of a concave profile curvature between the crown and the main scarp and a convex profile curvature between the foot and the toe of the mass involved.~~

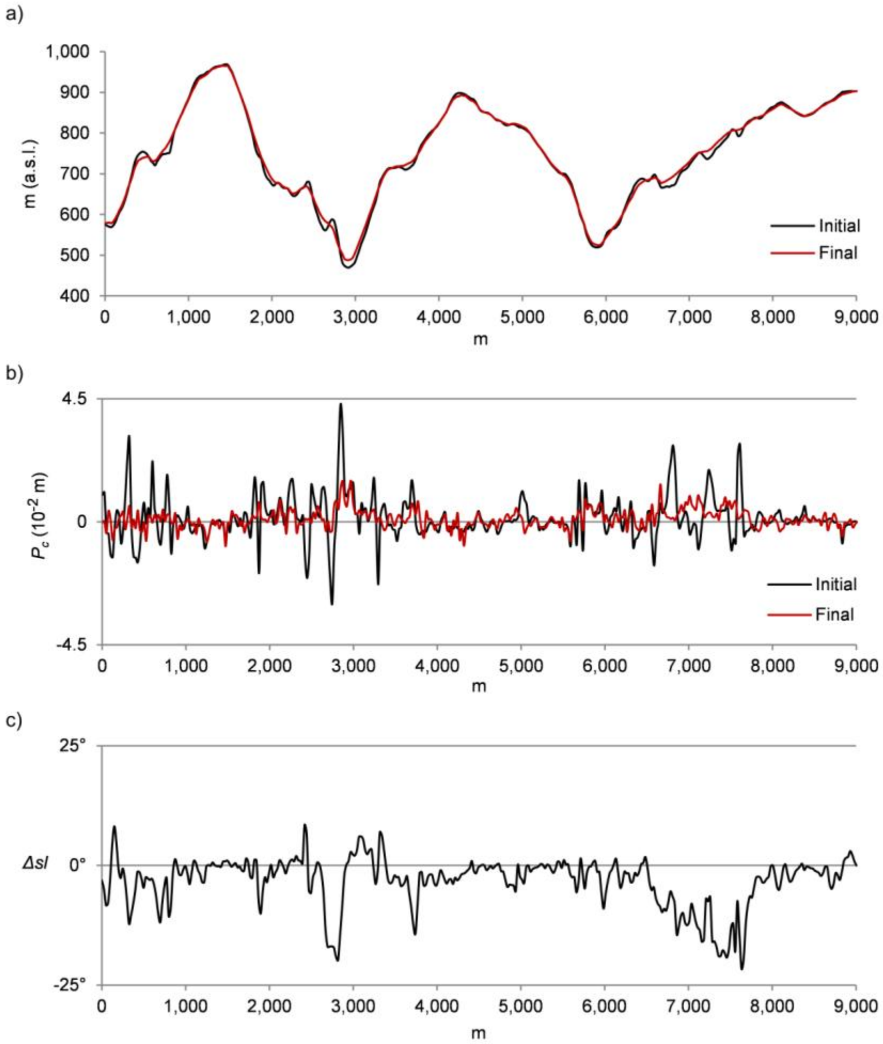


**Fig. 9** Change of topographic attributes along the cross-section made in Fig. 1. The change is evaluated between the initial topographic surface and the final one, obtained at $t_w$ = 5,000 and with $w$ = 1.5. a) Altitude; b) Profile curvature ($P_c$) in $10^{-2}$ m; c) Difference $\Delta sl$ between the initial and final slope angle (in degrees).

The curvatures were calculated using the algorithm in Spatial Analyst (ArcGIS10.0 © Esri), and are expressed in $10^{-2}$ m. Positive $P_c$ values indicate concave curvatures, while negative values indicate convex ones. In the graph we observe that the $P_c$ values of the final surface are closer to zero than those of the initial one, thus describing a decrease of both the convex and the concave curvature. Moreover, in the profile of the final curvature a general trend can be recognized, which consists in the shifting of the peaks corresponding to the maximum values of curvature toward lower values of linear distance (x-axis), compared to the peaks of the initial curvature profile. This could be due to a slope decline evolution, where the decrease of the slope angle is associated with a lateral movement of ridges and valley axes.

Fig. 9c displays the variation of the slope angle ($\Delta sl$) of the surface, calculated as the difference between the final and the initial slope. Overall, a decrease of the slope angle is observed, up to a maximum of about 21°. However, some exceptions can be noticed. A positive $\Delta sl$ corresponds to the medium and lower slope portions, where the moved mass increases ~~the curvature and consequently~~ the slope angle.

~~Overall, t~~These results are in agreement with real-world observations, where landslides dampen local relief removing mass from upper slopes and depositing it on lower slopes, thus producing a decrease of mean slope relief and relief variability, of slope angles and of their standard deviation (Korup, 2006; Korup et al., 2010). A more in-depth analysis of the change of the slope angles undergone by the relief will be addressed in Section 5.2. The evolution of the surface modeled also highlights that although the rules of the model apply to all cells of the lattice without discriminating between scar area, runout area and depositional area of landslides, this differentiation is intrinsically produced by the model. Indeed, the areas where we observe erosion represent the scar areas where landslides are triggered, i.e. where the instability is generated. These areas are located in the upper slope zones, which in real active mountain belts are the areas dominated by landslide erosion (Montgomery and Brandon, 2002; Korup et al., 2007). For the middle slopes we did not observe any significant change in altitude. Thus, they represent the runout areas of landslides where, in terms of the cells of the lattice, the instability is transferred from one cell to another but not generated. Finally, an increase in altitude is observed in the lower slopes overlooking the toe of slopes, which thus represent the depositional areas affected by the accumulation of landslide bodies.

### 5.2 Statistical properties of the slope angles

The topographic changes are driven by the dynamics of the model, which are controlled by the slope angles $\beta$ of the area. In Fig. 9c we observed that like other topographic attributes, slope angles also change over time. We thus investigated the temporal evolution of the slope angles and their possible dependence on the rate with which the system is driven to instability, in order to compare the behavior of the surface with the one observed for the scaling exponents of the frequency distribution of landslide sizes.

For each rate of weakening $w$ and number of model steps $t_w$ (i.e., 1,000; 2,000; 5,000) we calculated the respective frequency distribution of $\beta$ of the initial and the final topographic surface. Fig. 10 shows the non-cumulative (Fig. 10a) and the cumulative (Fig. 10b) distributions of $\beta$ for the initial surface and for those obtained with the maximum $t_w$, equal to 5,000 model steps. For clarity, in Fig. 10a only the frequency distributions corresponding to $w$ = 1, 2.5 and 2.75 are shown, since they offer a good description of the behavior of slope angles with increasing $w$.

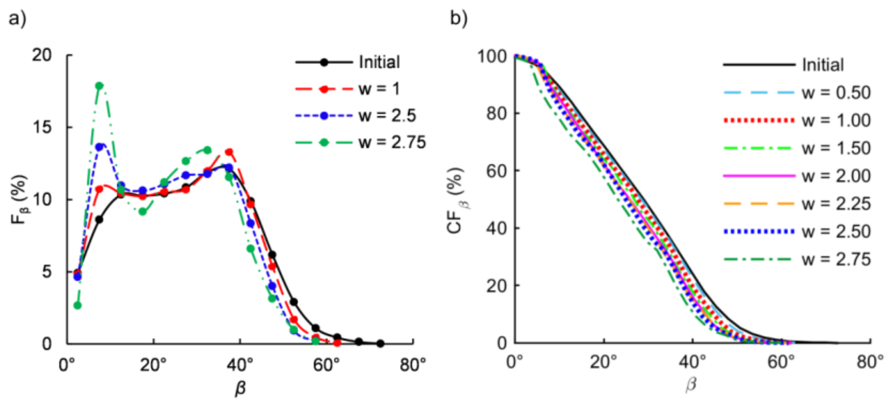


**Fig. 10** Non-cumulative (a) and cumulative (b) frequency distributions of the slope angle $\beta$ for the initial topographic surface and for those obtained at the maximum $t_w$, equal to 5,000 model steps, with $w$ = 1, 2.5, 2.75, in graph (a), and with all the $w$ applied in graph (b).

The initial frequency distribution of $\beta$ (black symbols in Fig. 10a) is representative of the topographic setting of the area, which is characterized by steep river valleys and flat surfaces at the top of the slopes. Because of this, in the slope angle series the intermediate classes ~~(between 12° and 37°)~~ are less represented than they would be in a Gaussian distribution, in favor of the frequency of classes corresponding to low and high slope angles. Landslide occurrence changes the shape of the curve. In comparison with the initial frequency distribution, for each $w$ tested we observe a decrease of the frequency of the angles higher than about 40° and an increase of those lower than about 13° (Fig. 10a). Moreover, landslide processes emphasize the bimodal character of the initial topographic setting~~, and this is particularly evident at the highest rate of weakening applied (w = 2.75, green series in Fig. 10a)~~. The smoothing produced on the surfaces by landslides is still more evident in the cumulative frequency distributions ($CF_\beta$), where we observe that for each $w$ the curve is shifted toward lower values of $\beta$. In order to quantify these changes, we calculated for each frequency distribution (thus considering all the $t_w$ and not just $t_w$=5,000) the following statistical parameters: maximum ($\beta_{max}$), mean ($\bar{\beta}$), standard deviation ($\sigma_\beta$), kurtosis ($k_\beta$), skewness ($sk_\beta$). Figure 11 shows the change of each statistical parameter in time. Also in this case, only results corresponding to some $w$ are displayed ($w$ = 1, 2 and 2.75), for clarity purposes.

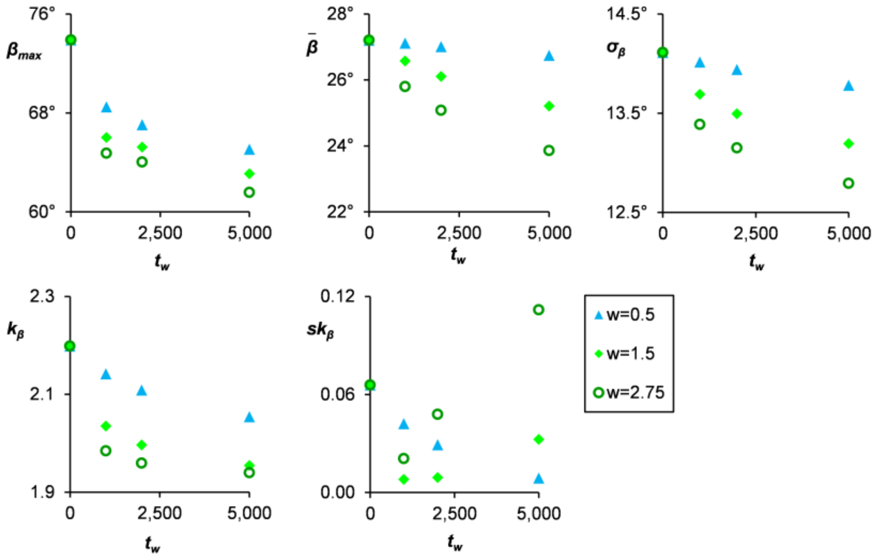


**Fig. 11** Temporal change of the statistical parameters of the slope angle frequency distribution, for $w$ = 0.5, 1.5, 2.75; $t_w$, number of model steps; $\beta_{max}$, maximum; $\bar{\beta}$, mean; $\sigma_\beta$, standard deviation; $k_\beta$, kurtosis; $sk_\beta$, skewness.

The overall temporal behavior of these parameters consists of a decrease of their value over time, although exceptions and some differences in the way these values decrease can be observed. The values of $\bar{\beta}$ and $\sigma_\beta$ ~~show a similar trend described by a linear~~ decrease ~~of their value~~ with increasing $t_w$~~. T~~ and this decrease is ~~steeper~~higher when the weakening is stronger. The parameter $\beta_{max}$ quickly decreases in the beginning (i.e., from t=0 to t=1,000) and then the decrease slows down. A similar behavior is observed for $k_\beta$, which is a measure of the peakedness or flattening of the distribution, when compared to a normal distribution. ~~The positive values of $k_\beta$ indicate a leptokurtic distribution – that is, a distribution with a higher weight of tails compared to a Gaussian distribution. Overall, also for this parameter the higher $t_w$ the lower the decrease of its value. The decrease indicates that the weight of the tails decreases and this can be observed in Fig. 10a, for the right tail.~~ A particular behavior is observed for $sk_\beta$~~: one can notice a slight asymmetry of the distribution~~, which quantifies the asymmetry of the distribution~~;~~. I~~i~~ts temporal evolution depends on $w$~~. F~~: for $w$ equal to 0.5, the parameter decreases over time, while for $w$ values of 1.5 and 2.75 there is an initial decrease followed by an increase of the value. This increase is due to the fact that ~~We interpret this difference as follows:~~ the change in topography takes place at a faster rate for higher $w$-values~~, while the decreasing trend of $sk_\beta$ for $w$ = 0.5 may be due to the fact that the system cannot manifest over the maximum $t_w$ of 5,000 model steps the increasing trend observed for the other values of $w$~~. Accordingly, ~~to this hypothesis~~ and in agreement with Fig. 10a, the initial decrease of the asymmetry is due to the difference between the decrease of the frequency of high $\beta$ values and the increase of the frequency of low $\beta$ values, while the subsequent increase of the asymmetry is mainly due to the increase of the relative importance of the lower $\beta$, over time. ~~The values of $\bar{\beta}$ and $\sigma_\beta$ show a similar trend described by a linear decrease of their value with increasing $t_w$. This decrease is steeper when the weakening is stronger.~~

The values of the statistical parameters of slope angles of the final topography also depend on the rate of weakening. In particular, we have found that $\bar{\beta}$ and $\sigma_\beta$ are linearly linked with $w$ according to the following equations:

$$\bar{\beta} = -m_{\bar{\beta}} \cdot w + c_{\bar{\beta}} \qquad (5)$$

$$\sigma_\beta = -m_\sigma \cdot w + c_\sigma \qquad (6)$$

where $m_{\bar{\beta}}$ and $m_\sigma$ are the angular coefficients of the best fit lines and $c_{\bar{\beta}}$ and $c_\sigma$ are constants, which depend on $t_w$ ($R^2 \cong 0.99$ for $\bar{\beta} = f(w)$ and $R^2 \geq 0.97$ for $\sigma_\beta = f(w)$). The relationships are illustrated in Fig. 12. According to Eqs. 5 and 6, the higher the rate of weakening the lower the values of $\bar{\beta}$ and $\sigma_\beta$ of the final surface - that is, the higher the change of the topographic surface caused by landslides.

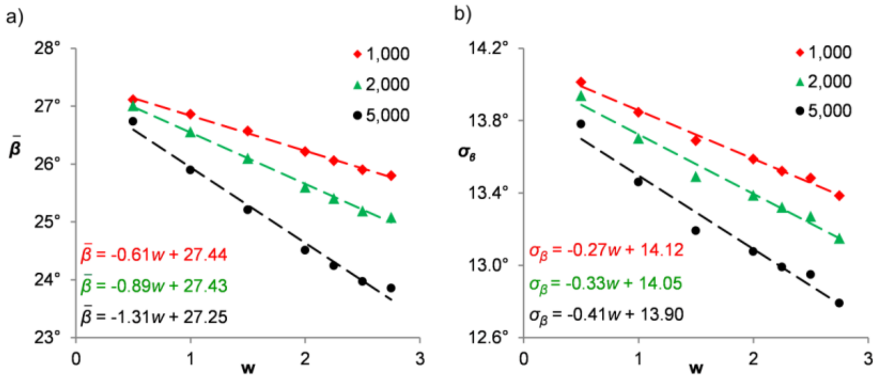


**Fig. 12** For each $t_w$ (1,000; 2,000; 5,000 model steps), (a) mean $\bar{\beta}$ and (b) standard deviation $\sigma_\beta$ of slope angles as a function of the rate of weakening *w*, and their respective linear best fit lines.

## 6. Relation between topographic changes and scaling properties of landslide sizes

In this section the relationship between topographic changes and the statistical behavior of landslide sizes is investigated.

We observed that landslide phenomena produce a smoothing of the topographic surface, which results in a decrease of the main statistical parameters of the frequency distribution of $\beta$, in time (Fig. 11). Unlike $\beta$, the scaling exponent *D* of the frequency distribution of landslide does not show any specific trend over time (Fig. 6d). Thus, the probability of landslide sizes and the changes undergone by the topographic surface exhibit different types of behavior over time. Instead, we observed that they manifest similar dependence on the rate of weakening *w*. In particular, we found that the scaling exponent *D*, the mean $\bar{\beta}$ and the standard deviation $\sigma_\beta$ of slope angles linearly decrease with increasing *w* (Figs. 6a, 6b, 6c and 12). Thus, by substituting in turn Eqs. 5 and 6 in Eq. 4 we obtain:

$$D = m_1 \cdot \bar{\beta} + c_1 \qquad (7)$$

$$D = m_2 \cdot \sigma_\beta + c_2 \qquad (8)$$

where $m_1 = m_D/m_{\bar{\beta}}$ and $m_2 = m_D/m_\sigma$ are the angular coefficients of the best fit lines, and $c_1$ and $c_2$ are constants. Figure~~.~~ 13 shows the same result obtained by plotting, for each *t*, *D* as a function of $\bar{\beta}$ (Fig. 13a) and $\sigma_\beta$ (Fig. 13b) obtained for the same $w$. The best fit lines have $R^2 \geq 0.95$ and $R^2 \geq 0.94$, in Fig.13a and 13b, respectively.

This result indicates that at each time span $t_w$, the scaling exponent $D$ that characterizes the probability of landslide sizes is linearly related, with a good approximation, to the values of the statistical parameters of the slope angles of the topographic surface where landslides occurred. In particular, the positive correlation of $D$ with $\bar{\beta}$ and $\sigma_\beta$ respectively, shows that an increase of $w$ (i.e., moving from the right extreme of the linear best fits to the left in Fig. 13) produces a decrease of $D$ and thus an increase of the probability of large landslide sizes, which is linearly related to the decrease of the mean and standard deviation of the slope angles of the final surface. In other words, the statistical parameters of the modeled topography preserve information about the probability of landslide sizes that occurred during a specific $t_w$ and under the action of a specific $w$.

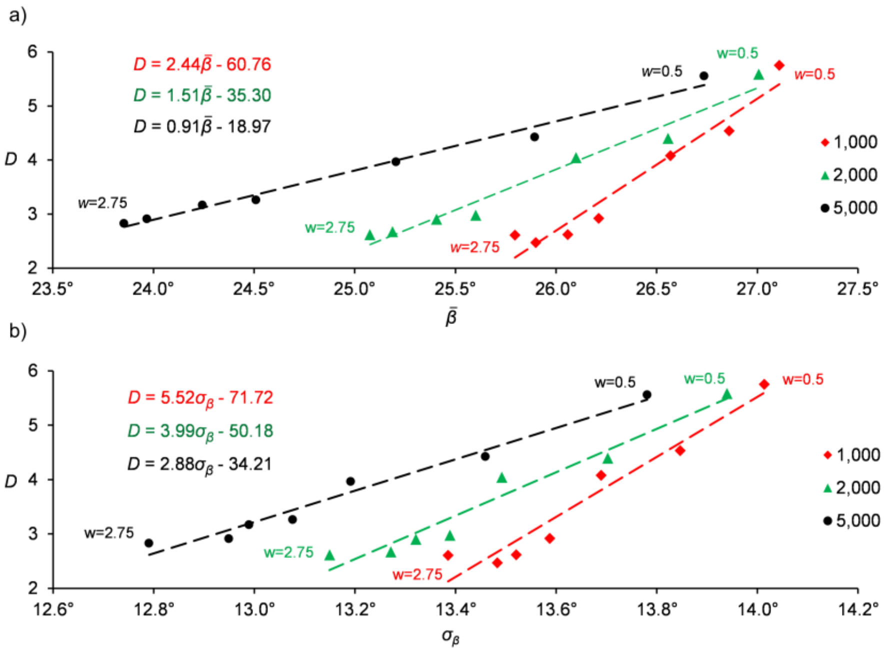


**Fig. 13** For each $t_w$ (1,000; 2,000; 5,000 model steps), $D$ as a function of (a) the mean $\bar{\beta}$ and (b) the standard deviation $\sigma_\beta$ of slope angles of the topographic surface, and their respective linear best fit. For each point, $w$ indicates the value of the rate of weakening at which $D$, $\bar{\beta}$ and $\sigma_\beta$ were obtained.

~~Although we observed that the way the system reacts in terms of landslide sizes and topographic changes depends on the way it is driven to instability (i.e. the configuration of the system changes as a function of the~~

~~external forces acting on it), t~~The Eqs. 4 to 8 indicate that the way the values of $D$, $\bar{\beta}$ and $\sigma_\beta$ change with $w$ may be described by linear mathematical laws, which respectively work for all the time spans $t_w$ tested and for which only the value of the linear fit parameters of the equation (slope and intercept) are different for the different $t_w$. Both in Figs. 13a and 13b we observe that going from $t_w = 1{,}000$ to $t_w = 5{,}000$ the steepness of the best fit lines decreases; that is, the angular coefficients $m_1$ and $m_2$ of Eqs. 7 and 8 decrease over time. This result indicates that the way $D$ is linked to the topographic change depends on the time span. In the next section we discuss outcomes, implications and limitations of the results obtained, including time-related aspects.

## 7. Discussion

The frequency distribution of landslide sizes characterizes the probability of landslide of a given magnitude. A property of this distribution identified in many landslide datasets around the world is the characteristic power-law decay of the frequency from medium to large sizes. Although small slope failures are the most frequent ones in landslide datasets, larger landslides represent the main hazard in terms of associated risk.

Despite its simple structure, the cellular automata model proposed in this paper has shown to be capable of reproducing key features of landslide processes related to the occurrence of medium to large slope failures. First, the distribution of landslide areas exhibits the typical scaling properties of real landslides, and a good agreement is observed for the values of the scaling exponents when a specific range of values is used for the parameters of the model. Given that in the model the topographic variability is the only component affecting the evolution of the system, this result suggests that the scaling properties of medium to large landslides could actually arise due to topography, thus supporting the conclusions of Frattini and Crosta (2013), who hypothesized that the scaling behavior of landslide sizes could find an explanation in the scaling properties of topography. Furthermore, the comparison of the frequency distributions of landslide areas obtained by using DEMs with different resolutions for the same initial topographic surface showed that neither the shape of the probability distribution nor the value of the scaling exponent are significantly affected by the change from one resolution to another. This indicates that the constraints imposed by topography on the probabilities of landslide areas are about the same at the investigated spatial scales, of 10 m and 25 m, respectively. Moreover, we observed that although the model does not use specific rules to distinguish between the processes of erosion, transport and deposition of landslides as other models do (Guthrie et al., 2008), these different parts of landslides may be recognized in the resulting topography. ~~In particular, we observed that scour areas are located in the upper slopes, runout areas in the middle slopes, and depositional areas in the lower slopes, in accordance with the natural behavior of landslides, which produce a smoothing of the relief.~~ Also, we found that landslide areas in the model increase with increasing rate of weakening. This result indicates that large landslides are more abundant when the intensity of the triggering mechanism is high, in agreement with findings from real geographic contexts (Saito et al., 2014). These similarities suggest that other properties observed for the model and discussed below may also describe properties of real systems.

We found that the scaling exponent of the landslide area frequency distribution linearly decreases with increasing driving rate, thus indicating that the faster the system is driven to instability the higher becomes the probability of large landslides. This result supports the hypothesis of Piegari et al. (2009), who conclude that the frequency-size distribution of landslides is controlled by the rate of approaching instability more than by the type of triggering mechanism per se. This could actually explain why landslide inventories generated for different triggering mechanisms, like rainfall and snowmelt, exhibit similar frequency–size statistics of landslides (Pelletier et al., 1997; Malamud et al., 2004). Additionally, our results suggest that the value of the scaling exponent is controlled by the way the topographic variability characterizing the area combines with the temporal effectiveness of the mechanism generating instability. A behavior similar to that of the scaling exponent was observed for the mean and standard deviation of the local slope angles of the surface, which under the action of landslides linearly decrease with increasing rate of weakening. Moreover, we observed that for the same driving rate, the value of the scaling exponent does not significantly change in time, contrary to what happens for the main statistical values of the slope angles of the surface, which show a decrease over time. Finally, we found that for a given time window, the scaling exponent of landslide areas, the driving rate, and the changes of the topographic setting are related to each other. In Section 2.2 we explained that the rate of weakening $w$ in the model may represent, for example, the rate of snow melt or the intensity of rainfall, or more generally, the temporal effectiveness with which the triggering mechanism weakens the soil, such as the temporal increase of the pore pressure by water, under the assumption of homogeneous soil properties. While in the model $t_w$ is the sum of both the weakening steps and the landsliding steps, and although $t_w$ does not have a characteristic scale length, the higher $t_w$ is, the wider is the time window during which the system is driven to instability. Thus, a higher $t_w$ represents a longer application of the triggering mechanism in real systems. With reference to rainfall, it has been widely shown that the triggering of landslides can be related to rainfall intensity-duration thresholds (or analogously, cumulated rainfall - rainfall duration thresholds) (Guzzetti et al., 2007; Peruccacci et al., 2012, Salciarini et al., 2012). Our results suggest that for an area of given topography, while this threshold governs the triggering of landslides, the probability of landslide areas depends on the intensity of the triggering mechanism ~~and is rather insensitive to~~more than on its duration, which mainly affects the number of landslides. Indeed, we found that the value of the scaling exponent is much more sensitive to the rate of weakening than to time (as shown in Fig. 6). Conversely, what we found to be strongly time-dependent is the footprint left on the topographic surface by landslides. ~~In the real world, for every rainfall event that exceeds the threshold (that is, when the intensity-duration conditions for the triggering of landslides are satisfied), the longer the duration of rainfall the higher the number of landslides triggered. Consequently, the longer the duration of the triggering mechanism, the more pronounced the topographic change of the topographic surface, caused by landslides. Interestingly, we found~~Moreover, we observed that the topographic setting of the area modeled preserves the information concerning the statistical distribution of landslide areas caused by a triggering event of given intensity and duration: based on the equations established above (Eqs. 7 and 8), by studying the topographic change of ~~the modeled~~ topography in the model, it would be possible to go back to the scaling exponent of the frequency distribution of landslide areas that caused that change. ~~This result opens up new potentially fruitful perspectives in the field of landslide forecasting. Indeed, while a numerical model is not meant to describe in detail real processes, given the correspondences observed between the behavior of the model and that of real systems, it is possible to hypothesize that a similar behavior could be observed in nature.~~

Some critical considerations must be added to the above. The model does not take into account river erosion and uplift, which are processes that allow for the rejuvenation of the system (Pucci et al., 2014) and landslide triggering. However, studies have shown that landslide erosion is not only the way in which hillslopes adjust in response to river channel incision. Rather, it plays an active role in shaping the landscape also independently of river processes and as a consequence of triggering mechanisms like rainfall (Korup, 2010; Reinhardt et al., 2015; Singh et al., 2015), and this role is mainly effective on smaller timescales (Korup, 2010). Thus, the choice whether or not to consider fluvial processes in the model should not affect the possibility to represent landslide dynamics and to investigate the scaling properties of this phenomenon.

Uplift is a long-term driving factor for landslide processes. Ignoring this process in the model implies that if we left the topographic surface free to evolve for a much larger number of model steps it would eventually become an almost flat surface. According to such a scenario, the surface would reach a maximum slope gradient equal to the one below which cells are always stable. This situation is not plausible in a dynamic geomorphological context affected by landslides. However, studies have shown that the rate of erosion by rivers and slope failures is regulated by the way the rate of uplift and the rate of precipitation interact with each other. Various scenarios have been described, where depending on the relative changes in uplift and precipitation the landscape evolves in different ways and with different erosion rates and mechanisms (Bonnet and Crave, 2006). The different types of system behavior have been described by defining, for example, specific uplift thresholds, which characterize the type of process that dominates the mountain range evolution, where slope failures occur in response to the rise of the surface (Ouchi, 2011, 2015). As explained above, in our model the driving rate could be thought of as representing the intensity of the landslide triggering mechanism, assuming constant intensity over time, and the higher the number of model steps, the longer the application of the triggering mechanism. Accordingly, although the model does not use a characteristic timescale, results from the model must be interpreted in the light of the possible maximum realistic duration of a triggering event, which can range from several days to several months depending on the climate of the area. Thus, we are studying the properties of the scaling behavior of landslides that occurred during one and the same erosion event, which happens in response to uplift – that is, the erosion operated by landslides in response to a rise of the topographic surface, which allows the equilibrium to be restored. In this context, while uplift affects the long-term evolution of landforms, for the single erosional event it only represents the underlying cause. Based on these considerations, it is reasonable to consider that the properties observed for the scaling behavior of landslides ~~can~~ could actually describe real properties of landslide processes. This idea is also supported by real-world studies, which found scaling properties in landslide datasets compiled both for long time spans and after a single triggering event (Guzzetti et al., 2002; Guthrie and Evan, 2004; Malamud et al., 2004), thus suggesting that the scale-invariance of landslides does not appear in the system only as a consequence of its long-term evolution, but rather manifests itself in a landscape, whose configuration is the result of its evolutionary history.

~~Although ignoring uplift does not allow us to draw clear conclusions about specific aspects of the long-term system dynamics, some considerations can be made. All the mathematical relationships that we found are time independent; time only affects the value of their parameters. This means that the properties observed for landslides in the model do not have a characteristic timescale. In the case of real landscapes, experimental studies suggested that topography advances toward a dynamical steady state (Bonnet and Crave, 2003; Lague et al., 2003), which arises in space-time scale invariant dynamics (Reinhardt et al., 2015; Singh et al., 2015). Consequently, considering the time-independence of the laws derived, we hypothesize that the properties observed could also describe the long-term dynamics of landslide processes.~~ As for the possible SOC behavior of landslides, in Fig. 6d we observed that at the lowest rates of weakening, that is, at the rates at which the change of topography caused by landslides is low, the scaling exponent is nearly stable over time. Conversely, at the highest rates of weakening corresponding to the most ample changes in topography, a change of the exponent trough time is observed. In summary, small topographic changes lead to small temporal changes in the scaling exponent, while more significant transformations in topography are associated with major variation in the values of the scaling exponent. This result indicates that the behavior of the model does not exhibit SOC dynamics, and this is due to the fact that ~~in the model~~ rejuvenation processes such as uplift are neglected, thus implying that in the model, topography cannot tend toward a dynamical steady state, unlike what has been hypothesized for topography in nature (Bonnet and Crave, 2003; Lague et al., 2003).

**8. Conclusions**

The cellular automata model (CA) proposed in this paper is capable of reproducing the power-law decay of the probability distribution of real landslide areas for a range of model parameter values. In analogy with the CA model by Hergarten and Neugebauer (2000), who firstly used a time-dependent variable in a CA model, our results confirm the key role that the temporal rate of weakening exerts in landslide dynamics. Model outputs provide insights into the variability of the scaling exponents observed in reality, indicating that the power-law scaling of medium to large landslide areas results from the interplay of the topographic spatial variability and the rate at which the system is driven to instability, which in the real world may be thought of as representing, for example, rainfall intensity. The fundamental difference between this model and the previous CA models used to study the frequency distribution of landslide areas consists of the topographic control of both the displaced mass and instability direction; our results point to topography as a major controlling factor in the probability of landslide sizes. Although the spatial variability of a real system is due to the combination of many interdependent factors, it is worth noting that the correspondence between the model outcomes and real landslide sizes is obtained by considering topography as the only factor defining the spatial variability in the system modeled. This result is consistent with the fact that the shapes of the landscape are dependent on geological and structural aspects of the relief, which constrain the type of the physical processes modeling the surface. To conclude, topography seems to be a good candidate to explain the scaling properties of medium to large landslide sizes, thus supporting with numerical evidence hypotheses made in previous studies (Frattini and Crosta, 2013).

Moreover, according to our results, the modeled topography not only provides explanations for the power law decay of landslide sizes, but also conserves the information about the scaling exponent of the probability distribution of areas of landslides that caused changes in its characteristics.

Incorporating rejuvenation processes like uplift and river erosion in the model could support the further study of long term landslide dynamics, as well as the possible SOC behavior of these processes.

**Acknowledgments**

The authors would like to thank the reviewers for their useful input and their constructive criticism.

## REFERENCES

Alvioli, M., Guzzetti, F., Rossi, M., 2014. Scaling properties of rainfall induced landslides predicted by a physically based model. Geomorphology 14, 2637-2648.

Ayalew, L., Yamagishi, H., 2005. The application of GIS-based logistic regression for landslide susceptibility mapping in the Kakuda-Yahiko Mountains, Central Japan. Geomorphology 65, 15-31.

Bak, P., Tang, C., Wiesenfeld, K., 1988. Self-organized criticality. Phys. Rev. A 38(1), 364-374.

Bjerrum, L., 1967. Progressive failures in slopes of overconsolidated plastic clay and clay shales. J. Soil Mech. Fdns. Div. Am. Soc. Civ. Engrs. 93(5), 1-49.

Bonabeau, E., Dessalles, J.L., Grumbach, A., 1995. Characterizing emergent phenomena (1): A critical review. Revue Internationale de Systémique 9(3), 327-346.

Bonnet, S., Crave, A., 2003. Landscape response to climate change; Insights from experimental modeling and implications for tectonic versus climatic uplift of topography. Geology 31(2), 123-126.

Bonnet, S., Crave, A., 2006. Macroscale dynamics of experimental landscapes, In: Buiter, S.J.H., Schreurs, G. (Eds.), Analogue and numerical modelling of crustal-scale processes. The Geological Society, London, UK, pp. 327-340.

Brardinoni, F., Church, M., 2004. Representing the landslide magnitude-frequency relation: Capilano river basin, British Columbia. Earth Surf. Process. Landforms 29, 115-124.

Brunetti, M.T., Guzzetti, F., Rossi, M., 2009. Probability distributions of landslide volumes. Nonlin. Processes Geophys. 16, 179-188.

Chen, A., Darbon, J., Morel, J.-M., 2014. Landscape evolution models: A review of their fundamental equations. Geomorphology 219, 68-86.

Frattini, P., Crosta, G. B., 2013. The role of material properties and landscape morphology on landslide size distributions, Earth Planet. Sci. Lett. 361, 310–319.

Goltz, C, 1996. Multifractal and Entropic Properties of Landslides in Japan. Geol. Rundsch. 85, 71-84.

Guthrie, R.H., Evans, S.G., 2004. Magnitude and frequency of landslides triggered by a storm event, Loughborough Inlet, British Columbia. Nat. Hazards Earth Sys. Sci. 4, 475-483.

Guthrie, R.H., Deadman, P.J., Raymond Cabrera, A., Evans, S.G., 2008. Exploring the magnitude-frequency distribution: a cellular automata model for landslides. Landslides 5:151-159.

Guzzetti, F., Malamud, B.D., Turcotte, D.L., Reichenbach, P., 2002. Power-law correlations of landslide areas in central Italy. Earth Planet. Sc. Lett. 195, 169-183.

Guzzetti, F., Reichenbach, P., Cardinali, M., Galli, M., Ardizzone, F., 2005. Probabilistic landslide hazard assessment at the basin scale. Geomorphology 72, 272-299.

Guzzetti, F., Peruccacci, S., Rossi, M., Stark, C.P., 2007. Rainfall thresholds for the initiation of landslides in central and southern Europe. Meteorol. Atmos. Phys. 98, 239-267.

Hergarten, S., Neugebauer, H.J., 2000. Self-organized criticality in two-variable models. Phys. Rev. E 61, 2382-2385.

Hergarten, S., 2003. Landslides, sandpiles and self-organized Criticality. Nat. Hazards Earth Sys. Sci. 3, 505-514.

Hergarten, S., 2013. SOC in Landslides. In: Ashwanden, M.J. (Ed.), Self-organized criticality systems. Open Academic Press, Warsaw, Berlin, pp. 379-401.

Katz, O., Aharonov, E., 2006. Landslides vibrating sand box: what controls types of slope failure and frequency magnitude relations? Earth Planet. Sc. Lett. 247, 280–294.

Katz, O., Morgan, J.K., Aharonov, E., Dugan, B., 2014. Controls on the size and geometry of landslides: Insights from DEM computer simulations. Geomorphology 220, 104–113.

Korup, O., 2005, Distribution of landslides in southwest New Zeland. Landslides 2, 43-51.

Korup, O., 2006. Effect of large deep-seated landslides on hillslope morphology, western Southern Alps, New Zealand. J. Geophys Res. – Earth Surf. 111, F01018, doi:10.1029/2004JF000242.

Korup, O., Clague, J.J., Hermanns, R.L., Hewitt, K., Strom, A.L., Weidenger, J.T., 2007. Giant landslides, topography and erosion. Earth Planet. Sc. Lett. 261, 578-589.

Korup, O., Densmore, A.L., Schlunegger, F., 2010. The role of landslides in mountain range evolution. Geomorphology 120(1-2), 77-90.

Iverson, R.M., 2000. Landslide triggering by rain infiltration. Water Resour. Res. 36(7), 1897-1910.

Lague, D., Crave, A., Davy, P., 2003. Laboratory experiments simulating the geomorphic response to tectonic uplift. J. Geophys. Res. 108(B1), doi:10.1029/2002JB001785.

Lee, S., Min, K., 2001. Statistical analysis of landslide susceptibility at Yongin, Korea. Environ. Geol. 40, 1095-1113.

Lehmann, P., Or, D., 2012. Hydromechanical triggering of landslides: From progressive local failures to mass release, Water. Resour. Res., 48, W03535, doi:10.1029/2011WR010947.

Liucci, L., Melelli, L., Suteanu, C., 2014. Scale-Invariance in the Spatial Development of Landslides in the Umbria Region (Italy). Pure and Applied Geophysics 172(7), 1959-1973.

Malamud, B.D., Turcotte, D.L., 1999. Self-Organized Criticality Applied to Natural Hazards. Nat. Hazards 20, 93-116.

Malamud, B.D., Turcotte, D.L., Guzzetti, F., Reichenbach, P., 2004. Landslide inventories and their statistical properties. Earth Surf. Process. Landforms 29, 687-711.

Martin, Y., Rood, K., Shwab, J.W., Church, M., 2002. Sediment transfer by shallow landsliding in the Queen Charlotte Islands, British Columbia. Can. J. Earth Sci. 39, 189-205.

McNamara, J.P., Ziegler, A.D., Wood, S.H., Vogler, J.B., 2006. Channel head location with respect to geomorphologic threshold derived from a digital elevation model: A case of study in northern Thailand. Forest Ecol. Manag. 224, 147-156.

Melelli, L., Pucci, S., Saccucci, L., Mirabella, F., Pazzaglia, F., Barchi, M.R., 2014. Morphotectonics of the Upper Tiber Valley (Northern Apennines, Italy) through quantitative analysis of drainage and landforms. Rend. Fis. Acc. Lincei 25(Suppl 2), S129-S138.

Milledge, D. G., Bellugi D., McKean J. A., Densmore A. L., Dietrich W. E., 2015. A multi-dimensional stability model for predicting shallow landslide size and shape across landscapes, J. Geophys. Res. Earth Surf., 119(11), 2481-2504.

Montgomery, D.R., Brandon, M.T., 2002. Topographic controls on erosion rates in tectonically active mountain ranges. Earth Planet. Sc. Lett. 201, 481-489.

Moore, I.D., Grayson, R.B., Landson, A.R., 1991. Digital Terrain Modelling: A Review of Hydrological, Geomorphological, and Biological Applications. Hydrol. Process. 5(1), 3–30.

Olami, Z., Feder, H.J.S., Christensen, K., 1992. Self-Organized Criticality in a Continuous Nonconservative Cellular Automaton Modeling Earthquakes. Phys. Rev. Lett. 68, 1244-1247.

Ouchi, S., 2011. Effects of uplift in the development of experimental erosion landform generated by artificial rainfall. Geomorphology 127, 88-98.

Ouchi, S., 2015. Experimental landform development by rainfall erosion with uplift at various rates. Geomorphology 238, 68-77.

Packard, N.H., Wolfram, S., 1985. Two-dimensional cellular automata, J. Stat. Phys. 38, 901-946.

Pelletier, J.D., Malamud, B.D., Blodgett, T., Turcotte, D.L., 1997. Scale invariance of soil moisture variability and its implications for the frequency-size distribution of landslides. Eng. Geol. 48, 255-268.

Peruccacci, S., Brunetti, M.T., Luciani, S., Vennari, C., Guzzetti, F., 2012. Lithological and seasonal control on rainfall threshold for the possible initiation of landslides in central Italy. Geomorphology 139-140, 79-90.

Piegari, E., Cataudella, V., Di Maio, R., Milano, L., Nicodemi, M., 2006. A cellular automaton for the factor of safety field in landslides modeling. Geophys. Res. Lett. 33, L01403-L01407, doi: 10.1029/2005GL024759.

Piegari, E., Di Maio, R., Milano, L., 2009. Characteristics scales in landslide modelling. Nonlin. Processes Geophys. 16, 515-523.

Pucci, S., Mirabella, F., Pazzaglia, F., Barchi, M.R., Melelli, L., Tuccimei, P., Soligo, M., Saccucci, L., 2014. Interaction between regional and local tectonic forcing along a complex Quaternary extensional basin: Upper Tiber Valley, Northern Apennines, Italy. Quat. Sci. Rev. 102, 111-132.

Reinhardt, L., Ellis, M.A., 2015. The emergence of topographic steady state in a perpetually dynamic self-organized critical landscape. Water Resour. Res. 51(7), 4986-5002, doi: 10.1002/2014WR016223.

Saito, H., Korup, O., Uchida, T., Hayashi, S., Oguchi, T., 2014. Rainfall conditions, typhoon frequency, and contemporary landslide erosion in Japan. Geology 42, 999–1002.

Salciarini, D., Tamagnini, C., Conversini, P., Rapinesi, S., 2012. Spatially distributed rainfal thresholds for the initiation of shallow landslides. Nat. Hazards 61(1), 229-245.

Singh, A., Reinhardt, L., Foufoula-Georgiou, E., 2015, Landscape reorganization under changing climatic forcing : Results from an experimental landscape. Water Resour. Res. 51(6), 4320-4337, doi:10.1002/2015WR017161

Stark, C.P., Guzzetti, F., 2009. Landslide rupture and the probability distribution of mobilized debris volumes. J Geophys. Res. 114(F00A02):1-16.

Stark, C.P., Hovius, N., 2001, The characterization of landslide size distributions. Geophys. Res. Lett. 28(6), 1091-1094.

Taramelli, A., Melelli, L., 2009. Detecting alluvial fans using quantitative roughness characterization and fuzzy logic analysis using the SRTM data. Int. J. of Computer Sc. and Software Technology 2(1), 55-67.

Tarquini, S., Isola, I., Favalli, M., Mazzarini, F., Bisson, M., Pareschi, M.T., Boschi, E., 2007. TINITALY/01: a new Triangular Irregular Network of Italy, Ann. Geophys. 50, 407-425.

Tarquini, S., Vinci, S., Favalli, M., Doumaz, F., Fornaciai, A., Nannipieri, L., 2012. Release of a 10-m-resolution DEM for the Italian territory: Comparison with global-coverage DEMs and anaglyph-mode exploration via the web, Comput. Geosci. 38, 168-170. doi: doi:10.1016/j.cageo.2011.04.018

Turcotte, D. L., 1997. Fractals and Chaos in Geology and Geophysics, 2nd ed. Cambridge University Press, Cambridge, pp. 398.

Turcotte, D.L., Malamud, B.D., Guzzetti, F., Reichenbach, P., 2002. Self-organization, the cascade model and natural hazards. P Natl. Acad. Sci., USA 99, Supp. 1, 2530-2537.

Van Den Eeckhaut, M., Poesen, J., Govers, G., Verstraeten, G., Demoulin, A., 2007. Characteristics of the size distribution of recent and historical landslides in a populated hilly region. Earth Planet. Sc. Lett. 256, 588–603.

Wolfram, S., 2002. A New Kind of Science. Wolfram Media Inc., Champaign, pp. 1197.

# The role of topography in the scaling distribution of landslide areas: A cellular automata modeling approach

AUTHORS:

**1**. Luisa Liucci (Corresponding Author)

**2.** Laura Melelli

**3.** Cristian Suteanu

**4.** Francesco Ponziani

AFFILIATIONS

**1; 2**: Department of Physics and Geology, University of Perugia, Via Alessandro Pascoli snc, 06123 Perugia, Italy

**3**: Department of Geography & Environmental Studies and Department of Environmental Science, Saint Mary's University, 923 Robie St., Halifax, Nova Scotia, B3H 3C3 Canada

**4**: Umbria Region Civil Protection Department, Via Romana Vecchia, 06034 Foligno, Perugia, Italy

CORRESPONDING AUTHOR

email Luisa.Liucci.LL@gmail.com

Tel +393405816613

Fax +390755840302

**Abstract**

Power law scaling has been widely observed in the frequency distribution of landslide sizes. The exponent of the power-law characterizes the probability of landslide magnitudes and it thus represents an important parameter for hazard assessment. The reason for the universal scaling behavior of landslides is still debated and the role of topography has been explored in terms of possible explanation for this type of behavior. We built a simple cellular automata model to investigate this issue, as well as the relationships between the scaling properties of landslide areas and the changes suffered by the topographic surface affected by landslides. The dynamics of the model is controlled by a temporal rate of weakening, which drives the system to instability, and by topography, which defines both the quantity of the displaced mass and the direction of the movement. Results show that the model is capable of reproducing the scaling behavior of real landslide areas and suggest that topography is a good candidate to explain their scale-invariance. In the model, the values of the scaling exponents depend on how fast the system is driven to instability; they are less sensitive to the duration of the driving rate, thus suggesting that the probability of landslide areas could depend on the intensity of the triggering mechanism rather than on its duration, and on the topographic setting of the area. Topography preserves the information concerning the statistical distribution of areas of landslides caused by a driving mechanism of given intensity and duration.

Keywords: Landslide area; Topography; Cellular automata; Scaling

## 1. Introduction

Landslide occurrence is controlled by the interaction of many factors, such as geology, topography, hydrology, land use and climate. These factors affect both the proneness to slope failures and the type and magnitude of landslides. However, regardless of the local characteristics, it has been widely shown that landslide patterns (Goltz, 1996; Liucci et al., 2015) and the frequency distribution of landslide areas and volumes exhibit scaling properties (Malamud and Turcotte, 1999; Stark and Hovius, 2001; Guzzetti et al., 2002, Martin et al. 2002; Brardinoni and Church, 2004; Guzzetti et al., 2005; Korup, 2005; Brunetti et al., 2009). In particular, landslide sizes follow a power law with negative scaling exponent, which can also be similar for landslides triggered by different mechanisms (Pelletier et al., 1997; Malamud et al., 2004; Hergarten, 2013). This trend is found from medium to large landslide sizes, while an opposite trend is identified at smaller sizes. Several models have been built to investigate this behavior and hypotheses have been discussed that the scaling properties of landslides could arise in Self-Organized Critical dynamics (Malamud and Turcotte, 1999; Hergarten, 2003, 2013).

According to the work by Van Den Eeckhaut et al. (2007), who reviewed the values of the scaling exponent observed for about thirty landslide datasets around the world, the exponent of the non-cumulative frequency distribution of landslide areas ranges between 1.42 and 3.36.

Compared to regolith landslides, rockfalls exhibit, on average, smaller scaling exponents (Malamud et al. 2004, Brunetti et al., 2009), and this could depend on the physics of processes leading to rockfalls, which are different from those responsible for regolith landslides (Malamud et al., 2004). The comparison between the scaling behavior of these two types of mass movement commonly takes into account the mobilized volumes.

The understanding of the factors controlling this power law decay and the value of the scaling exponent is of much interest, since it would provide valuable information concerning the probability of occurrence of landslides of different magnitudes. Several studies suggested possible explanations for the characteristic shape of the landslide frequency distribution and for the factors responsible for landslide sizes. Katz and Aharonov (2006) induced landslides in a vibrating box of cohesive sands through the application of both horizontal and vertical acceleration. The analysis of the frequency-size distribution of the generated landslides showed that the power law behavior observed for medium to large sizes is due to the strength heterogeneity of the material caused by the fracture systems that form in response to the acceleration applied. Lehmann and Or (2012) used a hydromechanical physically based hillslope model inspired by concepts of Self-Organized Criticality (SOC) (Bak et al., 1988), to study the frequency distribution of rainfall-induced shallow landslide volumes. They observed that root reinforced soils and high slope angles lead to smaller values of the scaling exponent of landslide volumes, while soil textural class and rain intensity have less of an impact on its value. Conversely, the work by Alvioli et al. (2014) showed that the shape of the frequency distribution for medium to large landslides changes with rainfall intensity and rainfall duration, for given geotechnical parameters. Frattini and Crosta (2013) observed that topography exhibits power law scaling with a rollover at smaller scales, similarly to what was observed for landslide size-frequency distributions, and that the scaling exponent of the frequency distribution of areas of patches (triangular units used to tile the topographic surface) increases with the slope gradient of relief. This indicates that topography is characterized by a low number of large areas with high slopes. They conclude that the low number of large patches with a slope gradient high enough to have slope failure causes an increase of the scaling exponent of the frequency distribution of landslides compared to the case of unlimited availability of high-slope patches. However, the investigation of synthetic landslide inventories showed that the main factor controlling the scaling exponent of landslide sizes is the variation of the geotechnical properties with depth. Katz et al. (2014) investigated the possible factors controlling the size and geometry of an individual landslide through the use of a numerical model. They hypothesized that the size of small landslides is controlled by the amount of material disintegrated by pre-sliding rupture processes, which in turn is controlled by the peak strength of the material and by the slope angle, while the size of medium to large landslides is not necessarily related to material disintegration and is mainly affected by the preexisting discontinuity setting. Milledge et al. (2014) proposed a slope stability model to predict the size of shallow landslides. They suggested that the low number of small landslides observed in real inventories and their size depend on the so called ‘critical area’, defined as the minimum area necessary to overcome resistive forces like friction and (when present) cohesion and thus to become prone to failure. The critical area is controlled by the critical failure depth, which is the depth at which the critical area is minimized, and in both cohesion and cohesionless soils it is affected by the position of the water table, which thus indirectly controls landslide sizes. They also found that the critical area closely corresponds to the peak of the frequency distribution of landslide areas on the reference site. This peak delimitates the rollover that marks the transition from the part of the frequency distribution corresponding to small landslide areas and characterized by positive slope, to the part corresponding to the medium to large landslide areas, which follows a power law with negative exponent (Guzzetti et al., 2002; Guthrie and Evans, 2004; Malamud et al., 2004). There is a wide debate about the reasons for the rollover. A possible explanation is an underestimation of small landslides because of the resolution of the original data sources used to build the dataset (Stark and Hovious, 2001; Brardinoni and Church, 2004). For example, raster data with a certain spatial resolution do not allow us to identify landslides with areas lower than the resolution of cells. Moreover, erosional processes quickly remove the fingerprint of small landslides (Guzzetti et al., 2002) - the level of conservativeness of landforms increases with their size.

Another possible explanation for the low number of small landslides concerns the geomechanical properties of soil and their relative importance in the rupture mechanism, which depends on the scale at with the process occurs (Stark and Guzzetti, 2009). Another category of models widely applied to the study of the dynamics of such natural phenomena is that of cellular automata (CA) models. A cellular automaton is a discrete numerical model, in which the studied system is discretized in cells. Each cell is characterized by a state representing one or more physical properties. The states of cells are evaluated and updated at discrete time steps according to rules that concern the states of the neighboring cells. One can then study the overall behavior of the system in space and time as an effect of local interactions. One of the strengths of these models stems from their capability of reproducing the complexity of real world patterns by using a small number of input parameters and by reducing processes to simple rules, capable of fruitfully describing their dynamics. Although in reality the dynamics are quite more complex and the factors involved are many, in CA models complex patterns emerge from simple rules (Wolfram, 2002); that is, they manifest emergent behavior (Bonabeau et al., 1995) just like complex natural systems do.

Two pivotal CA models are the Bak-Tang-Wiesenfeld model (Bak et al., 1988) and the Olami-Feder-Christensen model (Olami et al., 1992). The former, known as 'sandpile model', describes the behavior of a system subject to constant input that drives the system to instability: the equivalent of adding grains to a sand pile causes local instabilities that may propagate throughout the system, in a chain reaction, as a function of local states, producing scale invariant features both in space and in time. Constant input is thus leading to outputs in a wide range of sizes, corresponding to a distribution governed by a power law. The second one belongs to the group of CA spring-block models and it was built to study earthquake dynamics. In this model, cells represent blocks connected with each other through springs. In its theoretical formulation, blocks are also connected to a rigid driver plate, slowly moving, thus increasing the forces acting on the blocks until one (or some of them) exceeds the static friction and becomes unstable. When the block becomes unstable it is displaced, possibly initiating a chain-reaction involving neighboring cells. The OFC model is considered as a paradigm for non-conservative SOC because it involves dissipation: the potential energy gradually accumulated in the springs is partially transferred to the driver plate, while a part of it is lost from the system.

Like other phenomena, landslides seem suitable to be treated as avalanche processes. For slides occurring on slopes of overconsolidated clay and clay shales, the development of a sliding surface follows a mechanism of progressive slope failures (Bjerrum, 1967): the instability starts in a small region and destabilizes the neighborhood, thus allowing the instability to propagate. Moreover, the behavior of CA models can be thought of as a self-similar inverse cascade (Turcotte et al., 2002), and this idea can be fruitfully applied to landslides by considering the cascade as a coalescence of metastable regions: small failures coalesce to form a large failure plane.

Attempts have been made to apply the sandpile model (Bak et al., 1988) and the OFC model (Olami et al., 1992) to landslides, but results showed that none of them works on a quantitative level if the surface gradient is the only parameter used to describe the state of cells in the model (Hergarten, 2003). Hergarten and Neugebauer (2000) presented a new type of model, which introduces a second variable to the one describing the state of cells. The second variable represents a time-dependent weakening, and when the model is applied to landslides it consists of a temporal decrease of the stability slope threshold of each site. The rate of weakening can be introduced in different ways in the stability criterion, for example as a sum approach or as a product approach. When the product approach is used, the model shows SOC behavior and the scaling exponent observed is in agreement with values observed for real landslides. Thus, when a second variable is introduced to describe slope stability, results improve.

The idea of a two-variable model was also applied by Piegari et al. (2006, 2009). Their model uses the inverse of a factor of safety as a dynamic variable describing the state of cells, while a second parameter drives the system to instability, which in practice is equivalent to the time-dependent weakening of Hergarten and Neugebauer (2000). In their model, the instability of cells is partly lost from the system, which means that unlike previous landslide models the system is non-conservative, in analogy with the non-conservative case of the OFC model. A good correspondence with real frequency-size distributions is obtained when a specific level of conservation and driving rate are used, and after spatially scaling the model. They conclude that the frequency-size distribution of landslides is controlled by the rate of approaching instability more than by the triggering mechanism. Hergarten (2013) points out that the introduction of a degree of dissipation represents a tuning parameter for the model, whose value cannot be conceptually interpreted based on physical arguments.

Both the CA by Hergarten and Neugebauer (2000) and by Piegari et al. (2006, 2009) describe landslides on an individual slope. However, as shown by Frattini and Crosta (2013), topography is a key factor affecting landslide sizes. The important role of topography in slope failure occurrence is also highlighted by landslide susceptibility analyses, which find the slope gradient to be a predominant factor in causing the instability of an area (Lee and Min, 2001; Ayalew and Yamagishy, 2005). More generally, the setting of the topographic surface plays a major role in all the geomorphological processes acting on the landscape. Topography is not a static property of an area. A topographic surface changes as a consequence of the processes acting on it and in turn it affects the dynamics of most of these processes. A large number of landscape evolution models aim to describe these mutual interactions (a recent review of these models is given by Chen et al., 2014), and the factors mainly considered are the tectonic uplift, the fluvial erosion, and the gravitational processes. Topography also implicitly contains information concerning the lithology and the structural aspects of the area, since the geological properties constrain the resulting landforms (Taramelli and Melelli, 2009; Melelli et al., 2014). Consequently, the variability of the topographic surface also reflects the variability of many other parameters and it can thus be considered representative of the specificities of an area.

The changes that the topographic surface incurs over time could play a key role in the explanation for the statistics of landslide sizes (Hergarten, 2013). This paper focuses on this specific aspect of landslide dynamics, in order to contribute to the understanding of the scaling properties observed for medium to large landslides. In particular, we explore the possible relationships between landslide scaling properties and the changes in topography, which to the authors' knowledge, represents a new contribution to the existing literature on this topic.

To this purpose, we use a cellular automata (CA) model. In the model, we consider the gravitational process as the only mechanism shaping the landscape, and the topographic surface as the only parameter defining the variability in the initial conditions. Given that the model does not take into account the subsoil and structural geology, it refers to shallow landslides involving the regolith layer of the slope, and triggered by moisture increase. Its basic structure is similar to the one proposed by Hergarten and Neugebauer (2000), which is also used in the non-conservative CA model by Piegari et al. (2006, 2009). The model dynamics is driven by two variables: a temporal rate of weakening and a variable describing the state of cells. However, the fundamental difference between the model proposed here and those models consists of the predominant role of topography in the evolution of the system and in landslide dynamics, since topography is decisive for both the displaced mass and the instability direction. Moreover, conversely to the model by Piegari et al. (2006, 2009), this model is based on the transfer of mass and thus it is conservative.

The steps involved in this work consisted in: *i*) building the CA model (described in Section 2); *ii*) investigating the frequency distribution of landslide areas resulting from the implementation of the model starting from a topographic surface (Section 3 and 4); *iii*) qualitatively and quantitatively investigating the changes undergone by the topographic surface (Sections 5); *iv*) exploring the possible relationships between the scaling behavior of landslide areas and the changes in topography (Section 6). Section 7 discusses the results and their implications in terms of landslide dynamics, the limitations of this study, and possible future developments.

## 2. A cellular automata model for landslides

### 2.1. Structure of the model

The cellular automata model presented in this study was designed and written by the authors using the Matlab® software. It consists of a square lattice of square cells. Each cell is characterized by an altitude value, which can change during the evolution of the model through local interactions between neighboring cells. The initial state of the system is represented by the altitude values acquired from the Digital Elevation Model (DEM) of a real area. The lattice has a size of 320×320 cells, while the original DEM corresponds to an area located in the Umbria region (central Italy) and has a cell size of 25x25m. The area represents a mountainous morphology characterized by steep river valleys with slopes up to about 68° and flat surfaces at the top of the slopes. Overall, the area exhibits low drainage density and wide interfluve areas. The maximum altitude is of 1,412 m a.s.l (Fig. 1). We would like to specify the fact that it is not our objective to study landslide phenomena in this specific area. Rather, we use a real DEM in order to represent the natural variability of topographic surfaces, which has been shown to possess self-affine statistics over a wide range of scales (Turcotte, 1997). The advantage of using a real topography instead of a synthetic self-affine surface is that the latter typically lacks some important features of the earth's surface, such as river valleys and morphological shapes resulting from a variety of processes, including tectonics (Hergarten, 2013). Moreover, real topographic surfaces exhibit deviations from scale invariance (Evans and McClean, 1995).

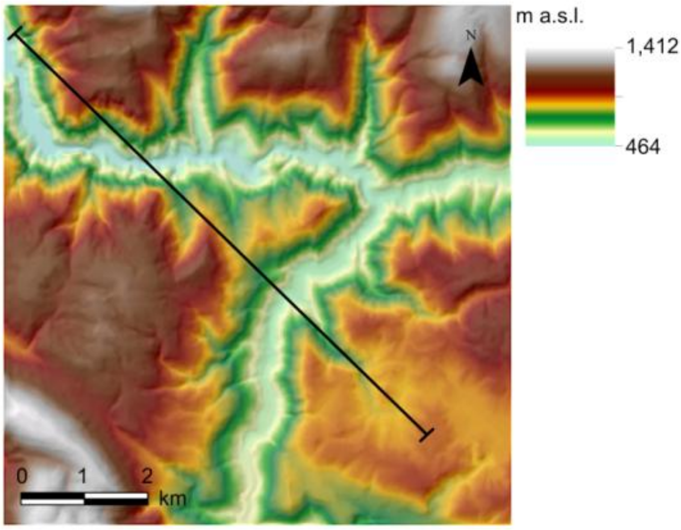


**Fig. 1** DEM of the area used as initial topographic surface in the CA model. The black line indicates the cross-section of profiles shown in Fig. 9.

The stability criterion for the cells is based on the local slope angle. The slope angle $\beta_c$ of each cell $c$ is defined as the maximum slope gradient between the cell and its eight Moore neighboring cells (Wolfram and Packard, 1985). The slope threshold is defined as the slope angle above which cells are unstable. The model starts from stable initial conditions; that is, the initial threshold $\alpha_0$ for all the cells is higher than the maximum $\beta_c$ of the area. Then, at each step the threshold decreases by a quantity $w$, driving the system towards instability. In analogy with the real world, the decrease of the stability threshold can be thought of as representative of the weakening of soil caused by triggering events such as rainfall and snowmelt, which produce a decrease of the resistive forces of soil until one or more slope failures occur. If the slope threshold of a cell at a given time $t$ has a value lower than or equal to $\alpha_{min}$, the decrease is no longer applied. The value used for $\alpha_{min}$ is 5°, which implies that a quasi-flat area is always stable. A cell $c$ is unstable when $\beta_c$ is higher than the slope threshold $\alpha_c$. When the cell $c$ is unstable, its altitude $e_c$ decreases by a quantity $\Delta e_c$. The value of $\Delta e_c$ is evaluated as the amount of altitude that $c$ must lose so that $\beta_c$ after perturbation becomes equal to $\alpha_c$, that is, the quantity necessary to bring cell $c$ back to a metastable state. The quantity $\Delta e_c$ is discharged to the $n_i$ neighboring cells identified as receiving cells ($n_i$, $i = 1\ldots, N$), thus resulting in an increase of their altitude $e_{n_i}$. Accordingly, in order to evaluate $\Delta e_c$ the model takes into account both the decrease of $e_c$ and the corresponding increase of $e_{n_i}$ of the receiving cells. There can be between one and three receiving cells ($1 \leq N \leq 3$) and they are evaluated based on the slope gradients between the eight Moore neighboring cells and the overcritical cell. The neighboring cell with the highest slope angle identifies the main landslide direction, which means that the avalanche follows the steepest descendent gradient. Then, if the two neighboring cells located at the two sides of the main landslide direction have an altitude that is lower than the altitude of *c*, they are also considered to be receiving cells. If $N > 1$, $\Delta e_c$ is anisotropically discharged among the $n_i$ cells. In particular, the fraction $f_{n_i}$ ($0 \leq f_{n_i} \leq 1$) of $\Delta e_c$ that each of the cells $n_i$ receives is proportional to the values of the slope angle between *c* and the cells $n_i$. If $N = 1$, $\Delta e_c$ is shifted in its entirety to the receiving cell in the direction of the maximum slope gradient (i.e., $f_{n_i} = 1$). Thus, both the landslide direction and the transfer of mass are constrained by the local topographic features of the surface. After perturbation, the threshold $\alpha_c$ of cell *c* is restored to its initial value $\alpha_0$. The instability of a cell may cause the instability of the neighboring cells, thus allowing the landslide to propagate within the system. At each model step *t* and for each cell *c*, the rules governing the dynamics of the model are summarized in Eqs. 1 and 2, which represent the driving rule and the transition rule, respectively.

$$\alpha_c(t) = \alpha_c(t-1) - w \qquad (1)$$

$$\text{if} \quad \beta_c(t) > \alpha_c(t) \rightarrow \begin{cases} e_c(t+1) = e_c(t) - \Delta e_c \\ e_{n_i}(t+1) = e_{n_i}(t) + f_{n_i} \cdot \Delta e_c \\ \alpha_c(t+1) = \alpha_0 \end{cases} \qquad (2)$$

In the model, landslides are considered instantaneous compared to the time scale of the overall evolution of the system. Thus, when the condition described in the transition rule (Eq. 2) is verified for at least one cell of the lattice (i.e. when there is at least one landslide in progress) the driving rule (Eq. 1) is no longer applied until all the cells become stable again.

Moreover, our model does not take into account a regenerating process such as uplift, since it is based on the assumption that the time scale at which the modeled landslides occur is much shorter than that of tectonic processes: the effect of these processes on the evolution of the system is negligible at the temporal scale considered and it does not significantly affect landslide dynamics.

### 2.2. Implementation of the model

The model was applied to the investigation of the frequency distribution of landslide areas. We used a series of values for the rate of weakening *w*. For each of these values we measured the areas of landslides that occurred over time windows $t_w$ defined as a number of model steps. The area of a landslide is calculated as the number of adjacent cells affected by instability during a single event. For each landslide area series we investigated the scaling properties of the resulting cumulative frequency distribution.

The choice of the values to be used for $w$ was constrained by the model outputs. In the next section it will be shown that in the model, landslide areas increase with $w$. Thus, the value of $w$ affects the sizes of the resulting landslides as well as the shape of the size frequency distribution. Accordingly, the model outputs drove the selection of the values of $w$ capable of representing the range of landslide sizes and the values of scaling exponents observed in the real world. In particular, we first tested a low value for $w$ ($w$ = 0.5). Then, we repeatedly ran the model by progressively increasing the value of $w$ by 0.5, until values were reached for which the behavior of the system was similar to real world observations. In the range of $w$ for which such similarity was observed, we reduced the distance between subsequent $w$ values to 0.25, to investigate the behavior of the system in more detail. The values tested for $w$ are 0.5, 1, 1.5, 2, 2.25, 2.5, 2.75.

As explained in Section 2.1, the weakening $w$ applied in the model through a decrease in the slope angle stability threshold is meant to correspond to the effect of rainfall or snowmelt events, which weaken the soil thus causing the instability of some sites of the system. In the real world, the rate of soil weakening depends both on the intensity of the triggering event and on the physical response of the soil (Iverson, 2000), which in turn depends on its physical properties. In our model we apply a constant rate of weakening in space and in time, which means to assume that the factors that create unstable conditions are constant in time, and that the only variable affecting the response of the system is topography, while all the other physical properties are homogeneous in space. Thus, a higher $w$ can be associated with a higher rainfall intensity or snowmelt rate, or more generally with a higher rate of increase of the resulting pore pressure, under the assumption of homogeneous soil properties.

To summarize, the way we implement the model allows us to study how landslide dynamics evolves when the system is subjected to a constant driving mechanism over time, with different predefined intensities.

The time windows $t_w$ used for the model consist of 1,000; 2,000; and 5,000 model steps. Accordingly, $t_w$ represents the sum of the "landsliding steps", that is, the steps at which the instability is communicated from the unstable cells to their neighbors, and the "weakening steps", that is, the steps at which the decrease of the slope stability threshold is applied. This implies that for a given time window $t_w$, the larger the areas of landslides of the resulting landslide series, the higher the number of landslide steps in the $t_w$-window, since the avalanche process involves a larger number of cells.

Figure 2 shows an example of stability conditions (Fig. 2a) and of the pattern of the slope stability threshold (Fig. 2b) of the examined topography, after 1,000 steps and for $w$ = 2. In Fig. 2a, yellow denotes the unstable cells at the 1,000$^{th}$ step of the model. In Fig. 2b we observe that under the effect of the driving rule (Eq.1, taking $w$ = 2), the slope threshold $\alpha_c$, which at time $t$ = 0 is uniform for all cells of the matrix (Eq.1, with $\alpha_c$ =75°; that is, $\tan \alpha_c$=3.7), has become strongly variable after 1,000 steps: its values vary from cell to cell, depending on the stability history of the cells during this time span.

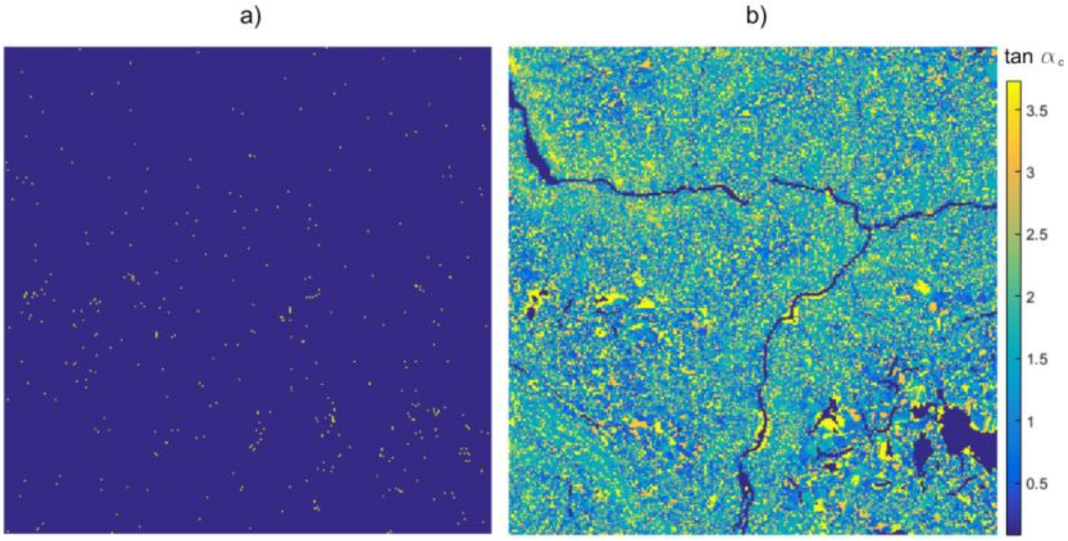


**Fig. 2** Stability conditions of the matrix, at the 1,000th step of the model. a) unstable cells (yellow) and stable cells (blue); b) Map of the tangent of the slope stability threshold $\alpha_c$.

## 3. Analysis of the probability of landslide areas obtained from the model

In this section, we first describe results obtained with all the rates of weakening ($w$) tested, and then compare these results with the real world observations in order to define the range of $w$-values capable of reproducing the behavior of real landslides.

For each number of iterations $t_w$ and for each $w$-value tested, the outputs from the model consist of a series of landslide areas $A_i$, expressed as a number of cells. These values were converted in in m$^2$ according to the resolution of the original DEM, in order to facilitate the comparison between the results obtained from the models and the behavior of real landslides.

Figure 3 shows how the mean area of landslides ($A_L$) of each landslide data series varies with the rate of weakening $w$ (Fig. 3a) and with the number of model steps $t_w$ (Fig. 3b). In both graphs we observe that the higher the value of $w$ the higher the mean area $A_L$. In particular, the two parameters are linked to each other by a linear equation (Fig. 3a). The increase of $A_L$ with $w$ is due to the spatial spread of instability, which increases with increasing rate of weakening. Indeed, according to the driving rule (Eq.1), a higher $w$ implies a faster decrease of the slope threshold $\alpha_c$ and thus a higher number of unstable cells with a higher probability to be in touch with each other. This results in larger landslide triggering areas, which consequently generate larger landslide bodies. Moreover, the wide spatial spread of instability can also cause the formation of coalescent landslides, which are identified in the model as a single landslide. Finally, a faster decrease of the slope threshold also implies that a larger mass must be lost from the unstable cell in order to restore equilibrium conditions. The increase of the landslide mass involved in the landslide process increases the probability for the neighboring cells that receive the mass to become in turn unstable and, as a result, landslide processes are more likely to generate large areas.

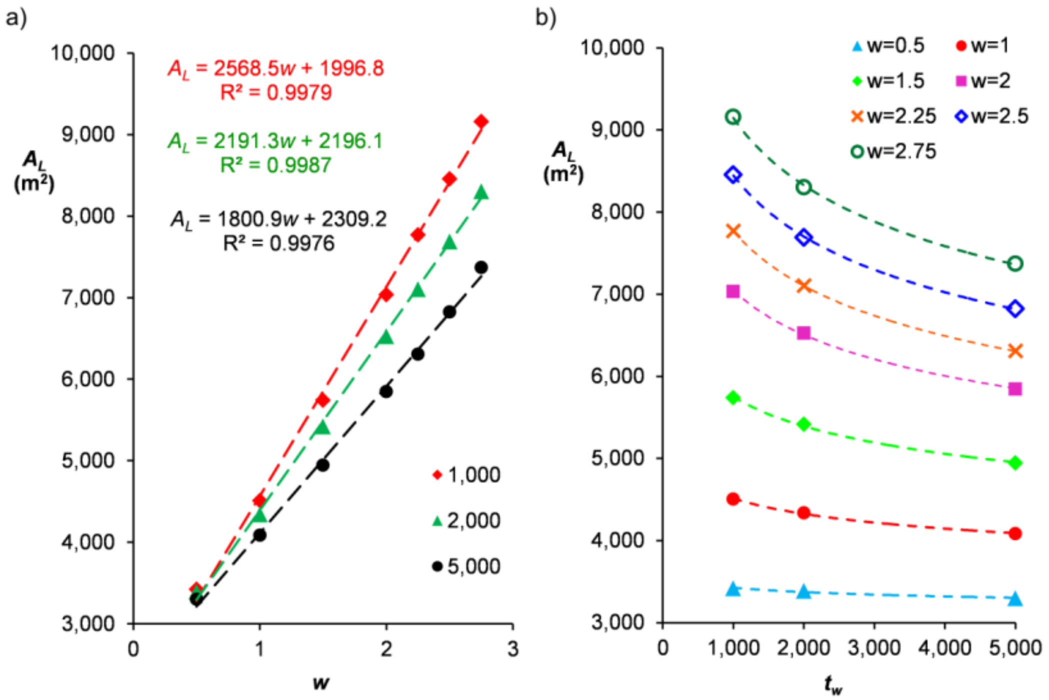


**Fig. 3** (a) For each number of model steps ($t_w$ = 1,000; 2,000; 5,000), mean area of landslides ($A_L$) of the respective landslide areas data series as a function of $w$, and the respective linear best fit. (b) For each $w$, $A_L$ as a function of $t_w$.

The slope of the linear best fit in Fig 3a decreases with increasing $t_w$, thus indicating that the largest landslides occur at the early stages of the evolution of the model, while the relative importance of smaller landslides in the data series increases with $t_w$, thus lowering the mean value of landslide areas $A_L$. This aspect of the behavior of the system is well depicted in Fig. 3b, where we observe that $A_L$ decreases with $t_w$, and that this decrease is higher for higher $w$. Since high values of $w$ lead to large landslide areas, we can hypothesize that like in real systems, relatively smaller topographic adjustments occur in response to large landslides, thus decreasing the value of $A_L$.

The complementary of the cumulative frequency distribution of landslide areas obtained from the model for each $w$ and $t_w$ tested, along with their scaling properties, are shown in Fig. 4.

Overall, landslide areas increase with increasing $w$ and vary from $2\times10^3$ to $2\times10^7$ $m^2$, which are values comparable with the range observed for real landslide areas (Pelletier et al., 1997; Guthrie and Evans, 2004; Malamud et al., 2004), although the highest order of magnitude represented in most real datasets is of $10^6$ $m^2$, while landslides obtained from the model reach $10^7$ $m^2$. Such large landslides are not often present in landslide inventories, since they require particular conditions in order to occur, that is, very high slope gradients like those observed in deeply incised river valley, and high-intensity rainfall events (Korup et al., 2007). Moreover, particular structural settings may favor the instability of large slope portions. In terms of slope gradients and rainfall intensity, these conditions match those of the system modeled. Indeed, the river valleys are up to 70° steep, and landslide areas with a magnitude of $10^7$ $m^2$ are obtained when the highest values for the rate of weakening are applied (w=2.5 and w=2.75), which according to the interpretation given in Section 2.2, correspond to the highest intensities of the triggering event. Moreover, as explained above, coalescent landslides are identified in the model as a single landslide, thus leading to larger areas.

The graphs in Fig. 4 show that the right tails of the frequency distributions of landslide areas always follow a power law trend (R > 0.99) (Eq.3).

$$N \propto A^{-(D-1)} \quad (3)$$

In Eq. 3, $N$ is the number of landslides with area greater than or equal to $A$, and $D$ is the scaling exponent.

The scaling exponents $D$ range from 2.67 to 5.75, with uncertainty intervals at the 95% confidence level between 0.07 and 0.19. Overall, scaling behavior is observed in ranges of landslide areas from 0.6 orders of magnitude (Figs.4d and 4f: series obtained at 1,000 model steps) to 2 orders of magnitude (Figs.4b and 4c: series obtained at 2,000 and 1,000 model steps, respectively). Later in this section we will show that only some of the $D$-values obtained are in the range detected for real landslides.

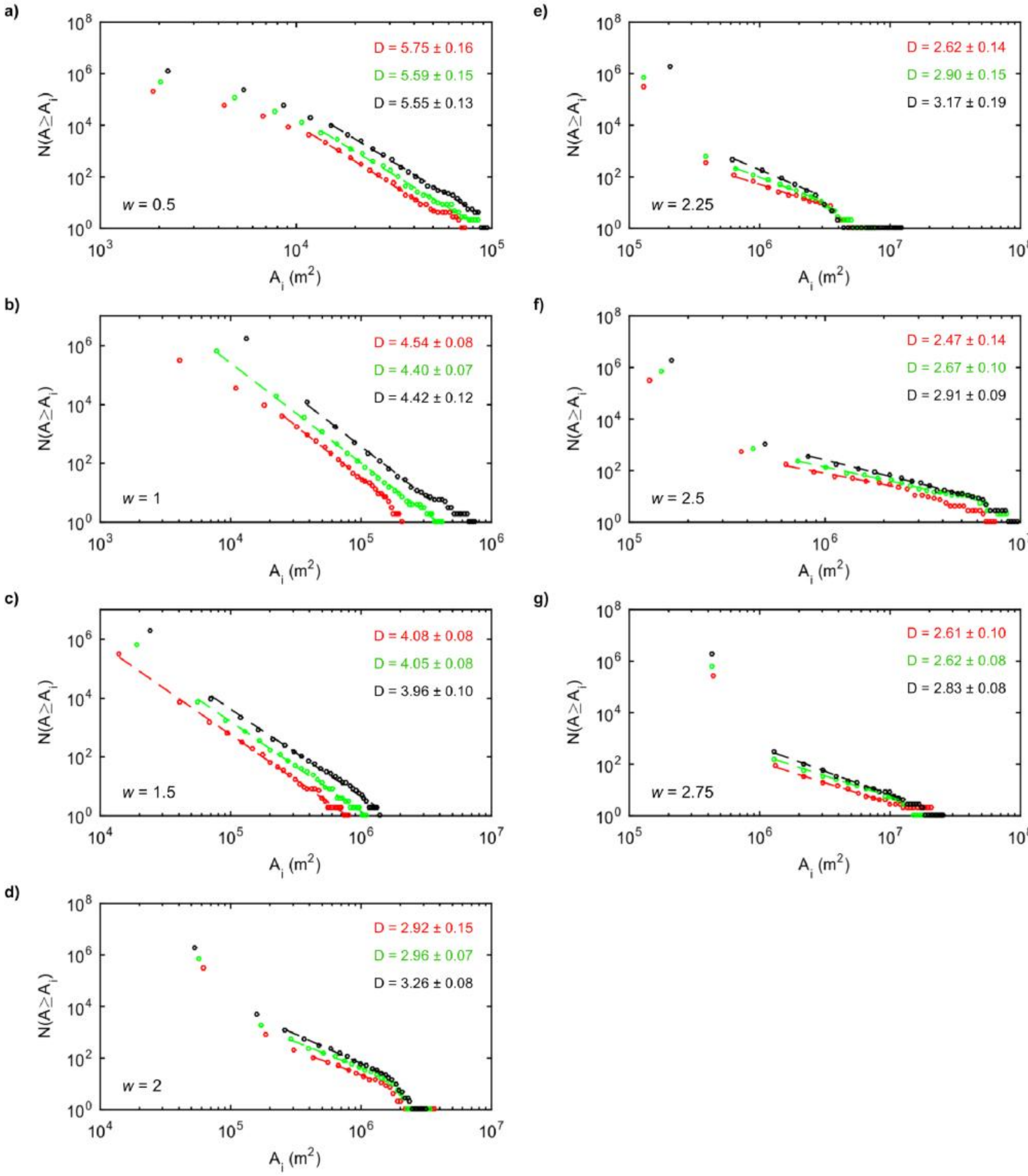


**Fig. 4** Complementary of the cumulative frequency distributions (*CFDs*) of landslide areas ($A_i$ in m$^2$) obtained with a) $w$ = 0.5, b) $w$ = 1, c) $w$ =1.5, d) $w$ = 2, e) $w$ = 2.25, f) $w$ = 2.5, g) $w$ = 2.75, for different time spans (1,000 model steps in red, 2,000 in green, and 5,000 in black). The dotted lines indicate the portions of the *CFD*s taken in consideration for the identification of the power law (dotted lines). For each power law the respective scaling exponent $D$ is shown.

A flattening of the frequency distributions is observed when landslide areas are lower than $10^4$ $m^2$ (Figs. 4a and 4b), thus indicating that small landslides are less frequent than predicted by the power law. A deviation from the power law at the smallest landslide sizes is also recognized in the *CFD*s obtained from real datasets. However, in the real world small landslides show a specific statistical behavior that is not observed in our *CFD*s: when non-cumulative frequency distributions are used, the interval corresponding to the smallest landslide areas is characterized by an opposite trend, with positive slope, followed by a rollover above which landslide areas start following the power law (Guzzetti et al., 2002; Guthrie and Evans, 2004; Malamud et al., 2004). Such a rollover is not present in the outcomes of this model: non-cumulative frequency distributions calculated for the same landslide data series for which the cumulative distributions are shown in Fig. 4a and 4b, exhibit a flattening rather than a rollover for the smallest sizes of landslide areas. As explained in Section 1, the rollover in real landslide inventories may be associated with a range of explanations, such as an underestimation of small landslides (Stark and Hovious, 2001; Brardinoni and Church, 2004), and the physics of processes controlling the occurrence of small landslides (Stark and Guzzetti, 2009, Milledge et al., 2014). In this regard, our model does not consider the physical parameters and processes invoked to explain the frequency distribution of small landslides, and it cannot be affected by the resolution of the data sources of the landslide inventory either. This could explain why the *CFD*s obtained do not exhibit a rollover. In our model, the only variable affecting landslide areas is the topography. Thus, the flattening that we observe for these series at the smallest landslide areas is expected to be related to the constraints represented by the topographic surface.

The first part of the frequency distributions obtained with *w* from 2 to 2.75 (Figs. from 4d to 4g) exhibits a behavior that it is not the same with the one from real landslide inventories. In particular, although the smallest sizes of these series are in a range at which scaling behavior is observed in nature, in this part of the *CFD* the number of the modeled landslides is higher than that predicted by the power law. The difference can again be related to the fact that the only constraint to model dynamics is represented by topography: as we deduced from Fig. 3, topographic adjustments occur in response to the large landslides caused by high rates of weakening, thus leading to a high number of slope failures with smaller area.

While model choices affect the first part of the area-frequency distributions, results indicate that the model is capable of reproducing the scaling properties of real landslides, when specific values for the parameters of the model are used. The values of $D$ were compared to those observed for real landslide inventories by taking as a reference the work by Van Den Eeckhaut et al. (2007), which provides an overview of the values of $D$ observed for about thirty landslide inventories around the world, published in twenty-seven papers (please refer to Van Den Eeckhaut et al. (2007) for the related bibliography). According to this paper, for real landslide inventories the values of $D$ range between 1.42 and 3.36, with many of them around 2.5. The landslide inventories considered are both historical and post-event. Since like most CA models, the one presented in this paper does not have a timescale, for the comparison of the model outputs with reality we preferred not to refer to a specific type of inventory, but rather to include both post-event inventories and historical ones, also considering that the main difference between historical and post-event inventories is observed in the frequency distribution of small landslides, which is not the focus of this study, while in the portion of the frequency distribution that exhibits power law scaling, the scaling exponent does not show any specific behavior for the two types of datasets.

The comparison indicates that the power law decay of the modeled landslide areas is in accordance with that of real landslide inventories for rates of weakening between 2 and 2.75 (Figs. from 4d to 4g). Indeed, in this range of $w$ the exponents are comprised between 2.47 and 3.26, while for lower values of $w$ the exponent is too high compared to real values, thus indicating an underestimation of large landslides and suggesting that although power law behavior is observed for all the $w$ applied, only the highest rates of weakening among those tested are capable of reproducing the action exerted by real landslide triggering events. The histogram in Fig. 5 shows the values of the $D$-exponent in literature. The $D$ classes are 0.3 wide and the values in the x-axis represent the middle value of each class. Most of the real observations are in the $D$ class from 2.4 to 2.6. In Fig. 5, the arrow delimitates the range of $D$-exponents observed for the landslide series obtained from the model, with rates of weakening $w$ between 2 and 2.75. The comparison with literature shows that in this range of $w$-values, the scaling behavior of landslide areas is well reproduced by the model: the scaling exponents of the modeled landslide series range from 2.5 to 3.2.

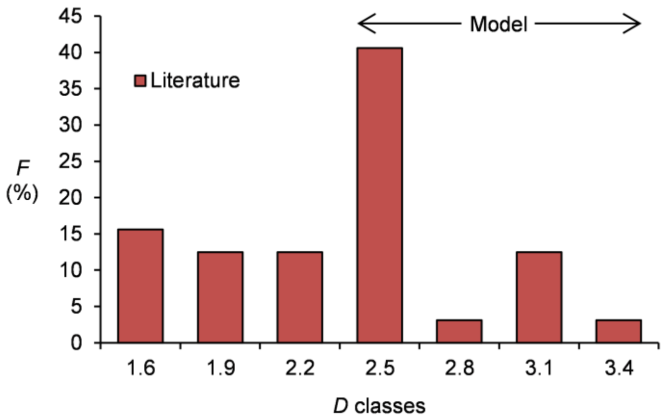


**Fig. 5** Comparison of the percentage frequency (*F*) of the values of *D* observed within each *D* class, in literature (Tab. 1 in Van Den Eeckhaut et al. (2007)) and for the landslide data series obtained with *w* from 2 to 2.75. The *D* classes are 0.3 wide.

In the next section we will show that the shape of the frequency distributions is not affected by the resolution of the DEM used, at least for the resolutions tested. This means that although the results presented in Fig. 4 correspond to landslide areas expressed in $m^2$ (based on the resolution of the original DEM of 25x25 m), the represented constraints exercised by topography on the landslide probability should correspond to a wider range of landslide areas than the one represented in the figure.

We studied the way the scaling exponents depend on (*i*) the rate of weakening *w* and (*ii*) time $t_w$. For this analysis, all the values of *w* were used, although only those higher than or equal to 2 lead to scaling exponents similar to the real ones (as shown above). This allows us to better explore the behavior of the system, which according to the results obtained and shown below and in the next sections, may be described by mathematical rules that can be fitted to the whole range of rates of weakening *w* tested. Graphs a, b, and c in Fig. 6 show that for each $t_w$, *D* linearly decreases with an increasing rate of weakening *w* ($R^2 > 0.98$), thus indicating that the faster the system is driven to instability the higher becomes the probability of large landslides. The decrease is described by:

$$D = -m_D \cdot w + c_D \qquad (4)$$

where $c_D$ is a constant.

This result indicates that a possible cause affecting the probability of occurrence of real landslide sizes is the rate at which the system is driven to instability, such as the rainfall intensity for rainfall triggered landslides. Fig. 6d indicates that when the rate of weakening *w* is lower than or equal to 1.5, *D* does not significantly change over time. Conversely, for higher $w$, $D$ slowly increases with $t_w$. However, the change of $D$ over time is much lower than that produced by the rate of weakening: for $t_w$ equal to 5,000 model steps, the maximum temporal change of $D$ is of 0.4 (Fig. 6d), while in the same time window, the change of $D$ with $w$ is of about 2.7. This result will be discussed in section 7.

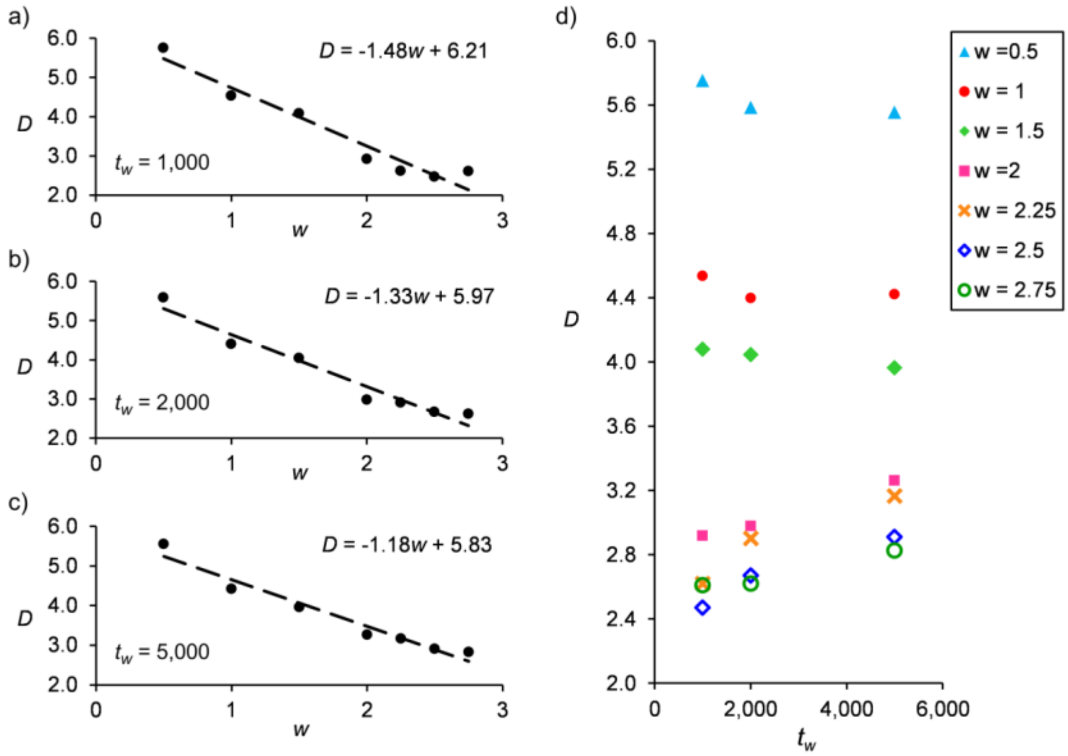


**Fig. 6** (a, b, c) For each $t_w$ (1,000; 2,000; 5,000 model steps), $D$ as a function of the rate of weakening $w$, and the respective linear best fit. (d) For each $w$, $D$ as a function of $t_w$.

## 4. Investigation of the effect of model choices and computational techniques

The model is based on a lattice of 320×320 cells, and the DEM used to define the altitude values of cells has a resolution of 25×25 meters, thus implying that the smallest possible landslide in the model is of 625 $m^2$ (i.e, when the instability involves only one cell). We investigated the ways in which these choices affect the landslide area distribution, by keeping the same area as the initial surface for the model, but changing the DEM resolution to 10×10 meters (the DEM was built by Tarquini et al., 2007, 2012). Accordingly, the resulting lattice has a size of 800×800 cells and the smallest possible landslide area is of 100 $m^2$. We used a low ($w$=1) and a high value ($w$=2.75) among the rates of weakening $w$ applied in the model (1,000 model steps were used for this comparison) and obtained similar results for both of them. The outcomes of the model for $w$=2.75 are shown in Fig. 7.

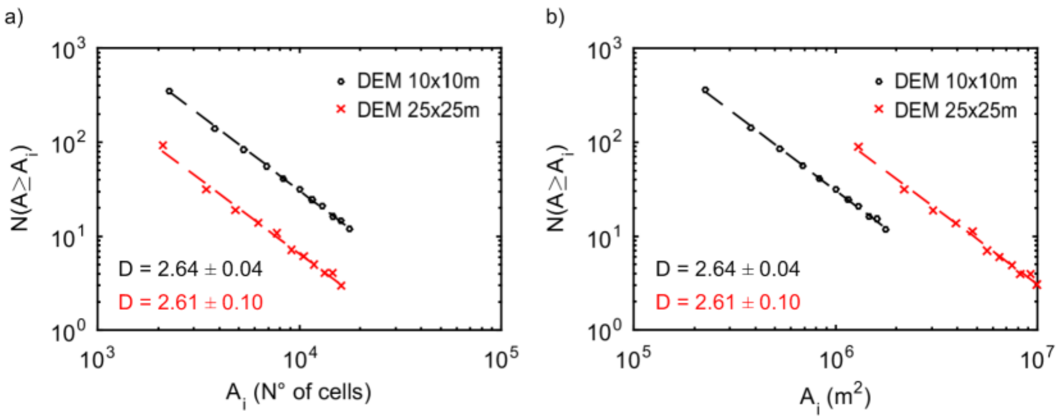


**Fig. 7** Portions of the cumulative frequency distributions (*CFD*) of landslide areas ($A_i$) that can be described by power laws (dotted lines) and their respective scaling exponents (*D*), for the series of $A_i$ obtained with a DEM of 25×25 m (lattice size of 320×320 cells) and with a DEM of 10×10 m (lattice size of 800×800 cells) ($t_w$=1,000;), with a rate of weakening of $w$ = 2.75: a) $A_i$ values as number of cells; b) $A_i$ values in m$^2$.

Figure 7a) shows the power law fit of the *CFD* of landslide areas, with the latter expressed as a number of cells, that is, without converting these values in m$^2$. The range of landslide areas obtained from the model is about the same for the two DEMs used, while the number of landslides is higher for the DEM of 10×10m. The scaling exponents *D* of the power laws observed for the two DEMs are very similar, as well as their scaling ranges. This result shows that while the size of the lattice affects, as expected, the number of landslides (the higher the model size, the higher the number of cells available to become unstable, and the higher the number of landslides), it does not affect the shape of the distribution and the dynamics of the system. The same applies to the resolution of the original DEM, which according to the results obtained does not produce any significant effect on the value of the scaling exponent, for the two resolutions tested. This result suggests that the control of topography on the size frequency distribution of the modeled landslides is the same at the two scales of analyses used, and this may be explained by the scale-invariant character of topography (Frattini and Crosta, 2013). Accordingly, after converting landslide areas from number of cells to m$^2$ (Fig. 7b) the only effect is a shift of the power laws along the x-axis. As a result, while the range of the scaling regimes for the landslide series obtained from the two DEMs are different, the values of their exponents do not change. This also indicates that a *D*-value of about 2.6 characterizes the scaling behavior of landslide areas in a range from about 2×10$^5$ to 10$^7$ (Fig. 7b), considering the scaling ranges observed for both the DEMs.

These outcomes also suggest that the fact that the model does not accurately represent the first part of the frequency distribution of real landslides (Section 3) is not due to the scale of analysis but rather, as hypothesized in the previous section, due to the choice of topography as the main way of describing the spatial variability of the system.

## 5. Changes of the topographic surface modeled

The initial topographic surface is subjected to changes caused by the mass distribution occurring during the time window $t_w$. In the present section we investigate these changes focusing on different morphometric and geomorphological features of the landscape. We must remember that according to the dynamics of the model, these changes represent the evolution of an area only subjected to the action of the gravitational process and whose variability is only represented by topography.

### 5.1 Topographic attributes

Fig. 8 shows the difference in altitude between the final surface obtained at $t_w$ = 5,000 steps, and the initial one, for $w$ equal to 1, 2 and 2.75, respectively. The difference is expressed in meters, according to the altitude values of the original DEM. Red zones indicate a decrease in altitude (areas affected by erosion), while blue zones indicate an increase in altitude (areas affected by deposition). When $w$ grows from 1 (Fig. 8a) to 2.75 (Fig. 8c), the difference in altitude increases. This is due to the observed property of the frequency distribution of landslides, which indicates that for the same $t_w$ the number of large landslides increases with increasing rate of weakening. Consequently, the higher $w$ the larger the change of the surface configuration.

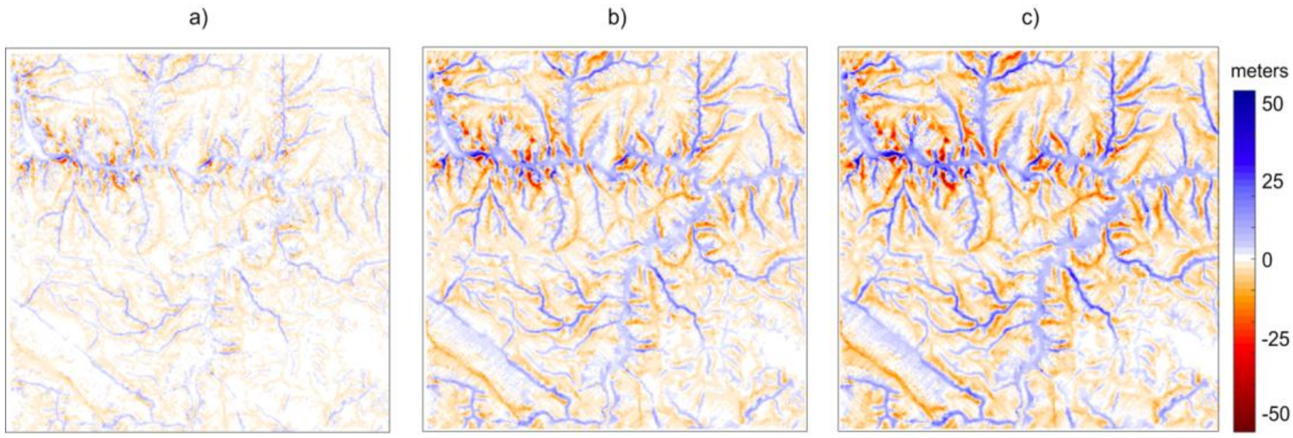


**Fig. 8** Difference in altitude between the final surface obtained at $t_w$ equal to 5,000, and the initial one. a) $w$=1; b) $w$=2; c) $w$=2.75.

In order to highlight the variation of specific topographic attributes a cross-section through the surface is made (Fig. 1). The section is traced so as to cross the main ridges and valleys to highlight the evolution of the slopes. Fig. 9 shows how specific topographic attributes change along the cross-section after an interval $t_w$ equal to 5,000 model steps and with $w$ = 2.75, i.e. the situation in which we observed the more pronounced topographic changes. Fig. 9a displays the initial and the final topographic profiles. The comparison of the two profiles indicates that landslides that occurred over the time interval $t_w$ cause a decrease of the altitude of mountain ridges and the filling of valleys, thus producing a smoothing of the relief. Fig. 9b shows the initial and the final profile curvature ($P_c$) of the topographic surface (Moore et al., 1991), which describes the curvature of the surface along the direction of the steepest gradient.

The curvatures were calculated using the algorithm in Spatial Analyst (ArcGIS10.0 © Esri), and are expressed in $10^{-2}$ m. Positive $P_c$ values indicate concave curvatures, while negative values indicate convex ones. In the graph we observe that the $P_c$ values of the final surface are closer to zero than those of the initial one, thus describing a decrease of both the convex and the concave curvature. Moreover, in the profile of the final curvature a general trend can be recognized, which consists in the shifting of the peaks corresponding to the maximum values of curvature toward lower values of linear distance (x-axis), compared to the peaks of the initial curvature profile. This could be due to a slope decline evolution, where the decrease of the slope angle is associated with a lateral movement of ridges and valley axes.

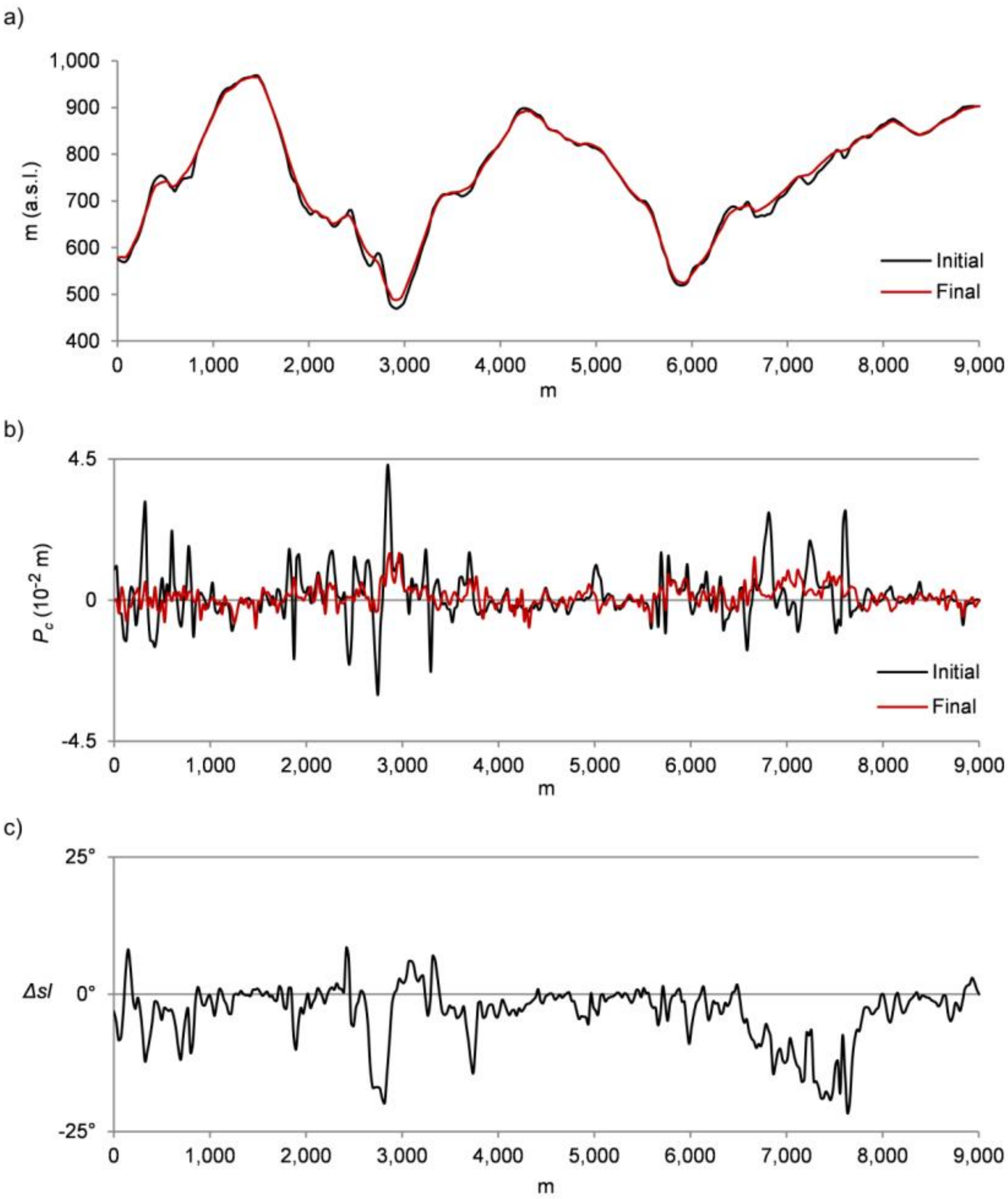


**Fig. 9** Change of topographic attributes along the cross-section made in Fig. 1. The change is evaluated between the initial topographic surface and the final one, obtained at $t_w$ = 5,000 and with $w$ = 1.5. a) Altitude; b) Profile curvature ($P_c$) in $10^{-2}$ m; c) Difference $\Delta sl$ between the initial and final slope angle (in degrees).

Fig. 9c displays the variation of the slope angle ($\Delta sl$) of the surface, calculated as the difference between the final and the initial slope. Overall, a decrease of the slope angle is observed, up to a maximum of about 21°. However, some exceptions can be noticed. A positive $\Delta sl$ corresponds to the medium and lower slope portions, where the moved mass increases the slope angle.

These results are in agreement with real-world observations, where landslides dampen local relief removing mass from upper slopes and depositing it on lower slopes, thus producing a decrease of mean slope relief and relief variability, of slope angles and of their standard deviation (Korup, 2006; Korup et al., 2010). A more in-depth analysis of the change of the slope angles undergone by the relief will be addressed in Section 5.2. The evolution of the surface modeled also highlights that although the rules of the model apply to all cells of the lattice without discriminating between scar area, runout area and depositional area of landslides, this differentiation is intrinsically produced by the model. Indeed, the areas where we observe erosion represent the scar areas where landslides are triggered, i.e. where the instability is generated. These areas are located in the upper slope zones, which in real active mountain belts are the areas dominated by landslide erosion (Montgomery and Brandon, 2002; Korup et al., 2007). For the middle slopes we did not observe any significant change in altitude. Thus, they represent the runout areas of landslides where, in terms of the cells of the lattice, the instability is transferred from one cell to another but not generated. Finally, an increase in altitude is observed in the lower slopes overlooking the toe of slopes, which thus represent the depositional areas affected by the accumulation of landslide bodies.

### 5.2 Statistical properties of the slope angles

The topographic changes are driven by the dynamics of the model, which are controlled by the slope angles $\beta$ of the area. In Fig. 9c we observed that like other topographic attributes, slope angles also change over time. We thus investigated the temporal evolution of the slope angles and their possible dependence on the rate with which the system is driven to instability, in order to compare the behavior of the surface with the one observed for the scaling exponents of the frequency distribution of landslide sizes.

For each rate of weakening $w$ and number of model steps $t_w$ (i.e., 1,000; 2,000; 5,000) we calculated the respective frequency distribution of $\beta$ of the initial and the final topographic surface. Fig. 10 shows the non-cumulative (Fig. 10a) and the cumulative (Fig. 10b) distributions of $\beta$ for the initial surface and for those obtained with the maximum $t_w$, equal to 5,000 model steps. For clarity, in Fig. 10a only the frequency distributions corresponding to $w$ = 1, 2.5 and 2.75 are shown, since they offer a good description of the behavior of slope angles with increasing $w$.

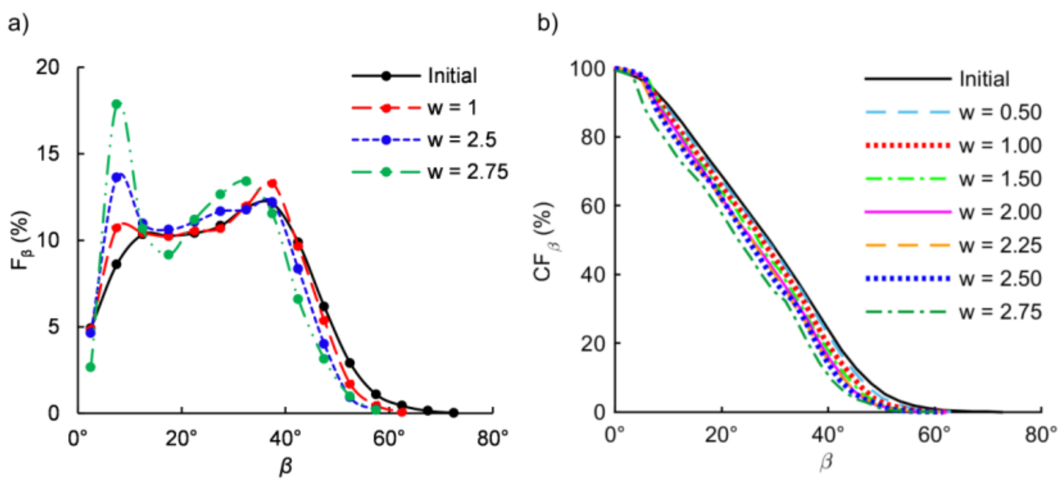


**Fig. 10** Non-cumulative (a) and cumulative (b) frequency distributions of the slope angle $\beta$ for the initial topographic surface and for those obtained at the maximum $t_w$, equal to 5,000 model steps, with $w$ = 1, 2.5, 2.75, in graph (a), and with all the $w$ applied in graph (b).

The initial frequency distribution of $\beta$ (black symbols in Fig. 10a) is representative of the topographic setting of the area, which is characterized by steep river valleys and flat surfaces at the top of the slopes. Because of this, in the slope angle series the intermediate classes are less represented than they would be in a Gaussian distribution, in favor of the frequency of classes corresponding to low and high slope angles. Landslide occurrence changes the shape of the curve. In comparison with the initial frequency distribution, for each $w$ tested we observe a decrease of the frequency of the angles higher than about 40° and an increase of those lower than about 13° (Fig. 10a). Moreover, landslide processes emphasize the bimodal character of the initial topographic setting. The smoothing produced on the surfaces by landslides is still more evident in the cumulative frequency distributions ($CF_\beta$), where we observe that for each $w$ the curve is shifted toward lower values of $\beta$. In order to quantify these changes, we calculated for each frequency distribution (thus considering all the $t_w$ and not just $t_w$=5,000) the following statistical parameters: maximum ($\beta_{max}$), mean ($\bar{\beta}$), standard deviation ($\sigma_\beta$), kurtosis ($k_\beta$), skewness ($sk_\beta$). Figure 11 shows the change of each statistical parameter in time. Also in this case, only results corresponding to some $w$ are displayed ($w$ = 1, 2 and 2.75), for clarity purposes.

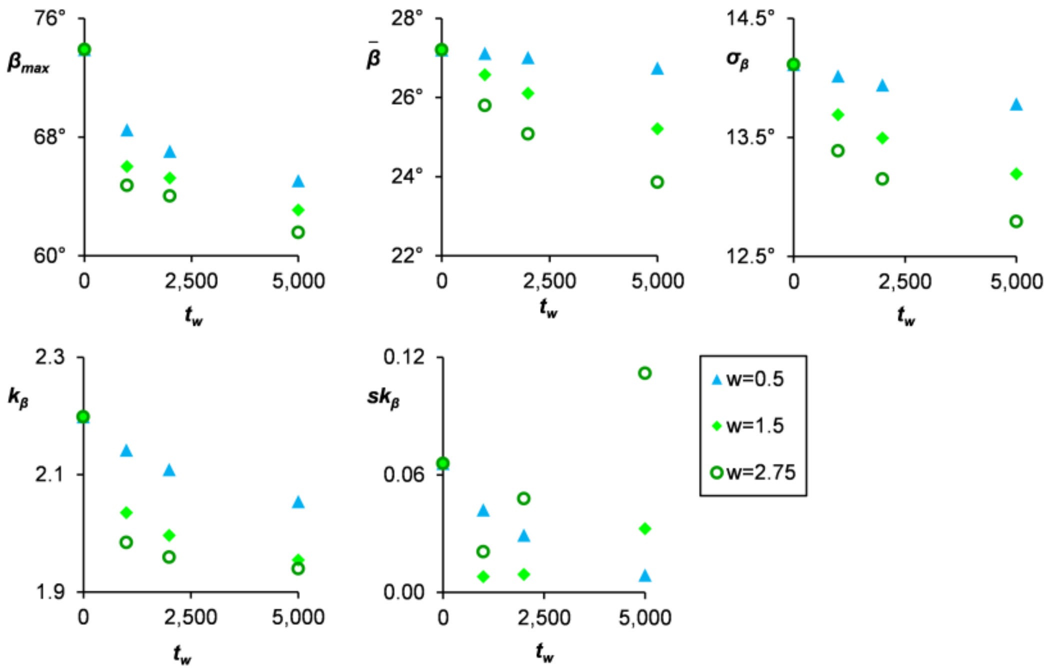


**Fig. 11** Temporal change of the statistical parameters of the slope angle frequency distribution, for $w$ = 0.5, 1.5, 2.75; $t_w$, number of model steps; $\beta_{max}$, maximum; $\bar{\beta}$, mean; $\sigma_\beta$, standard deviation; $k_\beta$, kurtosis; $sk_\beta$, skewness.

The overall temporal behavior of these parameters consists of a decrease of their value over time, although exceptions and some differences in the way these values decrease can be observed. The values of $\bar{\beta}$ and $\sigma_\beta$ decrease with increasing $t_w$ and this decrease is higher when the weakening is stronger. The parameter $\beta_{max}$ quickly decreases in the beginning (i.e., from t=0 to t=1,000) and then the decrease slows down. A similar behavior is observed for $k_\beta$, which is a measure of the peakedness or flattening of the distribution, when compared to a normal distribution. A particular behavior is observed for $sk_\beta$, which quantifies the asymmetry of the distribution. Its temporal evolution depends on *w*: for *w* equal to 0.5, the parameter decreases over time, while for *w* values of 1.5 and 2.75 there is an initial decrease followed by an increase of the value. This increase is due to the fact that the change in topography takes place at a faster rate for higher *w*-values. Accordingly, and in agreement with Fig. 10a, the initial decrease of the asymmetry is due to the difference between the decrease of the frequency of high $\beta$ values and the increase of the frequency of low $\beta$ values, while the subsequent increase of the asymmetry is mainly due to the increase of the relative importance of the lower $\beta$, over time.

The values of the statistical parameters of slope angles of the final topography also depend on the rate of weakening. In particular, we have found that $\bar{\beta}$ and $\sigma_\beta$ are linearly linked with $w$ according to the following equations:

$$\bar{\beta} = -m_{\bar{\beta}} \cdot w + c_{\bar{\beta}} \qquad (5)$$

$$\sigma_\beta = -m_\sigma \cdot w + c_\sigma \qquad (6)$$

where $m_{\bar{\beta}}$ and $m_\sigma$ are the angular coefficients of the best fit lines and $c_{\bar{\beta}}$ and $c_\sigma$ are constants, which depend on $t_w$ ($R^2 \cong 0.99$ for $\bar{\beta} = f(w)$ and $R^2 \geq 0.97$ for $\sigma_\beta = f(w)$). The relationships are illustrated in Fig. 12. According to Eqs. 5 and 6, the higher the rate of weakening the lower the values of $\bar{\beta}$ and $\sigma_\beta$ of the final surface - that is, the higher the change of the topographic surface caused by landslides.

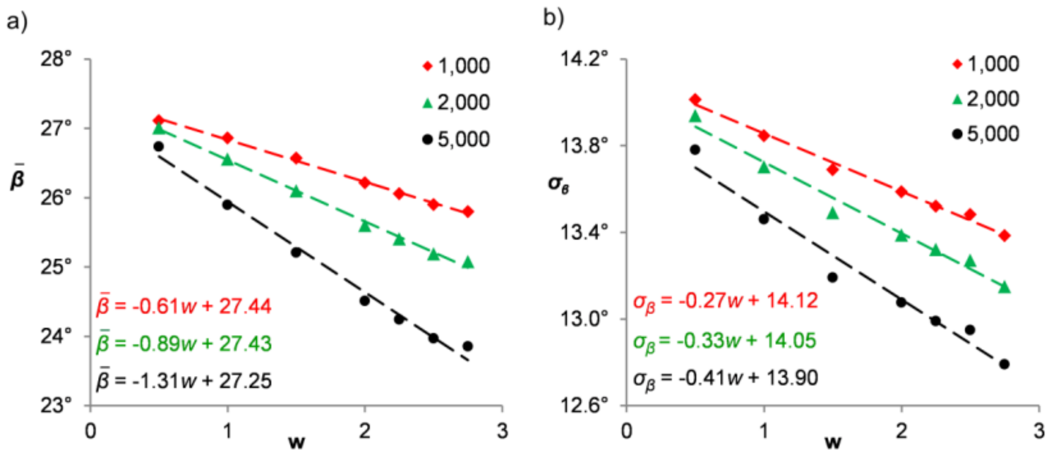


**Fig. 12** For each $t_w$ (1,000; 2,000; 5,000 model steps), (a) mean $\bar{\beta}$ and (b) standard deviation $\sigma_\beta$ of slope angles as a function of the rate of weakening $w$, and their respective linear best fit lines.

## 6. Relation between topographic changes and scaling properties of landslide sizes

In this section the relationship between topographic changes and the statistical behavior of landslide sizes is investigated.

We observed that landslide phenomena produce a smoothing of the topographic surface, which results in a decrease of the main statistical parameters of the frequency distribution of $\beta$, in time (Fig. 11). Unlike $\beta$, the scaling exponent $D$ of the frequency distribution of landslide does not show any specific trend over time (Fig. 6d). Thus, the probability of landslide sizes and the changes undergone by the topographic surface exhibit different types of behavior over time. Instead, we observed that they manifest similar dependence on the rate of weakening $w$. In particular, we found that the scaling exponent $D$, the mean $\bar{\beta}$ and the standard deviation $\sigma_\beta$ of slope angles linearly decrease with increasing $w$ (Figs. 6a, 6b, 6c and 12). Thus, by substituting in turn Eqs. 5 and 6 in Eq. 4 we obtain:

$$D = m_1 \cdot \bar{\beta} + c_1 \qquad (7)$$

$$D = m_2 \cdot \sigma_\beta + c_2 \qquad (8)$$

where $m_1 = m_D/m_{\bar{\beta}}$ and $m_2 = m_D/m_\sigma$ are the angular coefficients of the best fit lines, and $c_1$ and $c_2$ are constants. Figure 13 shows the same result obtained by plotting, for each $t$, $D$ as a function of $\bar{\beta}$ (Fig. 13a) and $\sigma_\beta$ (Fig. 13b) obtained for the same $w$. The best fit lines have $R^2 \geq 0.95$ and $R^2 \geq 0.94$, in Fig.13a and 13b, respectively.

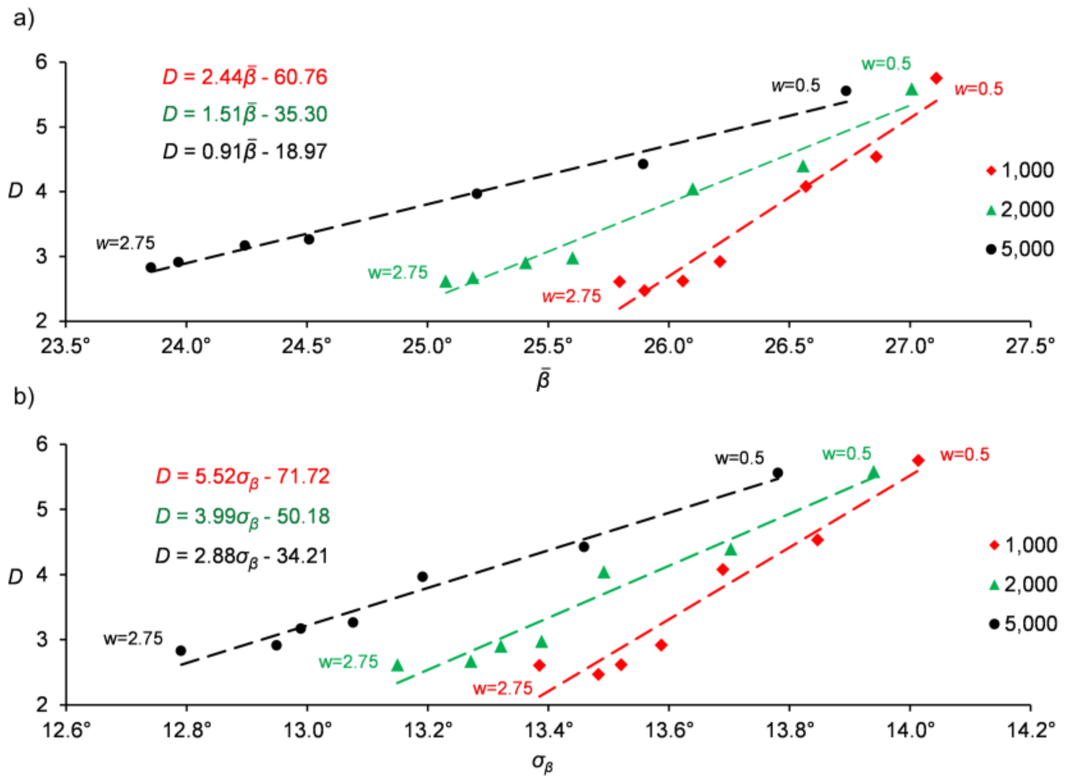


**Fig. 13** For each $t_w$ (1,000; 2,000; 5,000 model steps), $D$ as a function of (a) the mean $\bar{\beta}$ and (b) the standard deviation $\sigma_\beta$ of slope angles of the topographic surface, and their respective linear best fit. For each point, $w$ indicates the value of the rate of weakening at which $D$, $\bar{\beta}$ and $\sigma_\beta$ were obtained.

This result indicates that at each time span $t_w$, the scaling exponent $D$ that characterizes the probability of landslide sizes is linearly related, with a good approximation, to the values of the statistical parameters of the slope angles of the topographic surface where landslides occurred. In particular, the positive correlation of $D$ with $\bar{\beta}$ and $\sigma_\beta$ respectively, shows that an increase of $w$ (i.e., moving from the right extreme of the linear best fits to the left in Fig. 13) produces a decrease of $D$ and thus an increase of the probability of large landslide sizes, which is linearly related to the decrease of the mean and standard deviation of the slope angles of the final surface. In other words, the statistical parameters of the modeled topography preserve information about the probability of landslide sizes that occurred during a specific $t_w$ and under the action of a specific $w$. The Eqs. 4 to 8 indicate that the way the values of $D$, $\bar{\beta}$ and $\sigma_\beta$ change with $w$ may be described by linear mathematical laws, which respectively work for all the time spans $t_w$ tested and for which only the value of the linear fit parameters of the equation (slope and intercept) are different for the different $t_w$. Both in Figs. 13a and 13b we observe that going from $t_w = 1{,}000$ to $t_w = 5{,}000$ the steepness of the best fit lines decreases; that is, the angular coefficients $m_1$ and $m_2$ of Eqs. 7 and 8 decrease over time. This result indicates that the way $D$ is linked to the topographic change depends on the time span. In the next section we discuss outcomes, implications and limitations of the results obtained, including time-related aspects.

## 7. Discussion

The frequency distribution of landslide sizes characterizes the probability of landslide of a given magnitude. A property of this distribution identified in many landslide datasets around the world is the characteristic power-law decay of the frequency from medium to large sizes. Although small slope failures are the most frequent ones in landslide datasets, larger landslides represent the main hazard in terms of associated risk. Despite its simple structure, the cellular automata model proposed in this paper has shown to be capable of reproducing key features of landslide processes related to the occurrence of medium to large slope failures. First, the distribution of landslide areas exhibits the typical scaling properties of real landslides, and a good agreement is observed for the values of the scaling exponents when a specific range of values is used for the parameters of the model. Given that in the model the topographic variability is the only component affecting the evolution of the system, this result suggests that the scaling properties of medium to large landslides could actually arise due to topography, thus supporting the conclusions of Frattini and Crosta (2013), who hypothesized that the scaling behavior of landslide sizes could find an explanation in the scaling properties of topography. Furthermore, the comparison of the frequency distributions of landslide areas obtained by using DEMs with different resolutions for the same initial topographic surface showed that neither the shape of the probability distribution nor the value of the scaling exponent are significantly affected by the change from one resolution to another. This indicates that the constraints imposed by topography on the probabilities of landslide areas are about the same at the investigated spatial scales, of 10 m and 25 m, respectively. Moreover, we observed that although the model does not use specific rules to distinguish between the processes of erosion, transport and deposition of landslides as other models do (Guthrie et al., 2008), these different parts of landslides may be recognized in the resulting topography. Also, we found that landslide areas in the model increase with increasing rate of weakening. This result indicates that large landslides are more abundant when the intensity of the triggering mechanism is high, in agreement with findings from real geographic contexts (Saito et al., 2014). These similarities suggest that other properties observed for the model and discussed below may also describe properties of real systems.

We found that the scaling exponent of the landslide area frequency distribution linearly decreases with increasing driving rate, thus indicating that the faster the system is driven to instability the higher becomes the probability of large landslides. This result supports the hypothesis of Piegari et al. (2009), who conclude that the frequency-size distribution of landslides is controlled by the rate of approaching instability more than by the type of triggering mechanism per se. This could actually explain why landslide inventories generated for different triggering mechanisms, like rainfall and snowmelt, exhibit similar frequency–size statistics of landslides (Pelletier et al., 1997; Malamud et al., 2004). Additionally, our results suggest that the value of the scaling exponent is controlled by the way the topographic variability characterizing the area combines with the temporal effectiveness of the mechanism generating instability. A behavior similar to that of the scaling exponent was observed for the mean and standard deviation of the local slope angles of the surface, which under the action of landslides linearly decrease with increasing rate of weakening. Moreover, we observed that for the same driving rate, the value of the scaling exponent does not significantly change in time, contrary to what happens for the main statistical values of the slope angles of the surface, which show a decrease over time. Finally, we found that for a given time window, the scaling exponent of landslide areas, the driving rate, and the changes of the topographic setting are related to each other. In Section 2.2 we explained that the rate of weakening $w$ in the model may represent, for example, the rate of snow melt or the intensity of rainfall, or more generally, the temporal effectiveness with which the triggering mechanism weakens the soil, such as the temporal increase of the pore pressure by water, under the assumption of homogeneous soil properties. While in the model $t_w$ is the sum of both the weakening steps and the landsliding steps, and although $t_w$ does not have a characteristic scale length, the higher $t_w$ is, the wider is the time window during which the system is driven to instability. Thus, a higher $t_w$ represents a longer application of the triggering mechanism in real systems. With reference to rainfall, it has been widely shown that the triggering of landslides can be related to rainfall intensity-duration thresholds (or analogously, cumulated rainfall - rainfall duration thresholds) (Guzzetti et al., 2007; Peruccacci et al., 2012, Salciarini et al., 2012). Our results suggest that for an area of given topography, while this threshold governs the triggering of landslides, the probability of landslide areas depends on the intensity of the triggering mechanism more than on its duration, which mainly affects the number of landslides. Indeed, we found that the value of the scaling exponent is much more sensitive to the rate of weakening than to time (as shown in Fig. 6). Conversely, what we found to be strongly time-dependent is the footprint left on the topographic surface by landslides. Moreover, we observed that the topographic setting of the area modeled preserves the information concerning the statistical distribution of landslide areas caused by a triggering event of given intensity and duration: based on the equations established above (Eqs. 7 and 8), by studying the topographic change of topography in the model, it would be possible to go back to the scaling exponent of the frequency distribution of landslide areas that caused that change. Some critical considerations must be added to the above. The model does not take into account river erosion and uplift, which are processes that allow for the rejuvenation of the system (Pucci et al., 2014) and landslide triggering. However, studies have shown that landslide erosion is not only the way in which hillslopes adjust in response to river channel incision. Rather, it plays an active role in shaping the landscape also independently of river processes and as a consequence of triggering mechanisms like rainfall (Korup, 2010; Reinhardt et al., 2015; Singh et al., 2015), and this role is mainly effective on smaller timescales (Korup, 2010). Thus, the choice whether or not to consider fluvial processes in the model should not affect the possibility to represent landslide dynamics and to investigate the scaling properties of this phenomenon.

Uplift is a long-term driving factor for landslide processes. Ignoring this process in the model implies that if we left the topographic surface free to evolve for a much larger number of model steps it would eventually become an almost flat surface. According to such a scenario, the surface would reach a maximum slope gradient equal to the one below which cells are always stable. This situation is not plausible in a dynamic geomorphological context affected by landslides. However, studies have shown that the rate of erosion by rivers and slope failures is regulated by the way the rate of uplift and the rate of precipitation interact with each other. Various scenarios have been described, where depending on the relative changes in uplift and precipitation the landscape evolves in different ways and with different erosion rates and mechanisms (Bonnet and Crave, 2006). The different types of system behavior have been described by defining, for example, specific uplift thresholds, which characterize the type of process that dominates the mountain range evolution, where slope failures occur in response to the rise of the surface (Ouchi, 2011, 2015). As explained above, in our model the driving rate could be thought of as representing the intensity of the landslide triggering mechanism, assuming constant intensity over time, and the higher the number of model steps, the longer the application of the triggering mechanism. Accordingly, although the model does not use a characteristic timescale, results from the model must be interpreted in the light of the possible maximum realistic duration of a triggering event, which can range from several days to several months depending on the climate of the area. Thus, we are studying the properties of the scaling behavior of landslides that occurred during one and the same erosion event, which happens in response to uplift – that is, the erosion operated by landslides in response to a rise of the topographic surface, which allows the equilibrium to be restored. In this context, while uplift affects the long-term evolution of landforms, for the single erosional event it only represents the underlying cause. Based on these considerations, it is reasonable to consider that the properties observed for the scaling behavior of landslides could actually describe real properties of landslide processes. This idea is also supported by real-world studies, which found scaling properties in landslide datasets compiled both for long time spans and after a single triggering event (Guzzetti et al., 2002; Guthrie and Evan, 2004; Malamud et al., 2004), thus suggesting that the scale-invariance of landslides does not appear in the system only as a consequence of its long-term evolution, but rather manifests itself in a landscape, whose configuration is the result of its evolutionary history.

As for the possible SOC behavior of landslides, in Fig. 6d we observed that at the lowest rates of weakening, that is, at the rates at which the change of topography caused by landslides is low, the scaling exponent is nearly stable over time. Conversely, at the highest rates of weakening corresponding to the most ample changes in topography, a change of the exponent trough time is observed. In summary, small topographic changes lead to small temporal changes in the scaling exponent, while more significant transformations in topography are associated with major variation in the values of the scaling exponent. This result indicates that the behavior of the model does not exhibit SOC dynamics, and this is due to the fact that rejuvenation processes such as uplift are neglected, thus implying that in the model, topography cannot tend toward a dynamical steady state, unlike what has been hypothesized for topography in nature (Bonnet and Crave, 2003; Lague et al., 2003).

**8. Conclusions**

The cellular automata model (CA) proposed in this paper is capable of reproducing the power-law decay of the probability distribution of real landslide areas for a range of model parameter values. In analogy with the CA model by Hergarten and Neugebauer (2000), who firstly used a time-dependent variable in a CA model, our results confirm the key role that the temporal rate of weakening exerts in landslide dynamics. Model outputs provide insights into the variability of the scaling exponents observed in reality, indicating that the power-law scaling of medium to large landslide areas results from the interplay of the topographic spatial variability and the rate at which the system is driven to instability, which in the real world may be thought of as representing, for example, rainfall intensity. The fundamental difference between this model and the previous CA models used to study the frequency distribution of landslide areas consists of the topographic control of both the displaced mass and instability direction; our results point to topography as a major controlling factor in the probability of landslide sizes. Although the spatial variability of a real system is due to the combination of many interdependent factors, it is worth noting that the correspondence between the model outcomes and real landslide sizes is obtained by considering topography as the only factor defining the spatial variability in the system modeled. This result is consistent with the fact that the shapes of the landscape are dependent on geological and structural aspects of the relief, which constrain the type of the physical processes modeling the surface. To conclude, topography seems to be a good candidate to explain the scaling properties of medium to large landslide sizes, thus supporting with numerical evidence hypotheses made in previous studies (Frattini and Crosta, 2013).

Moreover, according to our results, the modeled topography not only provides explanations for the power law decay of landslide sizes, but also conserves the information about the scaling exponent of the probability distribution of areas of landslides that caused changes in its characteristics.

Incorporating rejuvenation processes like uplift and river erosion in the model could support the further study of long term landslide dynamics, as well as the possible SOC behavior of these processes.


## Acknowledgments

The authors would like to thank the reviewers for their useful input and their constructive criticism.


## REFERENCES


Alvioli, M., Guzzetti, F., Rossi, M., 2014. Scaling properties of rainfall induced landslides predicted by a physically based model. Geomorphology 14, 2637-2648.

Ayalew, L., Yamagishi, H., 2005. The application of GIS-based logistic regression for landslide susceptibility mapping in the Kakuda-Yahiko Mountains, Central Japan. Geomorphology 65, 15-31.

Bak, P., Tang, C., Wiesenfeld, K., 1988. Self-organized criticality. Phys. Rev. A 38(1), 364-374.

Bjerrum, L., 1967. Progressive failures in slopes of overconsolidated plastic clay and clay shales. J. Soil Mech. Fdns. Div. Am. Soc. Civ. Engrs. 93(5), 1-49.

Bonabeau, E., Dessalles, J.L., Grumbach, A., 1995. Characterizing emergent phenomena (1): A critical review. Revue Internationale de Systémique 9(3), 327-346.

Bonnet, S., Crave, A., 2003. Landscape response to climate change; Insights from experimental modeling and implications for tectonic versus climatic uplift of topography. Geology 31(2), 123-126.

Bonnet, S., Crave, A., 2006. Macroscale dynamics of experimental landscapes, In: Buiter, S.J.H., Schreurs, G. (Eds.), Analogue and numerical modelling of crustal-scale processes. The Geological Society, London, UK, pp. 327-340.

Brardinoni, F., Church, M., 2004. Representing the landslide magnitude-frequency relation: Capilano river basin, British Columbia. Earth Surf. Process. Landforms 29, 115-124.

Brunetti, M.T., Guzzetti, F., Rossi, M., 2009. Probability distributions of landslide volumes. Nonlin. Processes Geophys. 16, 179-188.

Chen, A., Darbon, J., Morel, J.-M., 2014. Landscape evolution models: A review of their fundamental equations. Geomorphology 219, 68-86.

Frattini, P., Crosta, G. B., 2013. The role of material properties and landscape morphology on landslide size distributions, Earth Planet. Sci. Lett. 361, 310–319.

Goltz, C, 1996. Multifractal and Entropic Properties of Landslides in Japan. Geol. Rundsch. 85, 71-84.

Guthrie, R.H., Evans, S.G., 2004. Magnitude and frequency of landslides triggered by a storm event, Loughborough Inlet, British Columbia. Nat. Hazards Earth Sys. Sci. 4, 475-483.

Guthrie, R.H., Deadman, P.J., Raymond Cabrera, A., Evans, S.G., 2008. Exploring the magnitude-frequency distribution: a cellular automata model for landslides. Landslides 5:151-159.

Guzzetti, F., Malamud, B.D., Turcotte, D.L., Reichembach, P., 2002. Power-law correlations of landslide areas in central Italy. Earth Planet. Sc. Lett. 195, 169-183.

Guzzetti, F., Reichembach, P., Cardinali, M., Galli, M., Ardizzone, F., 2005. Probabilistic landslide hazard assessment at the basin scale. Geomorphology 72, 272-299.

Guzzetti, F., Peruccacci, S., Rossi, M., Stark, C.P., 2007. Rainfall thresholds for the initiation of landslides in central and southern Europe. Meteorol. Atmos. Phys. 98, 239-267.

Hergarten, S., Neugebauer, H.J., 2000. Self-organized criticality in two-variable models. Phys. Rev. E 61, 2382-2385.

Hergarten, S., 2003. Landslides, sandpiles and self-organized Criticality. Nat. Hazards Earth Sys. Sci. 3, 505-514.

Hergarten, S., 2013. SOC in Landslides. In: Ashwanden, M.J. (Ed.), Self-organized criticality systems. Open Academic Press, Warsaw, Berlin, pp. 379-401.

Katz, O., Aharonov, E., 2006. Landslides vibrating sand box: what controls types of slope failure and frequency magnitude relations? Earth Planet. Sc. Lett. 247, 280–294.

Katz, O., Morgan, J.K., Aharonov, E., Dugan, B., 2014. Controls on the size and geometry of landslides: Insights from DEM computer simulations. Geomorphology 220, 104–113.

Korup, O., 2005, Distribution of landslides in southwest New Zeland. Landslides 2, 43-51.

Korup, O., 2006. Effect of large deep-seated landslides on hillslope morphology, western Southern Alps, New Zealand. J. Geophys Res. – Earth Surf. 111, F01018, doi:10.1029/2004JF000242.

Korup, O., Clague, J.J., Hermanns, R.L., Hewitt, K., Strom, A.L., Weidenger, J.T., 2007. Giant landslides, topography and erosion. Earth Planet. Sc. Lett. 261, 578-589.

Korup, O., Densmore, A.L., Schlunegger, F., 2010. The role of landslides in mountain range evolution. Geomorphology 120(1-2), 77-90.

Iverson, R.M., 2000. Landslide triggering by rain infiltration. Water Resour. Res. 36(7), 1897-1910.

Lague, D., Crave, A., Davy, P., 2003. Laboratory experiments simulating the geomorphic response to tectonic uplift. J. Geophys. Res. 108(B1), doi:10.1029/2002JB001785.

Lee, S., Min, K., 2001. Statistical analysis of landslide susceptibility at Yongin, Korea. Environ. Geol. 40, 1095-1113.

Lehmann, P., Or, D., 2012. Hydromechanical triggering of landslides: From progressive local failures to mass release, Water. Resour. Res., 48, W03535, doi:10.1029/2011WR010947.

Liucci, L., Melelli, L., Suteanu, C., 2014. Scale-Invariance in the Spatial Development of Landslides in the Umbria Region (Italy). Pure and Applied Geophysics 172(7), 1959-1973.

Malamud, B.D., Turcotte, D.L., 1999. Self-Organized Criticality Applied to Natural Hazards. Nat. Hazards 20, 93-116.

Malamud, B.D., Turcotte, D.L., Guzzetti, F., Reichenbach, P., 2004. Landslide inventories and their statistical properties. Earth Surf. Process. Landforms 29, 687-711.

Martin, Y., Rood, K., Shwab, J.W., Church, M., 2002. Sediment transfer by shallow landsliding in the Queen Charlotte Islands, British Columbia. Can. J. Earth Sci. 39, 189-205.

McNamara, J.P., Ziegler, A.D., Wood, S.H., Vogler, J.B., 2006. Channel head location with respect to geomorphologic threshold derived from a digital elevation model: A case of study in northern Thailand. Forest Ecol. Manag. 224, 147-156.

Melelli, L., Pucci, S., Saccucci, L., Mirabella, F., Pazzaglia, F., Barchi, M.R., 2014. Morphotectonics of the Upper Tiber Valley (Northern Apennines, Italy) through quantitative analysis of drainage and landforms. Rend. Fis. Acc. Lincei 25(Suppl 2), S129-S138.

Milledge, D. G., Bellugi D., McKean J. A., Densmore A. L., Dietrich W. E., 2015. A multi-dimensional stability model for predicting shallow landslide size and shape across landscapes, J. Geophys. Res. Earth Surf., 119(11), 2481-2504.

Montgomery, D.R., Brandon, M.T., 2002. Topographic controls on erosion rates in tectonically active mountain ranges. Earth Planet. Sc. Lett. 201, 481-489.

Moore, I.D., Grayson, R.B., Landson, A.R., 1991. Digital Terrain Modelling: A Review of Hydrological, Geomorphological, and Biological Applications. Hydrol. Process. 5(1), 3–30.

Olami, Z., Feder, H.J.S., Christensen, K., 1992. Self-Organized Criticality in a Continuous Nonconservative Cellular Automaton Modeling Earthquakes. Phys. Rev. Lett. 68, 1244-1247.

Ouchi, S., 2011. Effects of uplift in the development of experimental erosion landform generated by artificial rainfall. Geomorphology 127, 88-98.

Ouchi, S., 2015. Experimental landform development by rainfall erosion with uplift at various rates. Geomorphology 238, 68-77.

Packard, N.H., Wolfram, S., 1985. Two-dimensional cellular automata, J. Stat. Phys. 38, 901-946.

Pelletier, J.D., Malamud, B.D., Blodgett, T., Turcotte, D.L., 1997. Scale invariance of soil moisture variability and its implications for the frequency-size distribution of landslides. Eng. Geol. 48, 255-268.

Peruccacci, S., Brunetti, M.T., Luciani, S., Vennari, C., Guzzetti, F., 2012. Lithological and seasonal control on rainfall threshold for the possible initiation of landslides in central Italy. Geomorphology 139-140, 79-90.

Piegari, E., Cataudella, V., Di Maio, R., Milano, L., Nicodemi, M., 2006. A cellular automaton for the factor of safety field in landslides modeling. Geophys. Res. Lett. 33, L01403-L01407, doi: 10.1029/2005GL024759.

Piegari, E., Di Maio, R., Milano, L., 2009. Characteristics scales in landslide modelling. Nonlin. Processes Geophys. 16, 515-523.

Pucci, S., Mirabella, F., Pazzaglia, F., Barchi, M.R., Melelli, L., Tuccimei, P., Soligo, M., Saccucci, L., 2014. Interaction between regional and local tectonic forcing along a complex Quaternary extensional basin: Upper Tiber Valley, Northern Apennines, Italy. Quat. Sci. Rev. 102, 111-132.

Reinhardt, L., Ellis, M.A., 2015. The emergence of topographic steady state in a perpetually dynamic self-organized critical landscape. Water Resour. Res. 51(7), 4986-5002, doi: 10.1002/2014WR016223.

Saito, H., Korup, O., Uchida, T., Hayashi, S., Oguchi, T., 2014. Rainfall conditions, typhoon frequency, and contemporary landslide erosion in Japan. Geology 42, 999–1002.

Salciarini, D., Tamagnini, C., Conversini, P., Rapinesi, S., 2012. Spatially distributed rainfal thresholds for the initiation of shallow landslides. Nat. Hazards 61(1), 229-245.

Singh, A., Reinhardt, L., Foufoula-Georgiou, E., 2015, Landscape reorganization under changing climatic forcing : Results from an experimental landscape. Water Resour. Res. 51(6), 4320-4337, doi:10.1002/2015WR017161

Stark, C.P., Guzzetti, F., 2009. Landslide rupture and the probability distribution of mobilized debris volumes. J Geophys. Res. 114(F00A02):1-16.

Stark, C.P., Hovius, N., 2001, The characterization of landslide size distributions. Geophys. Res. Lett. 28(6), 1091-1094.

Taramelli, A., Melelli, L., 2009. Detecting alluvial fans using quantitative roughness characterization and fuzzy logic analysis using the SRTM data. Int. J. of Computer Sc. and Software Technology 2(1), 55-67.

Tarquini, S., Isola, I., Favalli, M., Mazzarini, F., Bisson, M., Pareschi, M.T., Boschi, E., 2007. TINITALY/01: a new Triangular Irregular Network of Italy, Ann. Geophys. 50, 407-425.

Tarquini, S., Vinci, S., Favalli, M., Doumaz, F., Fornaciai, A., Nannipieri, L., 2012. Release of a 10-m-resolution DEM for the Italian territory: Comparison with global-coverage DEMs and anaglyph-mode exploration via the web, Comput. Geosci. 38, 168-170. doi: doi:10.1016/j.cageo.2011.04.018

Turcotte, D. L., 1997. Fractals and Chaos in Geology and Geophysics, 2nd ed. Cambridge University Press, Cambridge, pp. 398.

Turcotte, D.L., Malamud, B.D., Guzzetti, F., Reichenbach, P., 2002. Self-organization, the cascade model and natural hazards. P Natl. Acad. Sci., USA 99, Supp. 1, 2530-2537.

Van Den Eeckhaut, M., Poesen, J., Govers, G., Verstraeten, G., Demoulin, A., 2007. Characteristics of the size distribution of recent and historical landslides in a populated hilly region. Earth Planet. Sc. Lett. 256, 588–603.

Wolfram, S., 2002. A New Kind of Science. Wolfram Media Inc., Champaign, pp. 1197.

Figure 1 (Color)


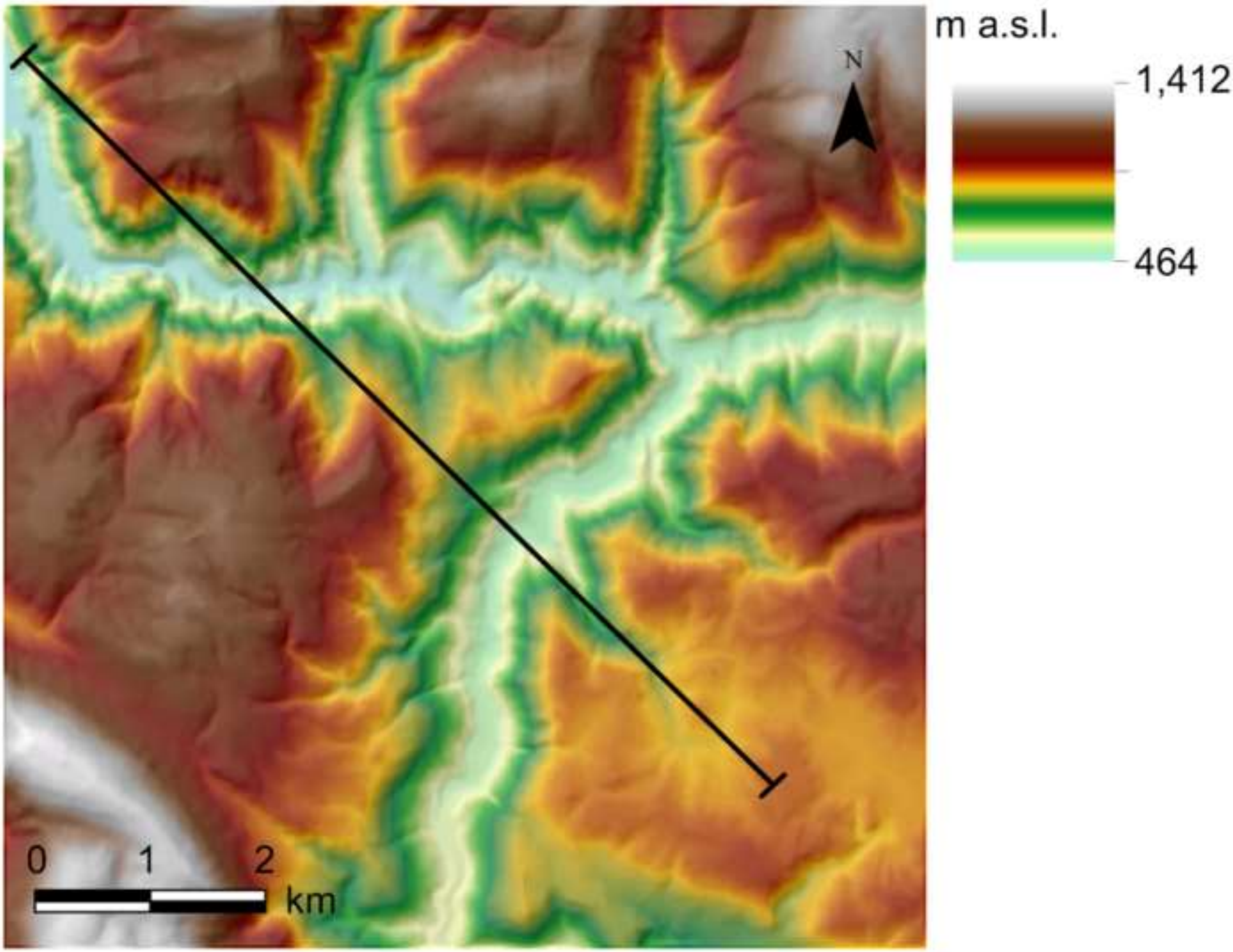

Figure 2 (Color)
Click here to download high resolution image

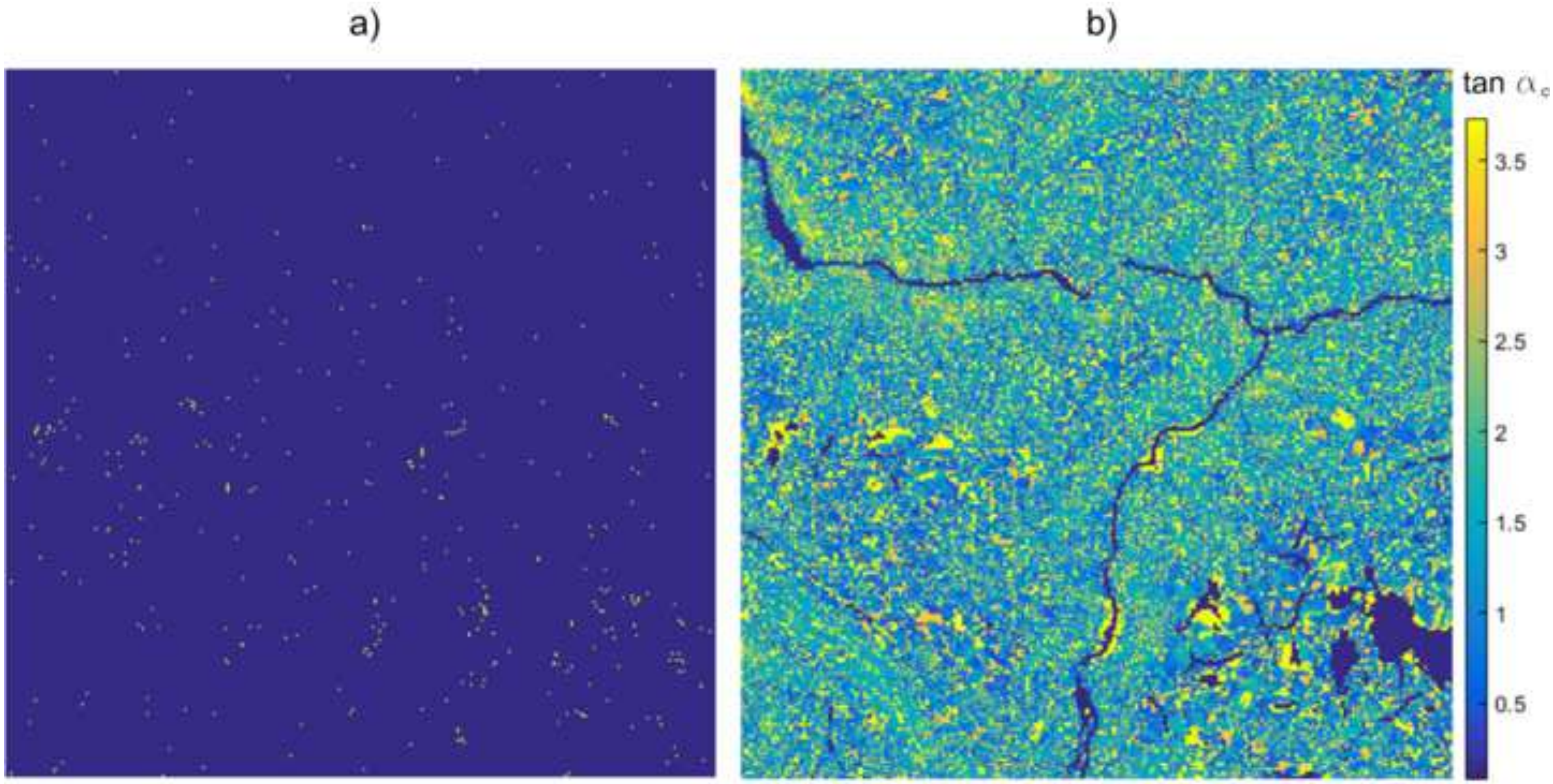

**Figure 3 (Color)**
Click here to download high resolution image

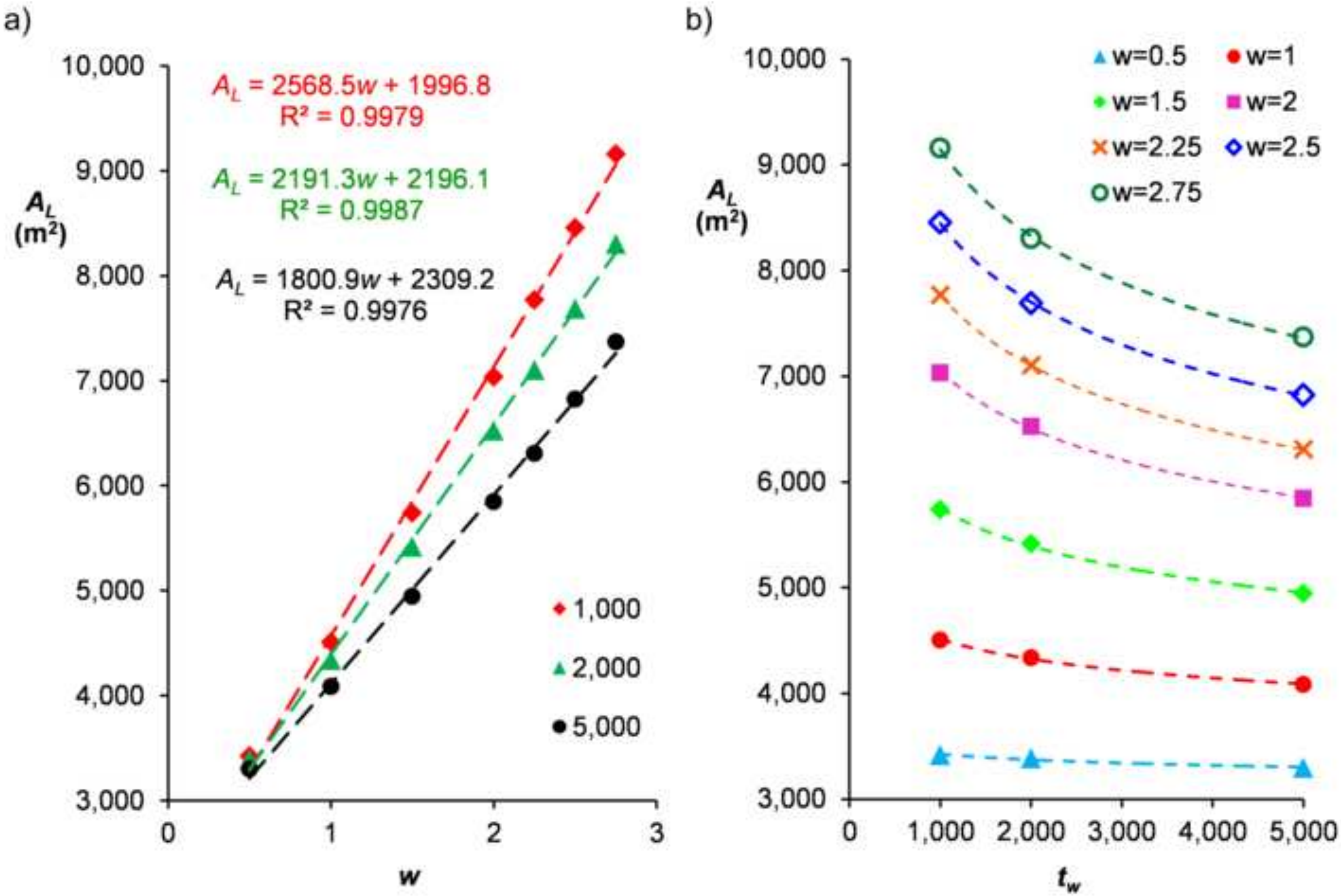

**Figure 4 (Color)**
**Click here to download high resolution image**

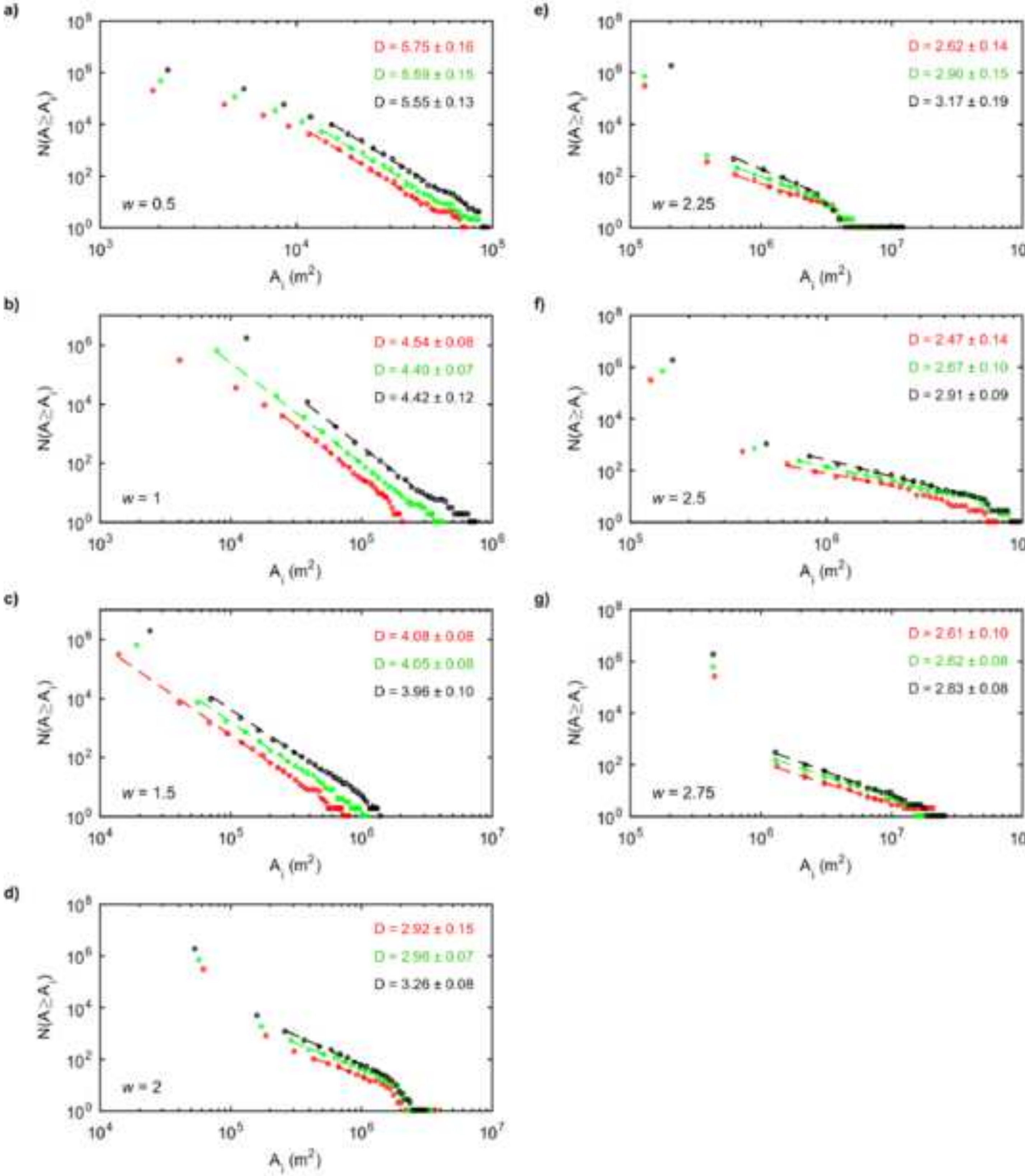

Figure 5 (Color)
Click here to download high resolution image

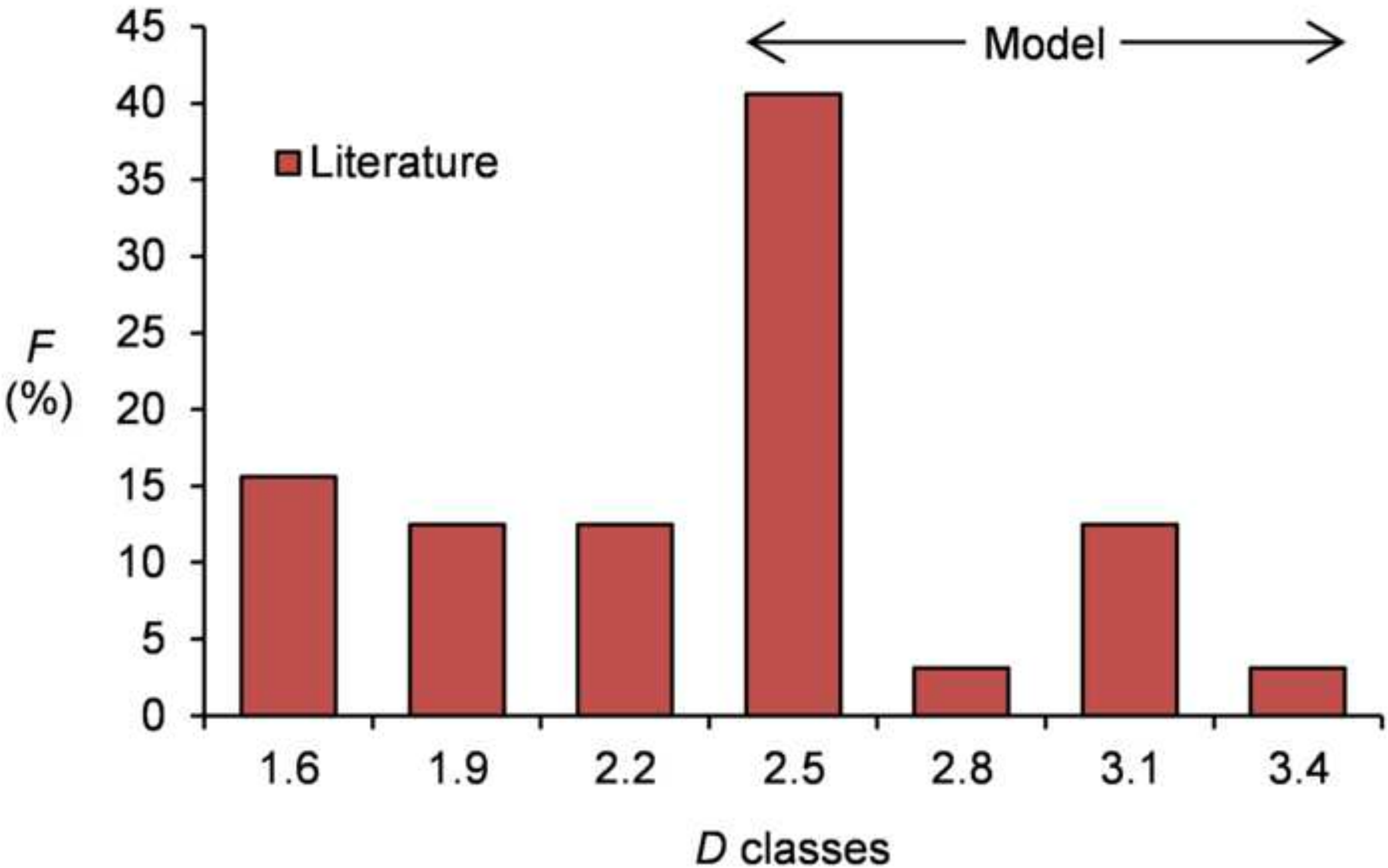

Figure 6 (Color)
Click here to download high resolution image

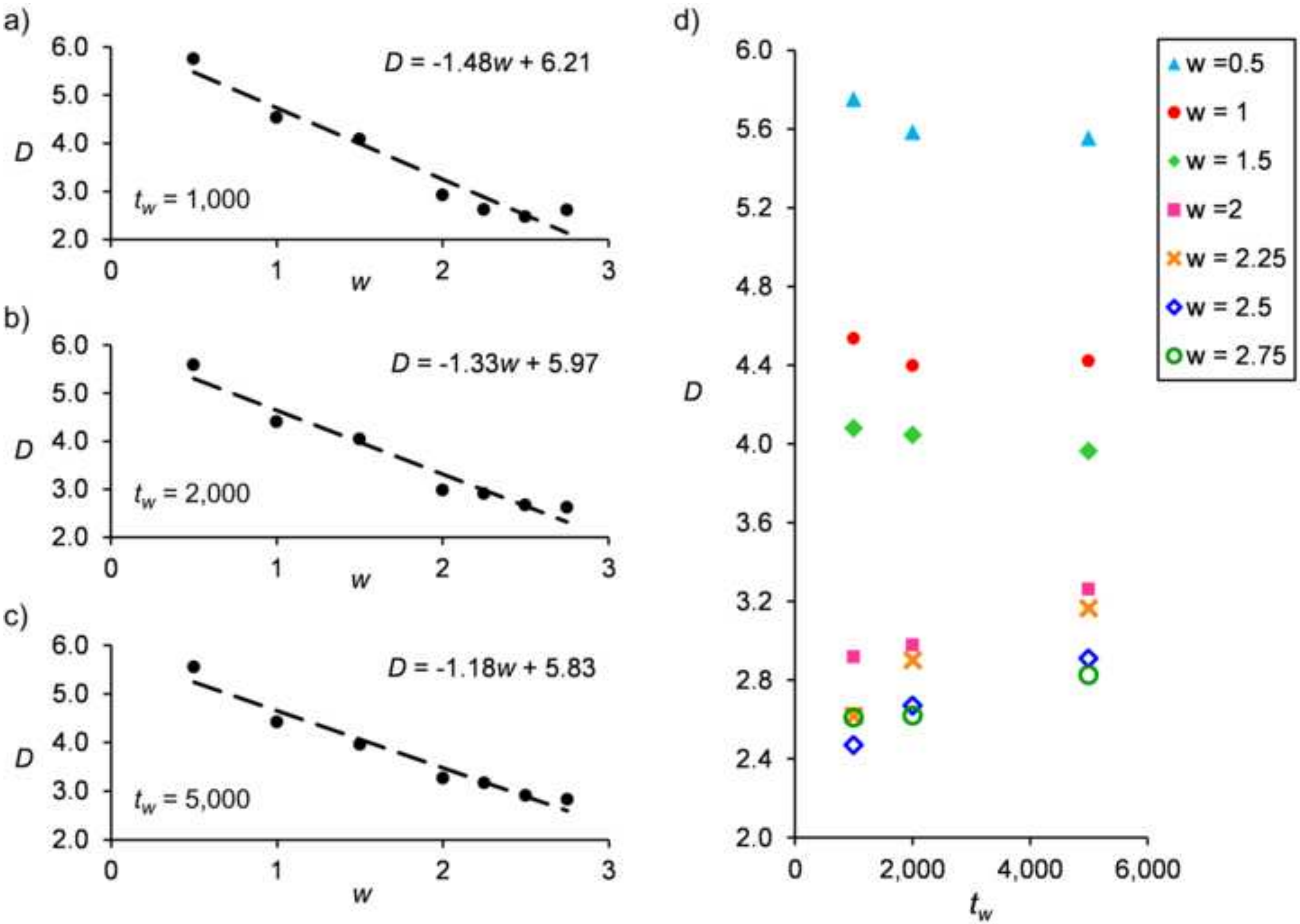

Figure 7 (Color)
Click here to download high resolution image

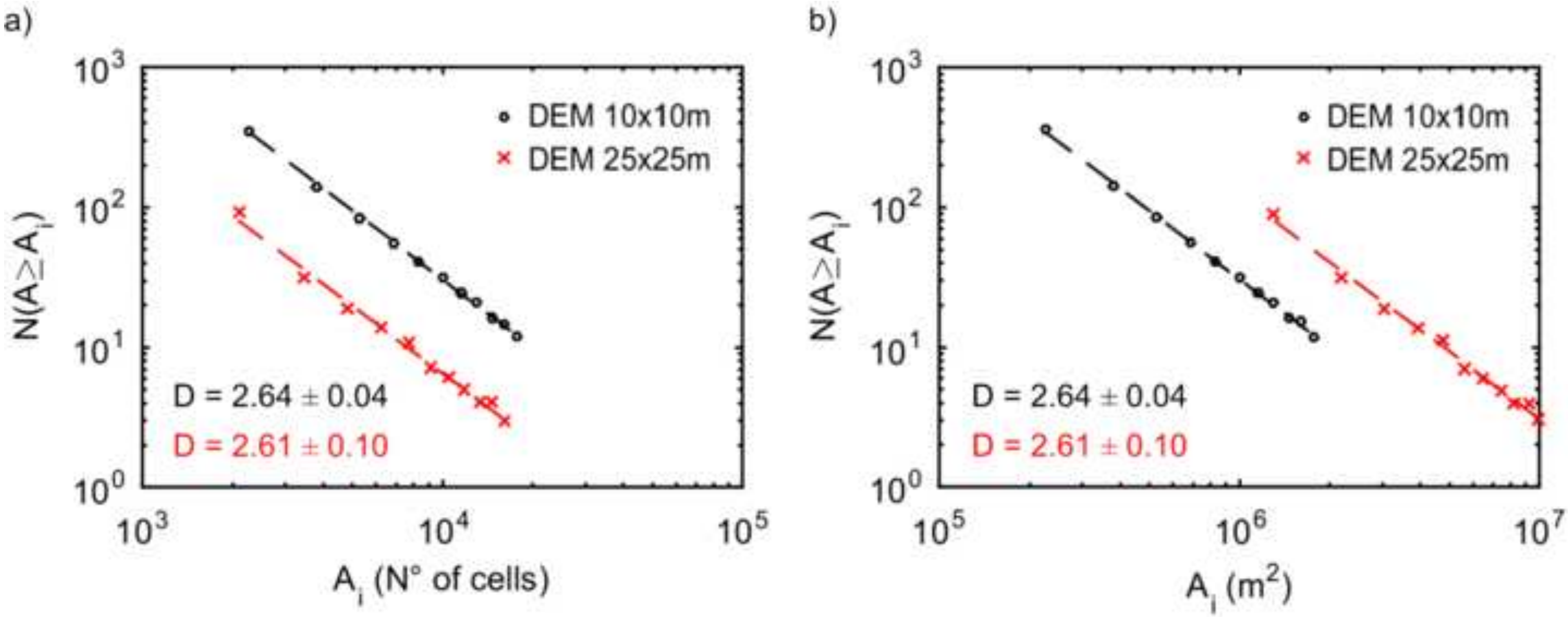

Figure 8 (Color)
Click here to download high resolution image

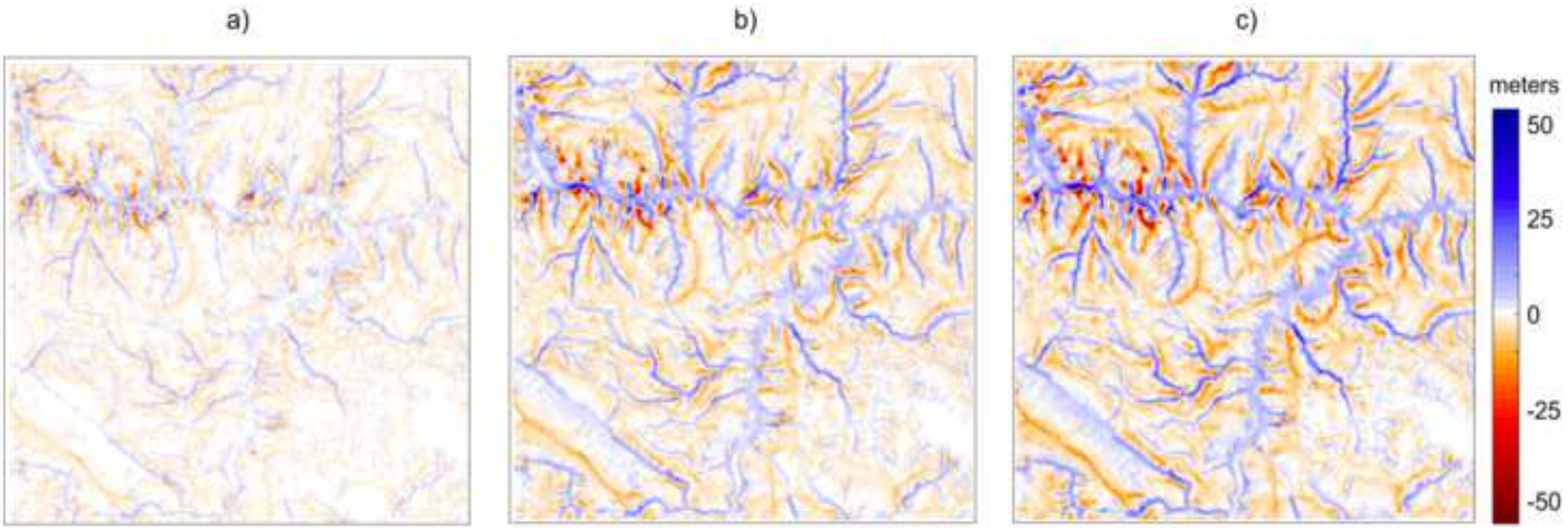

Figure 9 (Color)
Click here to download high resolution image

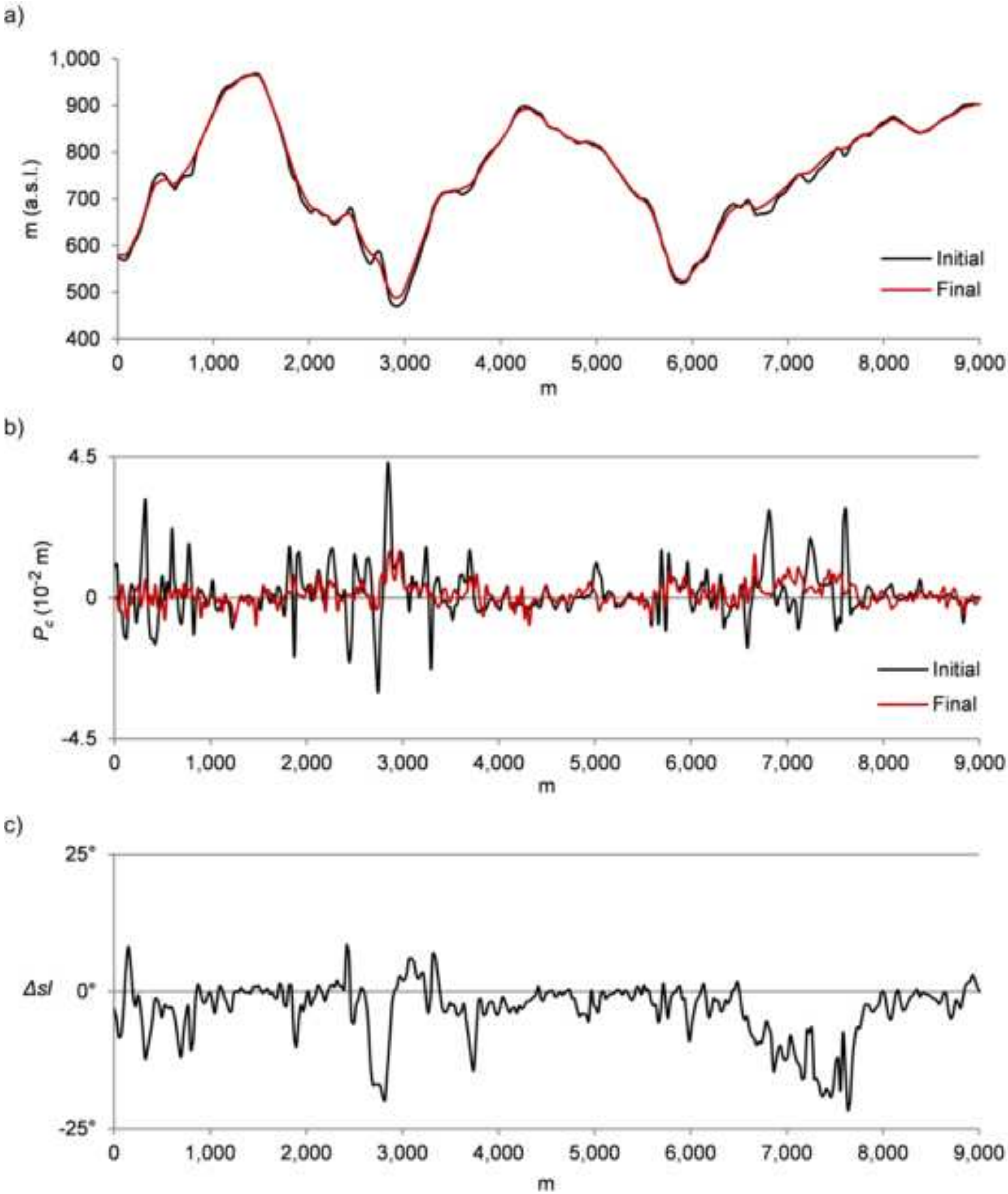

**Figure 10 (Color)**
**Click here to download high resolution image**

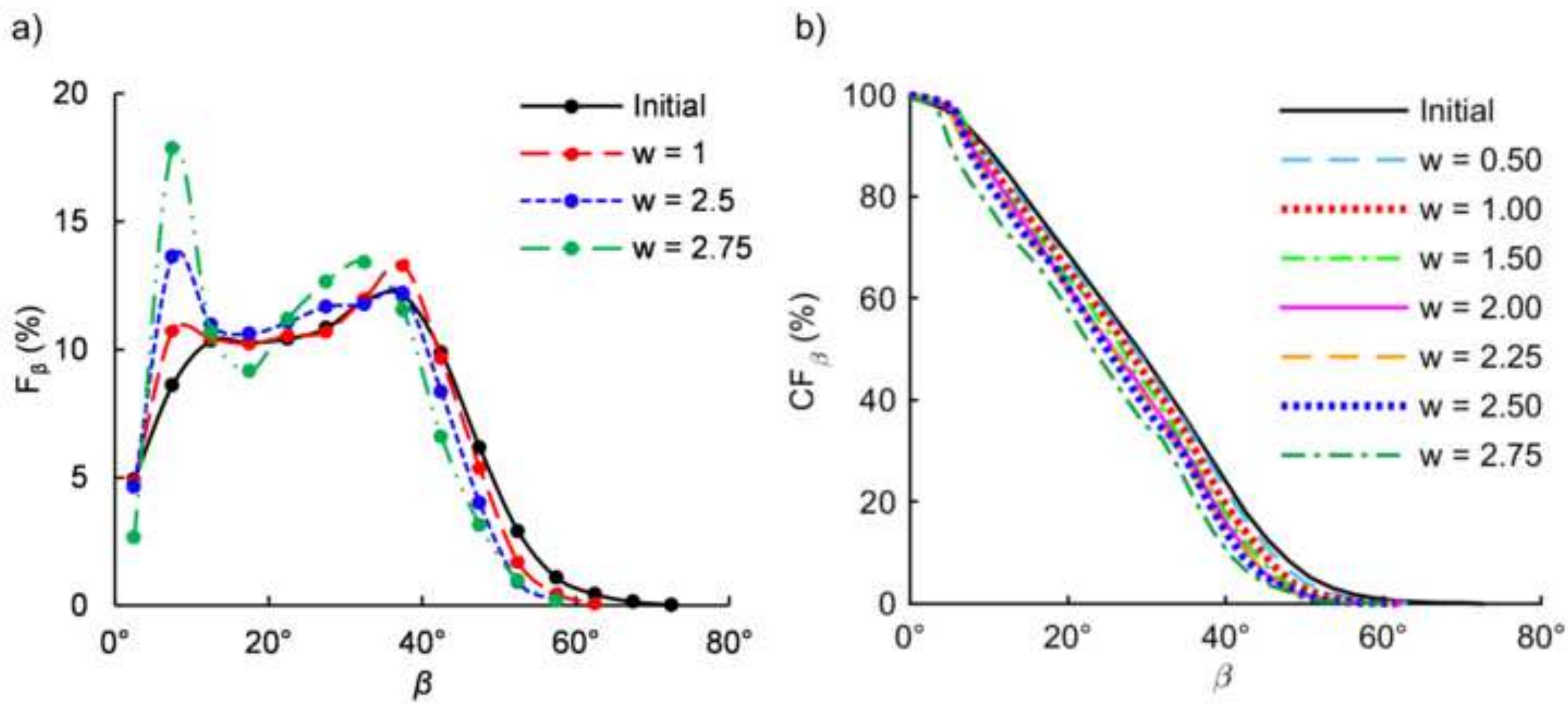

**Figure 11 (Color)**
Click here to download high resolution image

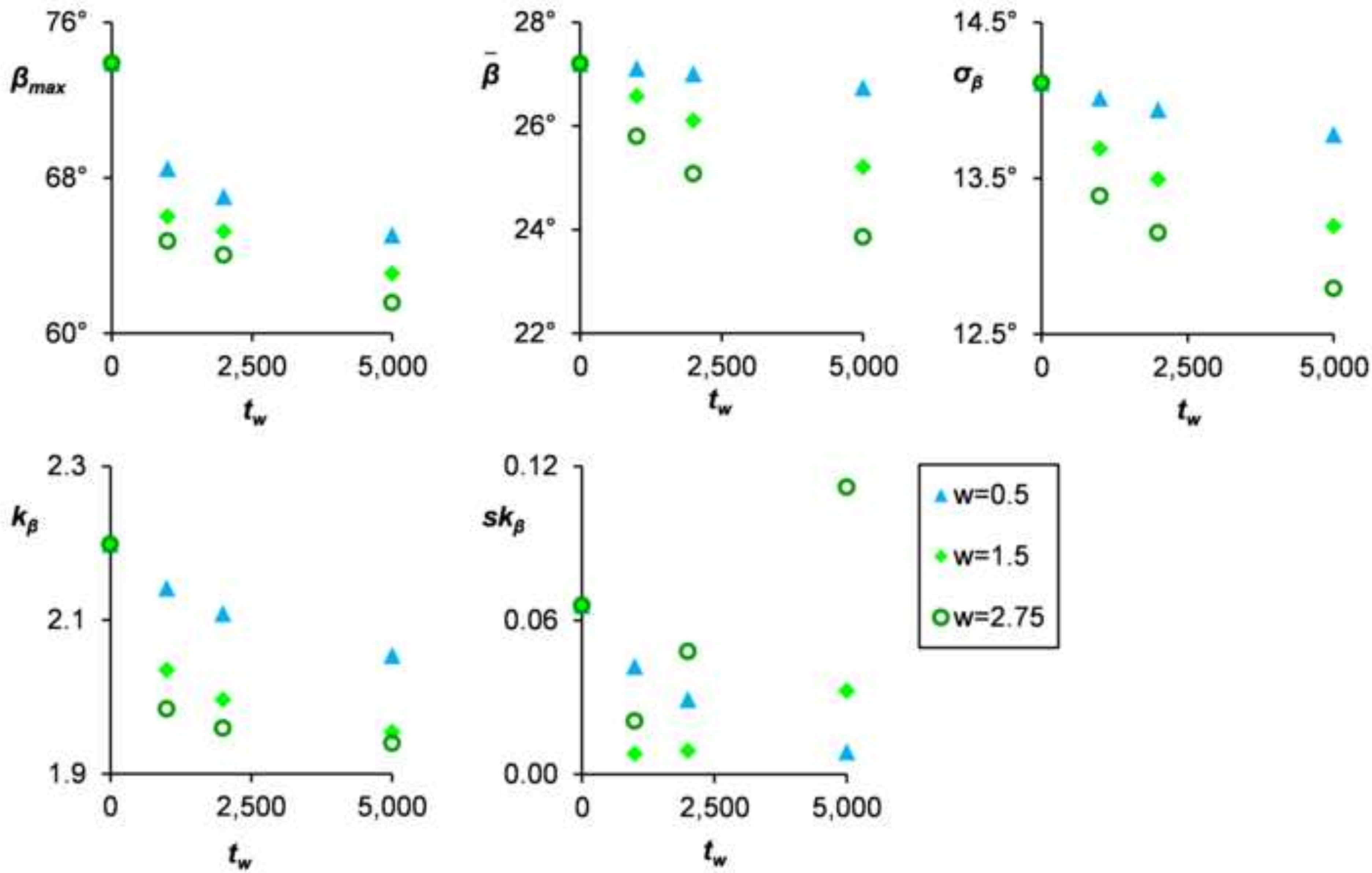

Figure 12 (Color)

Click here to download high resolution image

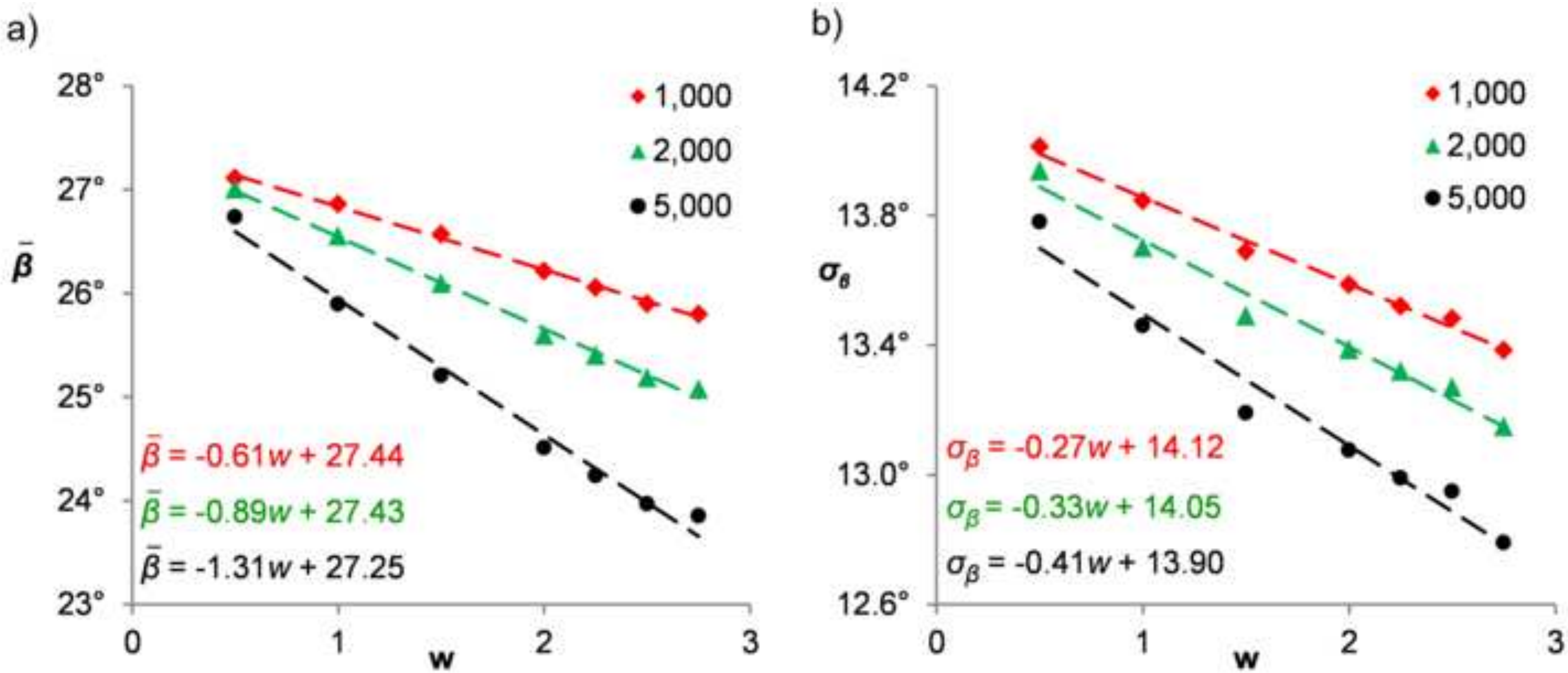

Figure 13 (Color)
Click here to download high resolution image

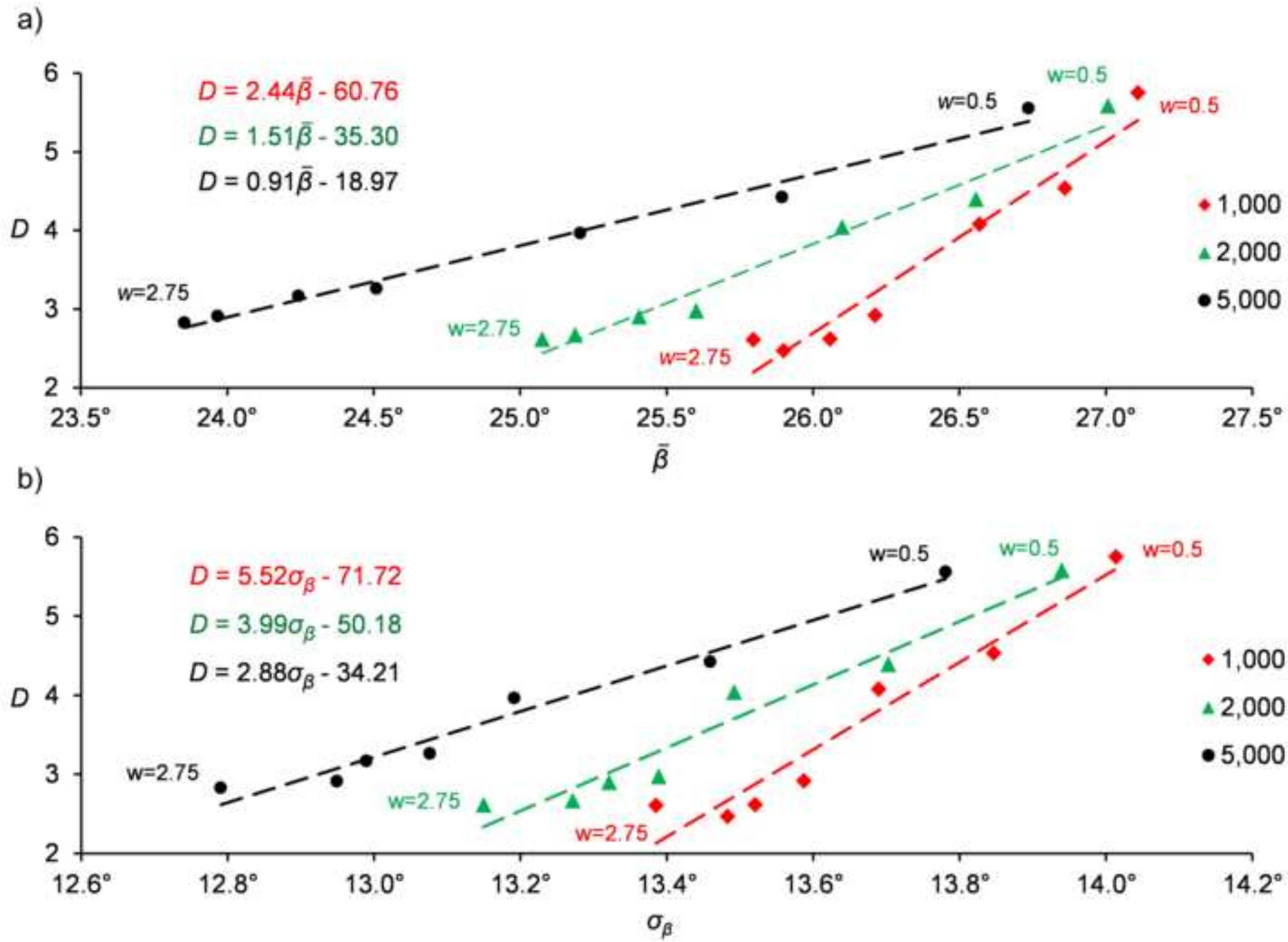

Figure 1 (Greyscale)
Click here to download high resolution image

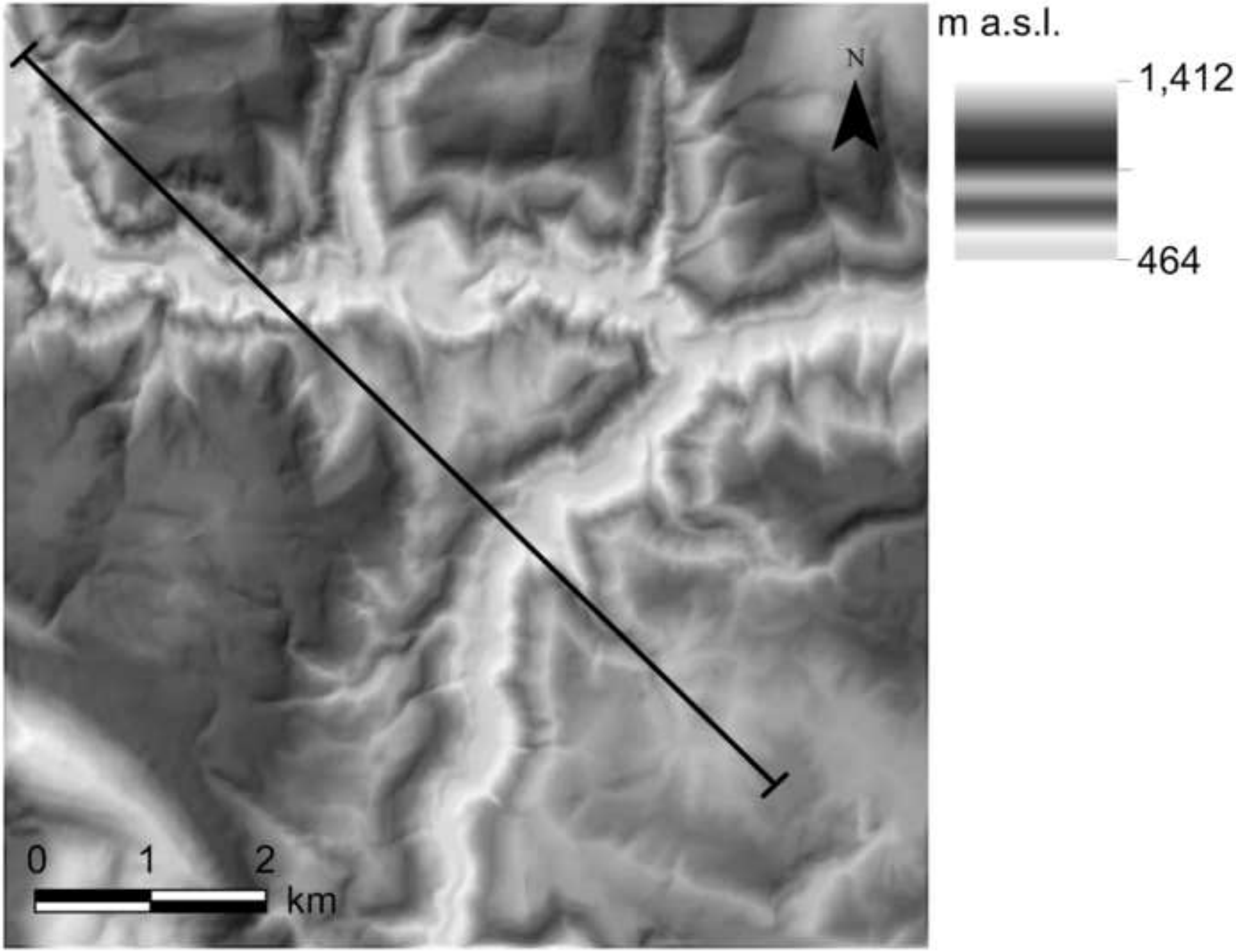

**Figure 2 (Greyscale)**

Click here to download high resolution image

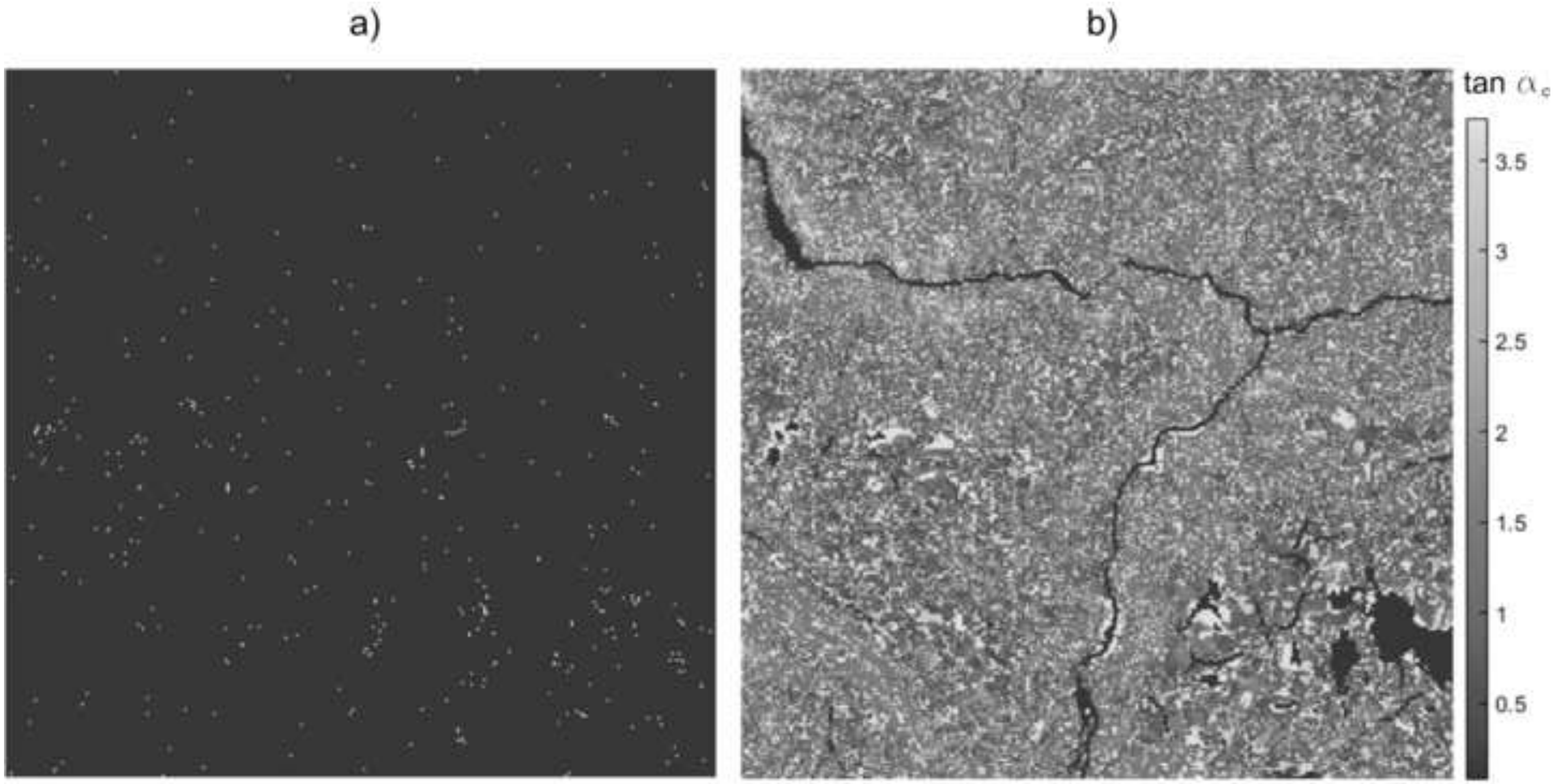

Figure 3 (Greyscale)
Click here to download high resolution image

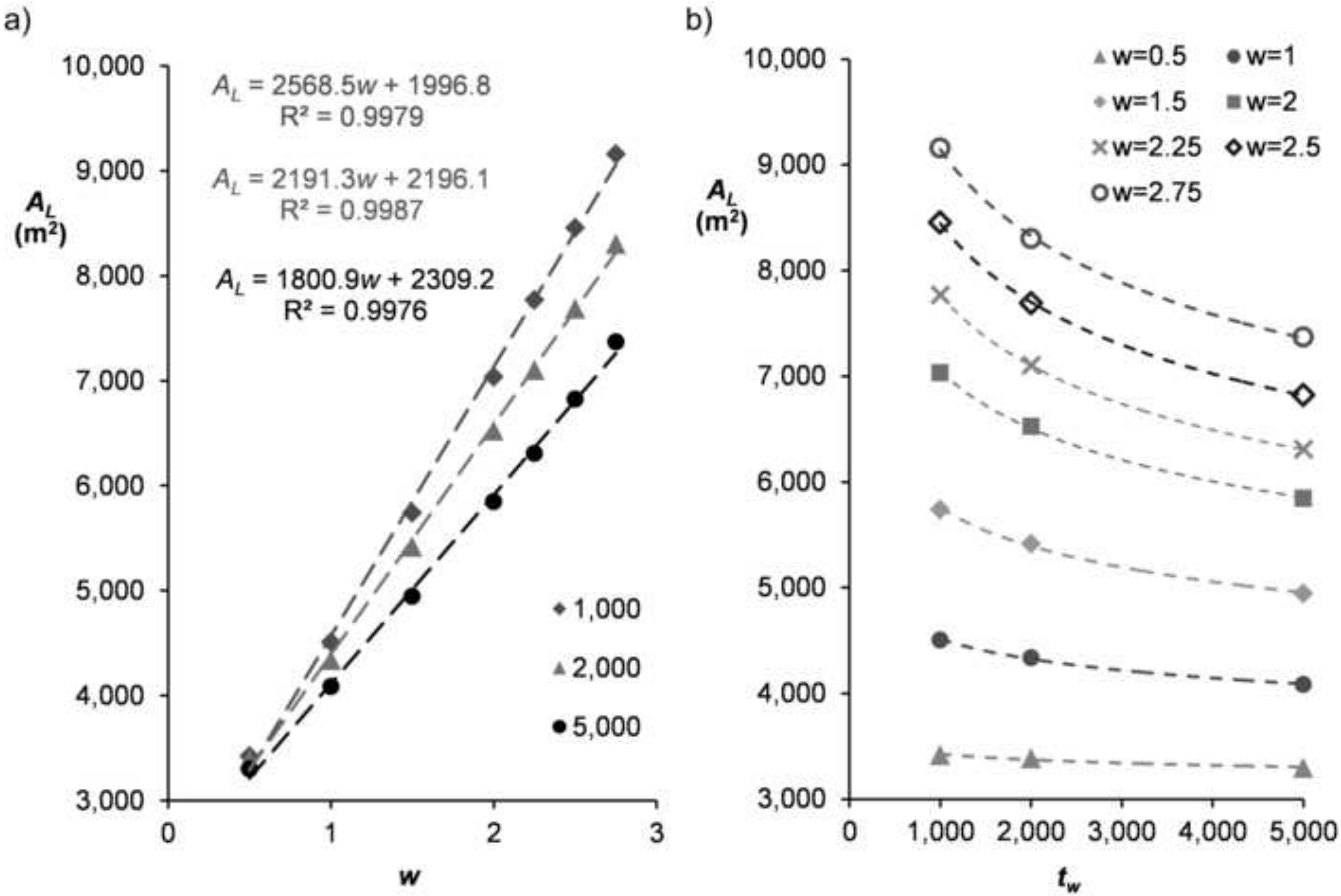

Figure 4 (Greyscale)
Click here to download high resolution image

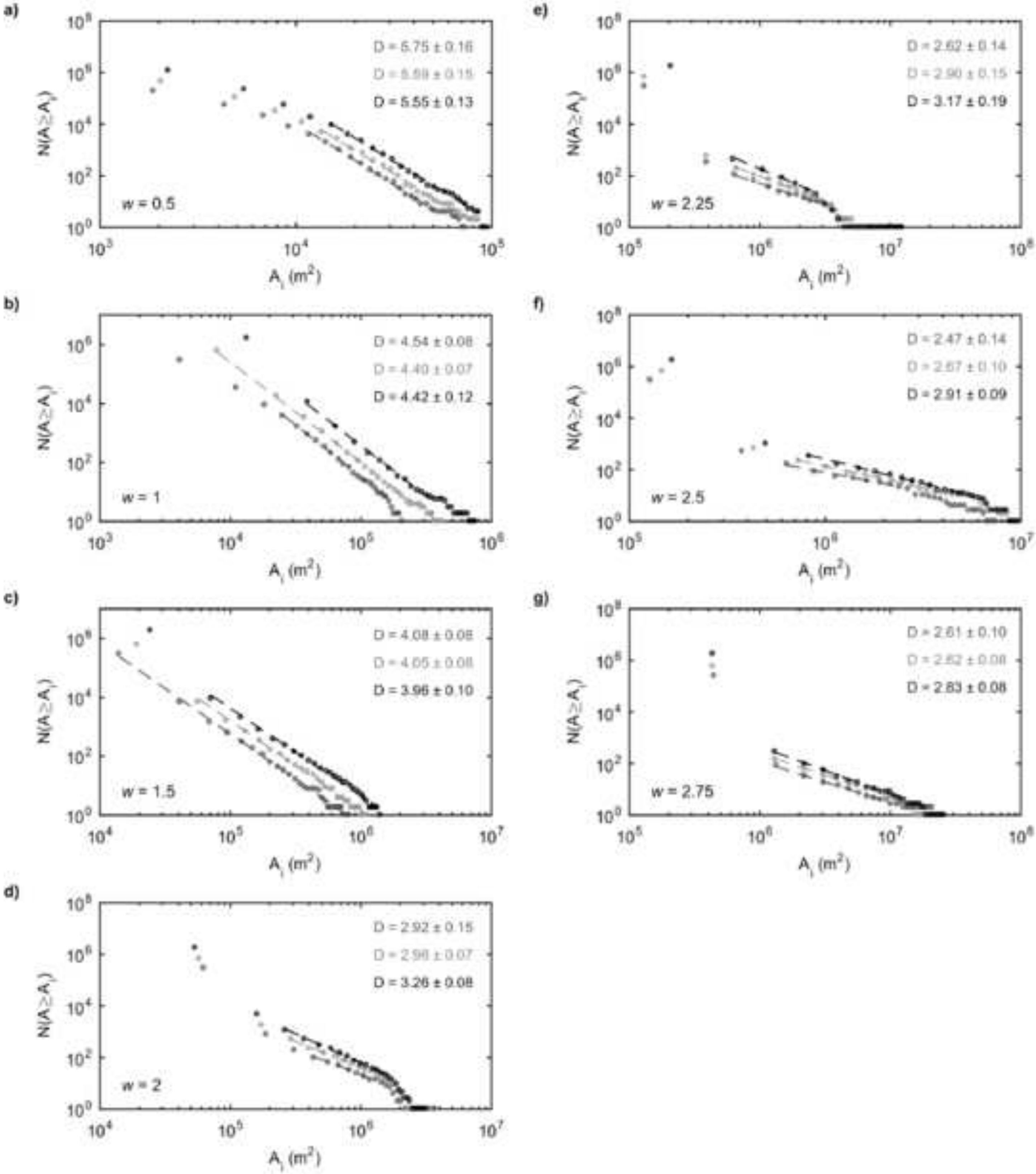

Figure 5 (Greyscale)
Click here to download high resolution image

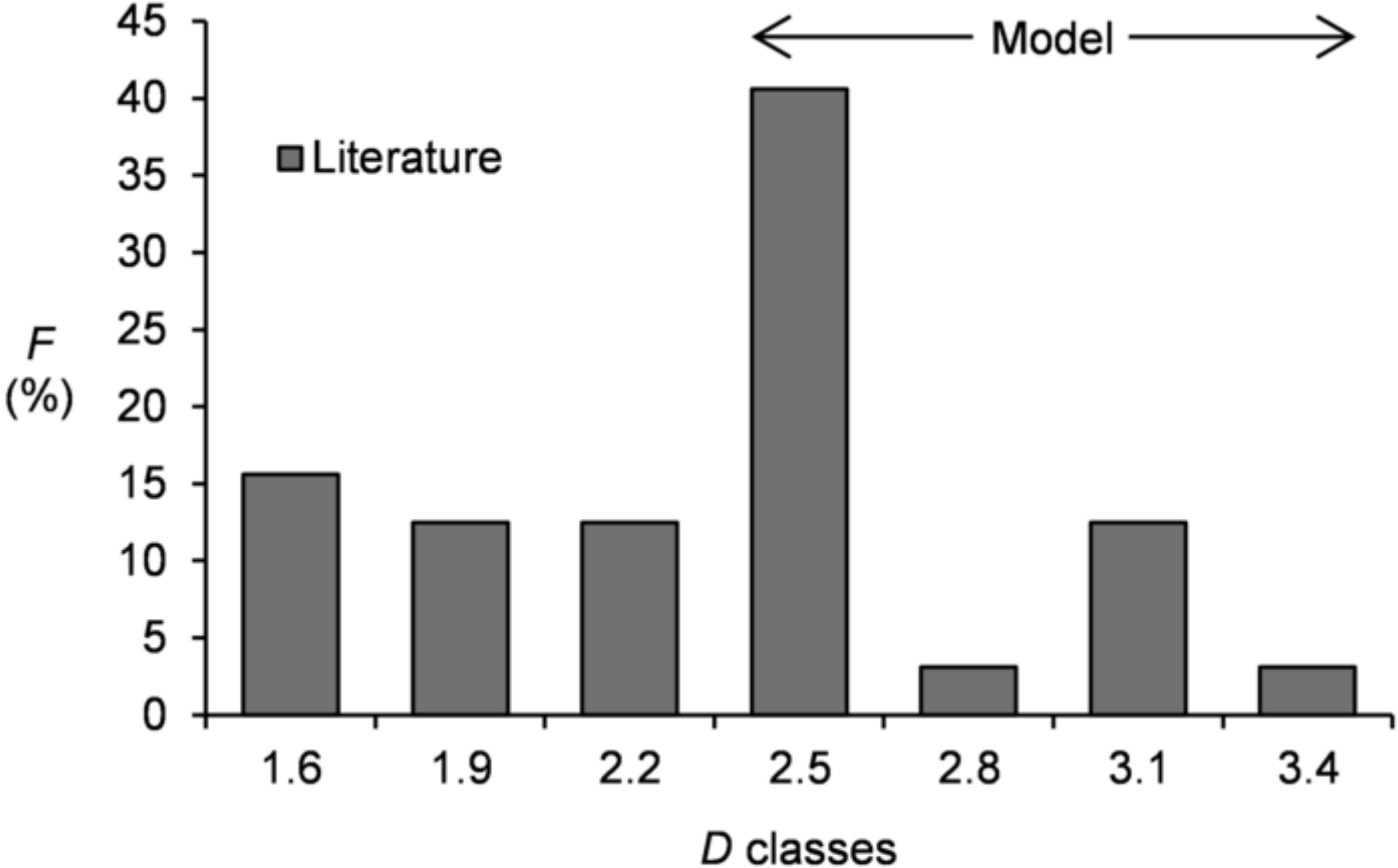

Figure 6 (Greyscale)
Click here to download high resolution image

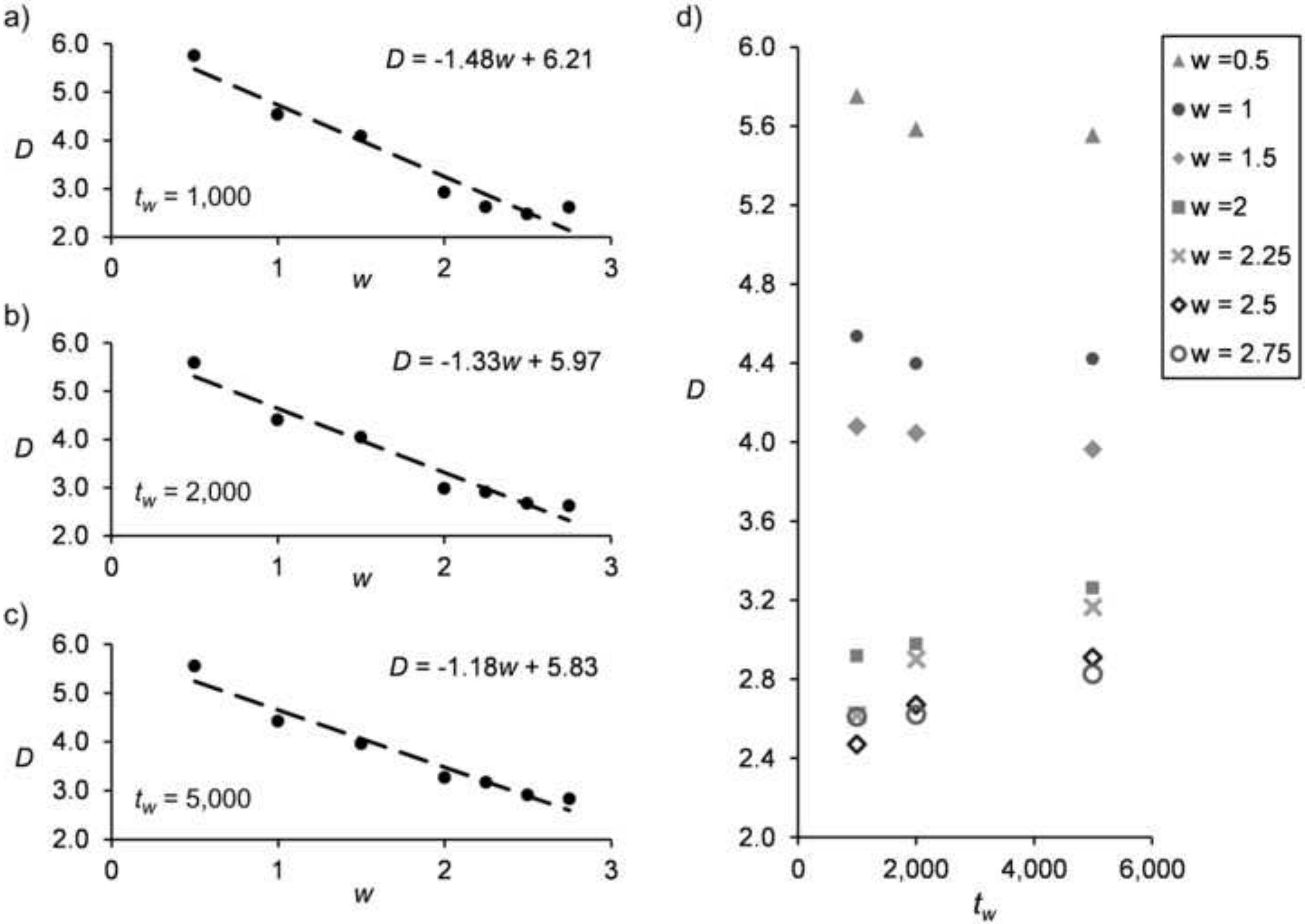

Figure 7 (Greyscale)
Click here to download high resolution image

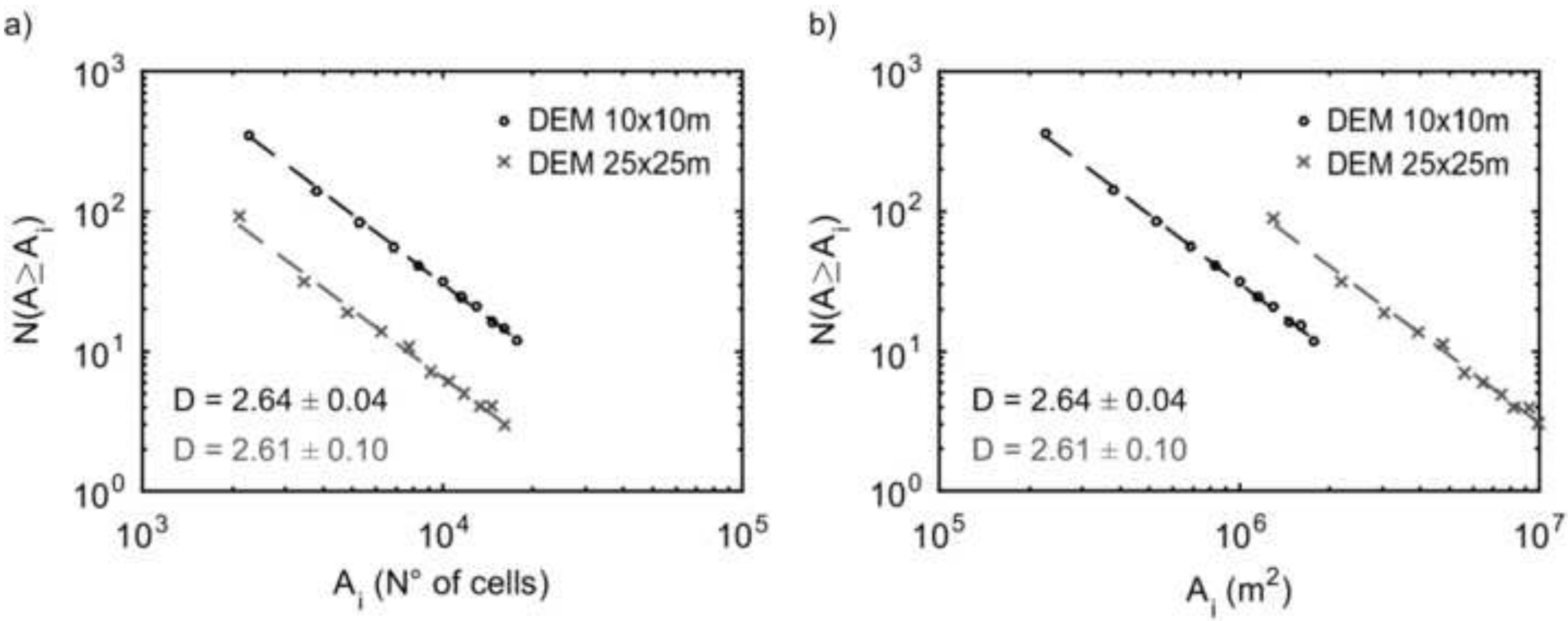

Figure 8 (Greyscale)
Click here to download high resolution image

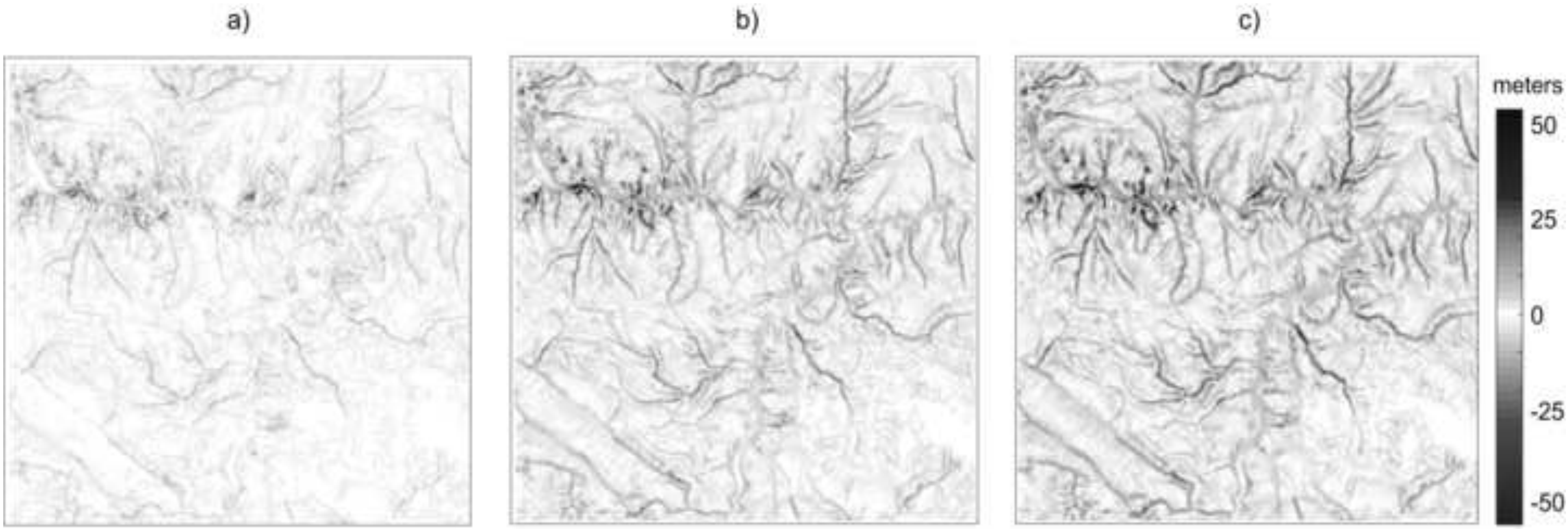

**Figure 9 (Greyscale)**
Click here to download high resolution image

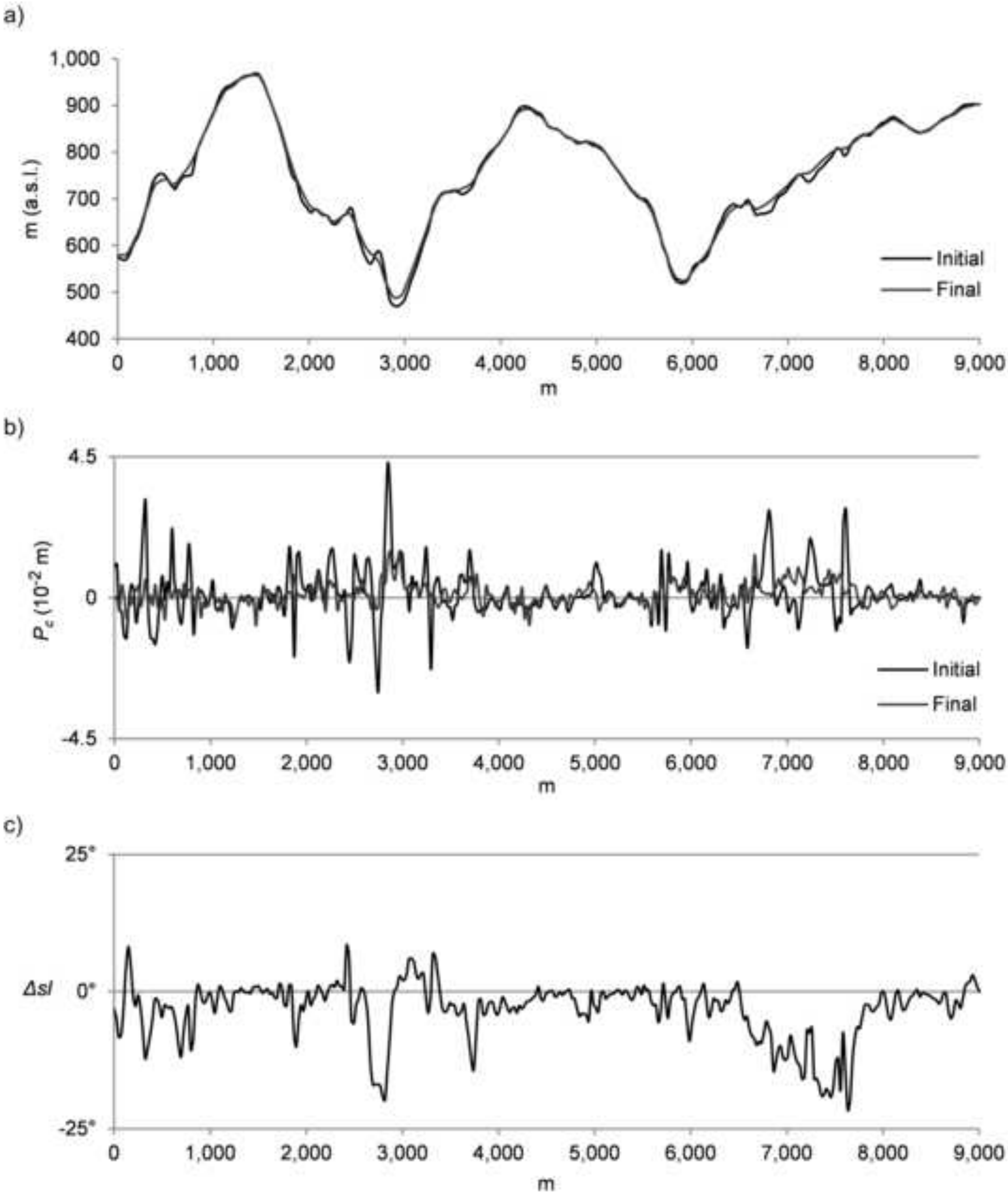

**Figure 10 (Greyscale)**
Click here to download high resolution image

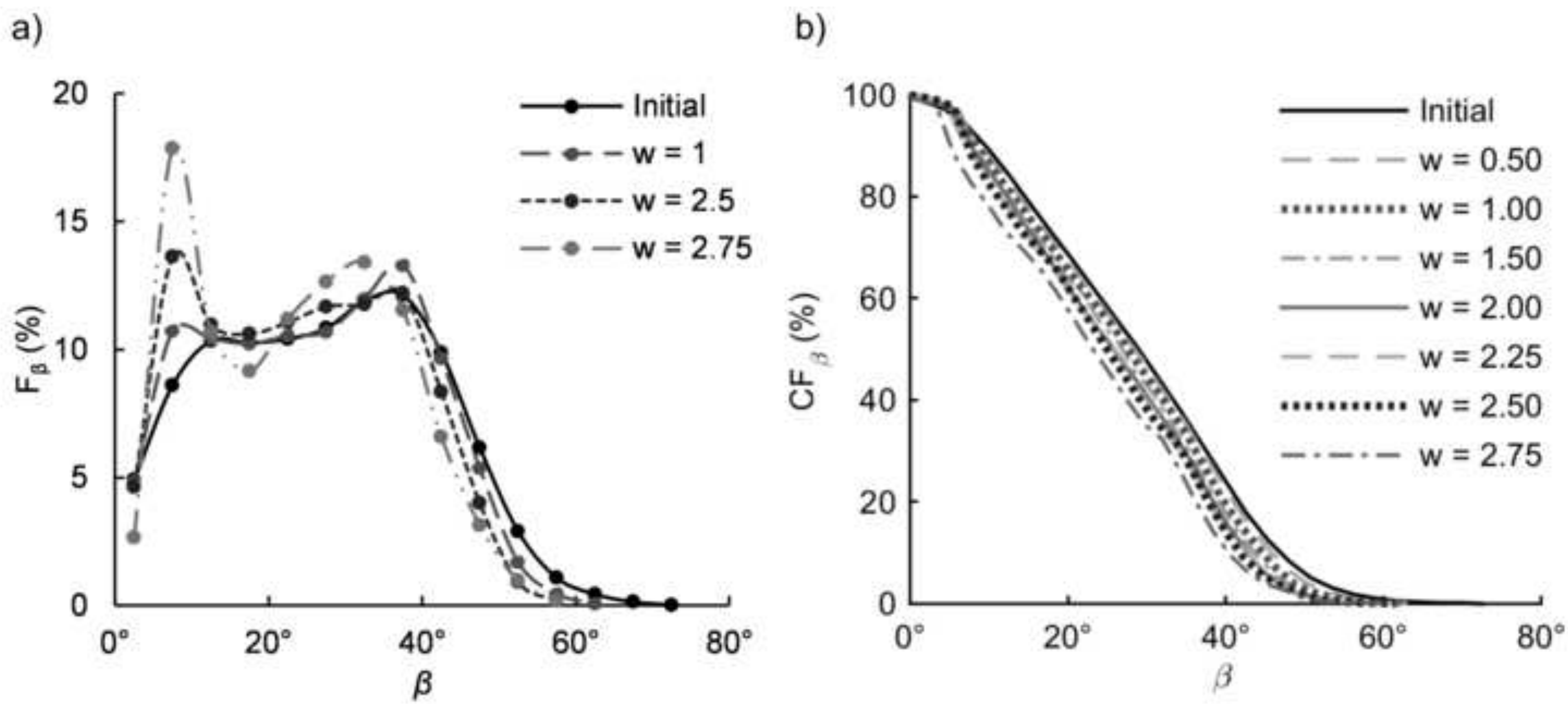

Figure 11 (Greyscale)
Click here to download high resolution image

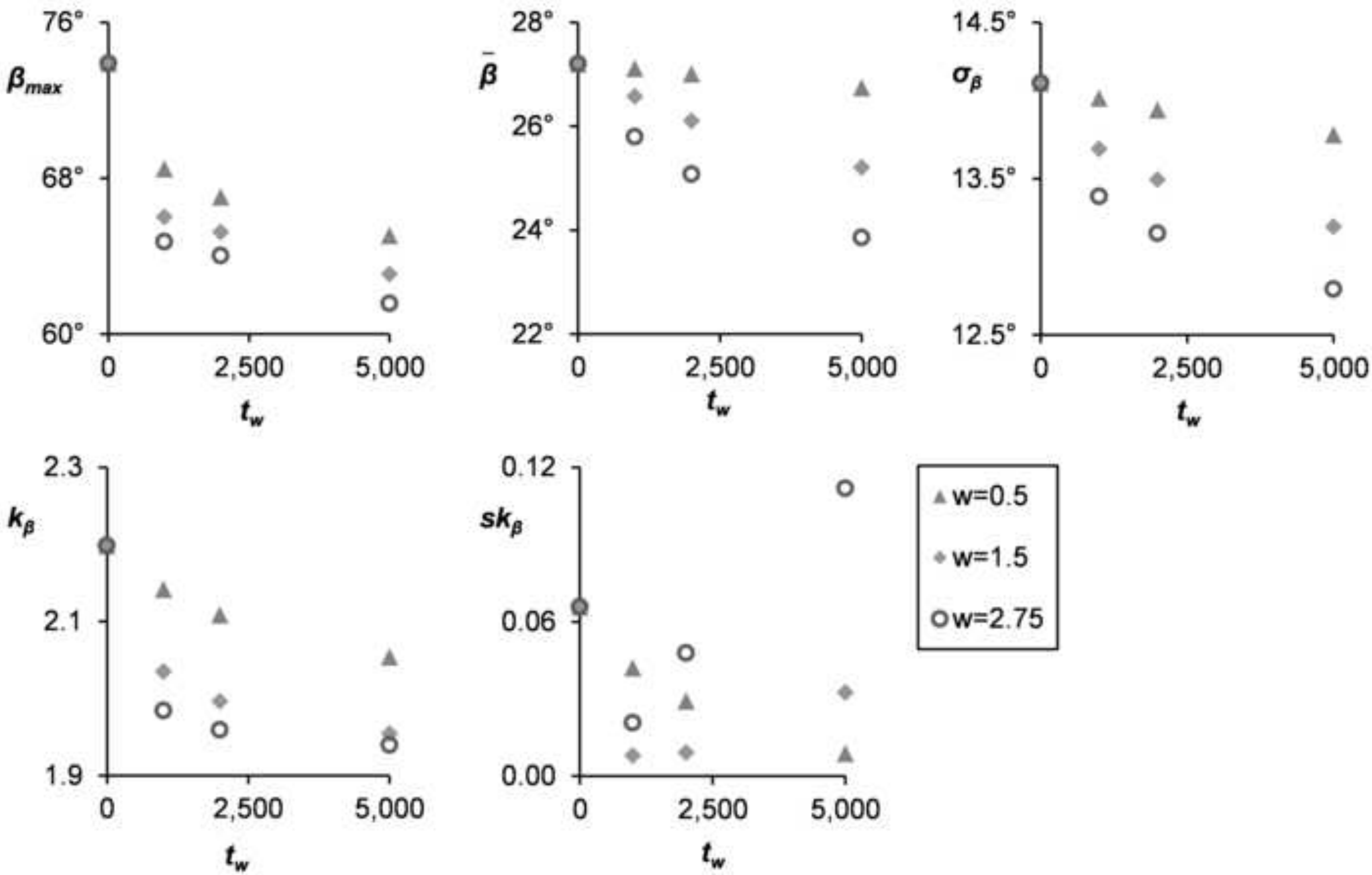

Figure 12 (Greyscale)
Click here to download high resolution image

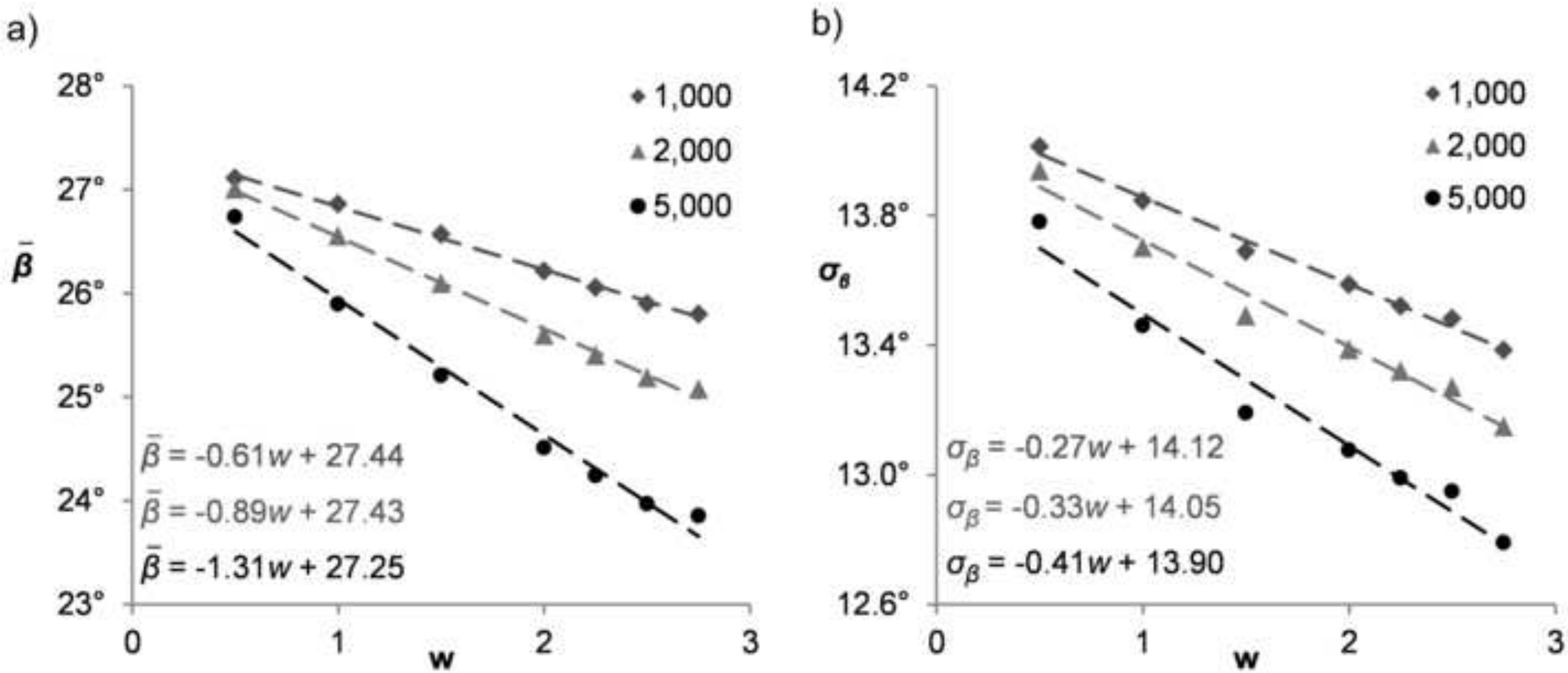

**Figure 13 (Greyscale)**
Click here to download high resolution image